Report No. K-TRAN: KSU-15-4 ▪ FINAL REPORT▪ April 2017

Characterizing Soil Erosion Potential Using Electrical Resistivity Imaging

Stacey Tucker-Kulesza, Ph.D.
Md Zahidul Karim

Kansas State University Transportation Center

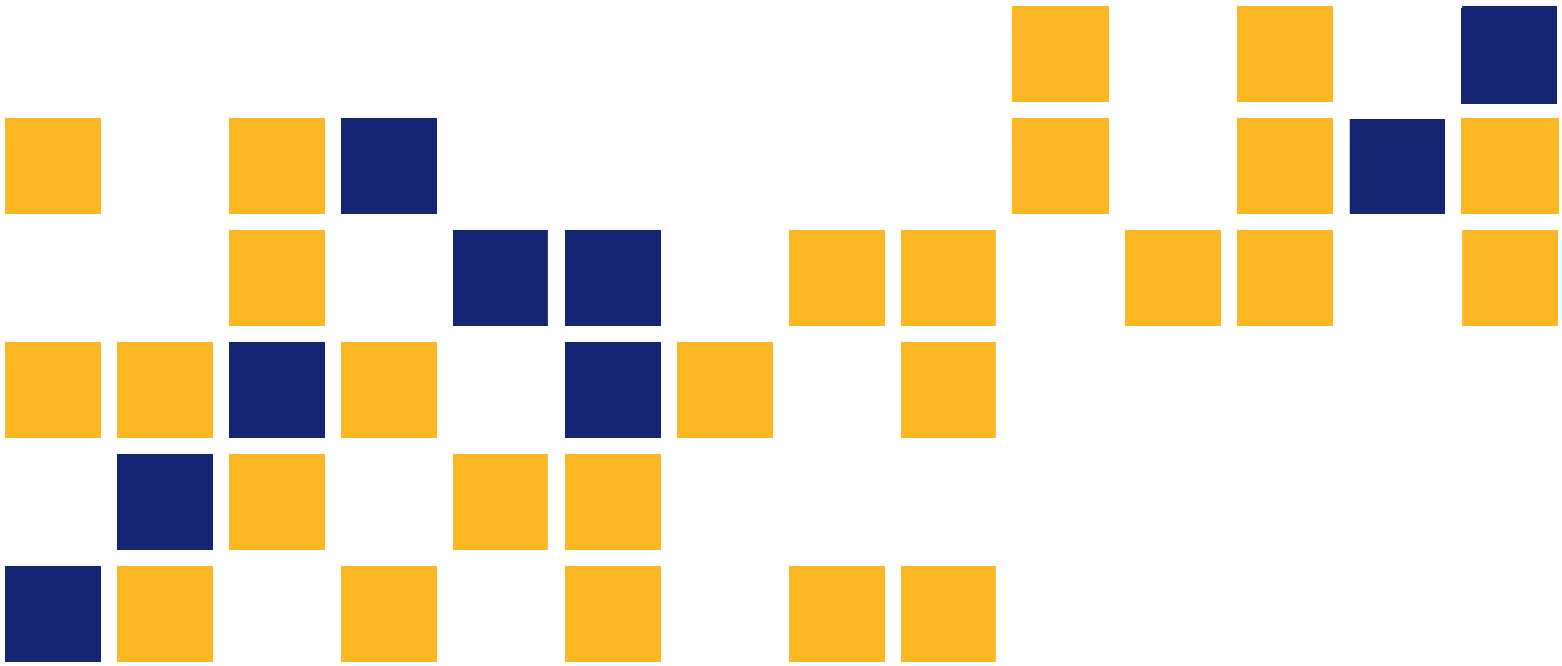

Kansas Department of Transportation

1 Report No. K-TRAN: KSU-15-4	**2 Government Accession No.**	**3 Recipient Catalog No.**
4 Title and Subtitle Characterizing Soil Erosion Potential Using Electrical Resistivity Imaging		**5 Report Date** April 2017 **6 Performing Organization Code**
7 Author(s) Stacey Tucker-Kulesza, Ph.D., Md Zahidul Karim		**7 Performing Organization Report No.**
9 Performing Organization Name and Address Kansas State University 2122 Fiedler Hall Manhattan, Kansas 66506-113		**10 Work Unit No. (TRAIS)** **11 Contract or Grant No.** C2045
12 Sponsoring Agency Name and Address Kansas Department of Transportation Bureau of Research 2300 SW Van Buren Topeka, Kansas 66611-1195		**13 Type of Report and Period Covered** Final Report August 2014 – February 2017 **14 Sponsoring Agency Code** RE-0655-01
15 Supplementary Notes For more information write to address in block 9.		

The erosion rate, or erodibility, of soil depends on many soil characteristics including: plasticity, water content, grain size, percent clay, compaction, and shear strength. Many of these characteristics also influence soil in situ bulk electrical resistivity (ER) measurements. The objective of this study was to characterize soil erosion potential by correlating the in situ ER of soil with erodibility measured in an Erosion Function Apparatus (EFA) at Kansas State University. ER surveys were conducted at 15 bridge sites. Five soil samples were also collected at each site with a drill rig from the surface to 10 ft (3 m) using thin-walled Shelby tubes. The samples were tested in the EFA and classified according to the Unified Soil Classification System. Analysis showed that the rapid in situ data obtained from an ER field survey can be used to categorize the level of soil erodibility. As such, ER surveys may be used to characterize the soils at future bridge sites or prioritize existing bridges for additional testing to measure the scour potential. Moreover, ER surveys may be used to determine which existing bridges should be closed or closely monitored for scour potential during a flood event. Preliminary analytical models to predict soil critical shear stress using ER and other soil parameters were constructed. The selected preliminary model and ER prediction of soil erodibility were validated using one site.

17 Key Words Soil Erosion, Erosion Rate, Electrical Resistivity Imaging		**18 Distribution Statement** No restrictions. This document is available to the public through the National Technical Information Service www.ntis.gov.	
19 Security Classification (of this report) Unclassified	**20 Security Classification (of this page)** Unclassified	**21 No. of pages** 104	**22 Price**

Form DOT F 1700.7 (8-72)

This page intentionally left blank.

Characterizing Soil Erosion Potential Using Electrical Resistivity Imaging

Final Report

Prepared by

Stacey Tucker-Kulesza, Ph.D.
Md Zahidul Karim

Kansas State University Transportation Center

A Report on Research Sponsored by

THE KANSAS DEPARTMENT OF TRANSPORTATION
TOPEKA, KANSAS

and

KANSAS STATE UNIVERSITY TRANSPORTATION CENTER
MANHATTAN, KANSAS

April 2017

PREFACE

The Kansas Department of Transportation's (KDOT) Kansas Transportation Research and New-Developments (K-TRAN) Research Program funded this research project. It is an ongoing, cooperative and comprehensive research program addressing transportation needs of the state of Kansas utilizing academic and research resources from KDOT, Kansas State University and the University of Kansas. Transportation professionals in KDOT and the universities jointly develop the projects included in the research program.

NOTICE

The authors and the state of Kansas do not endorse products or manufacturers. Trade and manufacturers names appear herein solely because they are considered essential to the object of this report.

This information is available in alternative accessible formats. To obtain an alternative format, contact the Office of Public Affairs, Kansas Department of Transportation, 700 SW Harrison, 2nd Floor – West Wing, Topeka, Kansas 66603-3745 or phone (785) 296-3585 (Voice) (TDD).

DISCLAIMER

The contents of this report reflect the views of the authors who are responsible for the facts and accuracy of the data presented herein. The contents do not necessarily reflect the views or the policies of the state of Kansas. This report does not constitute a standard, specification or regulation.

Abstract

The erosion rate, or erodibility, of soil depends on many soil characteristics including: plasticity, water content, grain size, percent clay, compaction, and shear strength. Many of these characteristics also influence soil in situ bulk electrical resistivity (ER) measurements. The objective of this study was to characterize soil erosion potential by correlating the in situ ER of soil with erodibility measured in an Erosion Function Apparatus (EFA) at Kansas State University. ER surveys were conducted at 15 bridge sites. Five soil samples were also collected at each site with a drill rig from the surface to 10 ft (3 m) using thin-walled Shelby tubes. The samples were tested in the EFA and classified according to the Unified Soil Classification System. Analysis showed that the rapid in situ data obtained from an ER field survey can be used to categorize the level of soil erodibility. As such, ER surveys may be used to characterize the soils at future bridge sites or prioritize existing bridges for additional testing to measure the scour potential. Moreover, ER surveys may be used to determine which existing bridges should be closed or closely monitored for scour potential during a flood event. Preliminary analytical models to predict soil critical shear stress using ER and other soil parameters were constructed. The selected preliminary model and ER prediction of soil erodibility were validated using one site.

Acknowledgements

The authors would like to thank the Kansas Department of Transportation and the Kansas Transportation Research and New-Developments (K-TRAN) Research Program for funding the research described in this report. The authors thank the KDOT project monitor Bradford Rognlie, as well as Mike Orth, Luke Metheny, and James Brennan. Finally, we appreciated the help of Mike Noguera, Ed Eneihen, and Kevin Vaughn for their assistance coordinating the drilling at each site and collecting soil samples in the field.

Table of Contents

List of Tables

List of Figures

Chapter 1: Introduction

The Federal Highway Administration (FHWA) defines scour as the result of erosive action of flowing water excavating and carrying away material from the bed and banks of streams and from around the piers and abutments of bridges (Calappi, Miller, & Carpenter, 2010). As of 2003, the National Bridge Inventory (NBI) contained 604,279 bridges including the federal, state, county, and city bridges (Richardson, Pagan-Ortiz, Schall, & Price, 2003). Of these bridges, approximately 84% (503,000) are built over waterways, of which, over 20,000 bridges are classified as "scour critical." Therefore, at least one out of every 25 bridges in the United States is vulnerable to scour. According to Nassif, Ertekin, and Davis (2002), about 80% of existing bridges require some sort of scour mitigation.

Over 1,500 bridges collapsed in the United States between 1965 and 2005; scour was responsible for nearly 60% of these failures (Calappi et al., 2010). For example, 73 bridges collapsed during the 1985 floods in Pennsylvania, Virginia, and West Virginia (Richardson & Davis, 2001). In 1987, following the deadly collapse of the Schoharie Creek Bridge, the FHWA issued a Technical Advisory T5140.20 titled "Scour at Bridges," accompanied by a publication titled "Interim Procedures for Evaluating Scour at Bridges" in 1988. The "Interim Procedures" divided the national scour problem at highway encroachments and crossings as (1) stream instability and channel movement, (2) long-term degradation or aggradation, (3) live-bed or clear-water contraction scour, and (4) local scour at piers and abutments. It also addressed the methods for determining and preventing stream instability, channel movement, and long-term streambed elevation changes. As a part of the continued process, the FHWA updated the "Interim Procedures" to Hydraulic Engineering Circular 18 (HEC-18) in 1991 (Richardson, Harrison, Richardson, & Davis, 1993). HEC-18 remains the primary tool for predicting scour depth and prioritizing bridge monitoring schedules.

Although HEC-18 has served as a useful benchmark for scour prediction, it is not applicable to all geologic, geotechnical, and hydraulic conditions. Therefore, numerous testing devices have been developed by researchers for directly measuring soil erosion in the laboratory and in the field. Some of the recent apparatuses for erosion measurements include the Sediment

Erosion Rate Flume (Bloomquist & Crowley, 2010), the Jet Erosion Testing apparatus (Hanson & Cook, 2004), the Erosion Function Apparatus (EFA; Briaud et al., 2001), and the Ex Situ Erosion Testing Device (ESTD; Shan, Shen, Kilgore, & Kerenyi, 2015). The ESTD was developed and utilized by the FHWA to predict erosion in cohesive soils using the HEC-18 scour framework (Shan et al., 2015). Ultimately, the goal of these apparatuses is to predict the amount of scour by measuring the critical shear stress, or the stress at which soil starts to erode. The Erosion Function Apparatus (EFA), utilized in this study at Kansas State University, is a flume style apparatus that measures the erosion of undisturbed soil samples, field collected in Shelby tubes. While soil erosion measurements are valuable using these devices, they are often time consuming. For example, a full test on a single sample takes 8 hours to finish in the EFA. For large projects, such as statewide prioritizing of bridge monitoring procedures, the application of such time-consuming testing may not be economically feasible.

The objective of this research was to predict soil erodibility. Unlike coarse-grained soil, where erosion is a function of median particle size only (Briaud et al., 2001), there is a complex system of factors that affects the erosion in fine-grained soil as shown in Figure 1.1. The effects of some of these factors on erosion are described in Chapter 3.

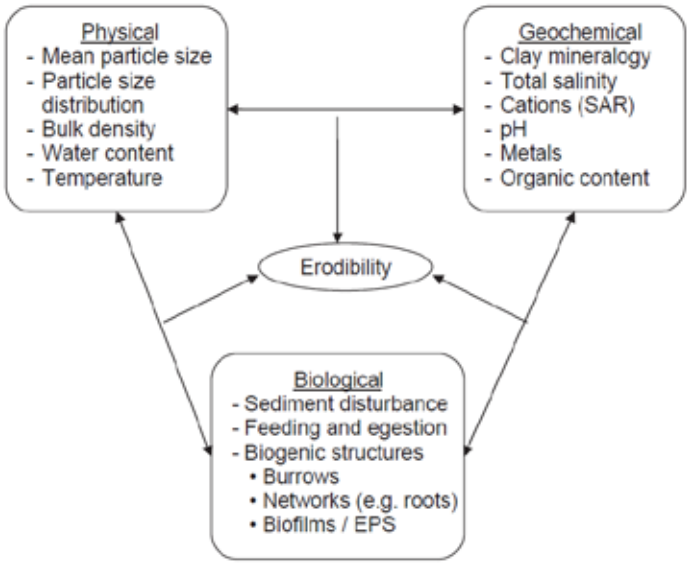

Figure 1.1: Factors Affecting Erosion in Fine-Grained Soils
Source: Grabowski, Droppo, and Wharton (2011)

Electrical Resistivity (ER) is an intrinsic property of every material and is measured as the capability of opposing the flow of electrical current. Typical ranges of ER for different geo-materials are outlined in Table 1.1. ER tomography, or surveys, have gained popularity as a geophysical testing method and are commonly used in geology, environmental science, archeology, and geotechnical engineering (Loke, 1999; Dahlin, 2001; Zonge, Wynn, & Urquhart, 2005). Applications within these fields include determining depth to groundwater (Vaudelet et al., 2011), detecting varying subsurface geology (Chambers et al., 2013), and the presence of subsurface structures (Arjwech et al., 2013). The major factors that affect the ER of soils are particle sizes, water content, porosity, bulk density, mineralogy, and plasticity (Zhou, Shimada, & Sato, 2001). From Figure 1.1, it is seen that many of these factors are the same as the physical factors of erosion. Therefore, correlating erodibility and ER of soil may provide rapid in situ measurement of erodibility. The objective of this study was to characterize the soil erosion potential, or erodibility, by correlating the in situ ER of soil with the erodibility measurements from an EFA.

Table 1.1: Typical Electrical Resistivity (ER) Values of Different Geo-Materials

Material	Resistivity (Ω−m)
Clay	5-100
Saturated Sand and Gravel	<50
Dry Sand and Gravel	>200
Shale	5-50
Sandstone	50-1,000
Conglomerates	1,000-10,000
Limestone and Dolomite	>1,000
Igneous Rocks	>1,000
Metamorphic Rocks	>1,000

Source: Knight and Endres (2005); Lucius, Langer, and Ellefsen (2006)

Due to its geographic position in the Upper Mississippi River basin, scour is a significant issue in Kansas. As mentioned earlier, erosion testing in the EFA can provide essential data for predicting erodibility, but is time consuming. ER surveys are rapid and can collect large amounts of subsurface data. Based on a correlation between ER and erodibility, ER data can be used to

determine which bridge sites are vulnerable to scour and need further testing for predicting erosion potential or erodibility. This has the potential to reduce the number of required erosion tests statewide.

Samples were collected from 15 bridge sites throughout eastern Kansas using Shelby tubes for erosion tests in an EFA. ER surveys were also conducted at each bridge site to obtain a two-dimensional distribution of subsurface ER. Data obtained in this manner were then used to correlate ER of soils with the erodibility of soils. This study showed that the rapid in situ data obtained from an ER survey can predict the presence of highly erosive soils. As such, ER surveys may be used to identify where further testing is necessary to measure the scour potential or determine which existing bridges should be closed or closely monitored for scour potential during a flood event.

There are five chapters in this report. Following this introduction, Chapter 2 includes a literature review of different soil erosion testing methods and electrical resistivity imaging. Chapter 3 describes the methodology of this research, including the subsurface sampling, erosion tests as well as the field setup for ER survey. It is followed by Chapter 4 where results and analysis of this research, including necessary statistical analysis, are provided. Conclusions, recommendations for implementation, and future work are discussed in the final chapter.

Chapter 2: Literature Review

2.1 Soil Erosion

Erosion is the process of soil loss due to water flow. Erosion occurs when exerted shear forces by the flowing water overcome the resistive forces within the soil mass. The resistive forces from the soil include gravity, friction, cohesion, and adhesion depending on the type of soil (Leeder, 1999; Winterwerp & Van Kesteren, 2004). This threshold for erosion can be measured in terms of critical shear stress. The process of erosion initiates once the shear stress exerted by the flowing water exceeds the critical shear stress of the soil. After this critical point, if flow continues, the amount of soil eroded per unit time is defined as the erodibility or erosion rate. This simple concept indicates that an erosion resistant soil is likely to have low erodibility and an erosion prone soil will have a high erodibility.

While coarse-grained soils erode as individual particles, fine-grained soils erode as blocks. Slow motion videos have shown erosion as blocks in fine-grained soils is associated with a combined rolling and plucking action (Briaud et al., 2001). In coarse-grained soils, resistance against erosion is controlled by the weight of soil whereas in fine-grained soils, inter-particular forces (i.e., cohesion and adhesion) provide the resistance against erosion in addition to the weight of soil (Grabowski et al., 2011). The excess shear stress equation (Partheniades, 1965; Hanson, 1990) is the common simplified equation for estimating soil erodibility, $\dot{z}$ (lb/ft2/s [$cm^3/hr/cm^2$]) such that

$$\dot{z} = K_d \exp(\alpha(\tau_e - \tau_c)^{\beta}) \qquad \textbf{Equation 2.1}$$

Where:

K_d is the erodibility coefficient (lb/ft^2/s [cm/hr/Pa]),

τ_e is the effective hydraulic stress (lb/ft^2 [Pa]),

τ_c is the critical shear stress (lb/ft^2 [Pa]), and

α, β are empirical constants.

When expressed in SI units, the exponent β is typically assumed to be equal to 1.0 (Hanson, Cook, & Simon, 1999); however, researchers have showed that *b* can vary from 1.0 to 6.8 (Van Klaveren & McCool, 1998; Knapen, Poesen, Govers, Gyssels, & Nachtergaele, 2007).

The critical shear stress, τ_c, in Equation 2.1 is the shear stress exerted by flowing water on the soil surface that initiates erosion. Any shear stress below τ_c will not cause the soil to erode. In coarse-grained soils, only the weight of the soil resists the shear force. Briaud et al. (1999) found that the ratio of critical shear stress, τ_c (in Pa), and median grain size (in mm), d_{50}, is 1.03 for coarse-grained soils. Therefore, τ_c (Pa) can be expressed by the following equation for coarse-grained soils:

$$\boldsymbol{\tau_c = d_{50}} \qquad \textbf{Equation 2.2}$$

Where:

d_{50} is the median grain size (mm; Briaud et al., 1999).

This equation is only valid for SI units. However, studies have shown that Equation 2.2 underestimates τ_c for fine-grained soils and overestimates the amount of erosion (Hanson & Simon, 2001). Laboratory tests on coarse-grained soils demonstrate that an increase in median grain size increases the critical shear stress. However, comprehensive laboratory studies on soil having particle size below 190 μm showed that critical shear stress decreases with increasing median grain size. The researchers concluded that silt-sized particles behave as fine-grained soil and the cohesion between organic materials supplies the inter-particular force (Johnson, Kranck, & Muschenheim, 1994; Lick, Jin, & Gailani, 2004). According to a field survey on both consolidated and unconsolidated soil by Thomsen and Gust (2000), it was found that natural marine mud has an inverse correlation between critical shear stress and particle size. However, when particle size and floc density were proportional, a positive correlation between critical shear stress and particle size was observed during laboratory studies (Lau & Droppo, 2000; Droppo, Lau, & Mitchell, 2001). Therefore, for fine-grained soils, particle size can be either positively or negatively related to critical shear stress depending on various factors.

2.1.1 Properties that Affect Fine-Grained Soil Erosion

Many researchers have developed empirical relationships between critical shear stress and erodibility for fine-grained soils based on laboratory tests. Common geotechnical parameters such as clay content (Panagiotopoulos, Voulgaris, & Collins, 1997; Van Ledden, Van Kesteren, &

Winterwerp, 2004; Winterwerp & Van Kesteren, 2004; Houwing, 1999; Dickhudt, Friedrichs, & Sanford, 2011; Debnath, Nikora, Aberle, Westrich, & Muste, 2007) and bulk density (Jepsen, Roberts, & Lick, 1997; Lick & McNeil, 2001; Amos et al., 2004; Bale, Stephens, & Harris, 2007) have been correlated with critical shear stress. Researchers have also related plasticity index (Smerdon & Beasley, 1961; Dunn, 1959) and the liquidity index to soil erosion (Amaryan, 1993; Bale et al., 2007). Despite the wealth of research, critical shear stress is governed by the inter-particular forces and the chemistry between pore-water and flowing water. These are site-specific properties and are very difficult to estimate (Heinzen, 1976; Grissinger, 1982; Knapen et al., 2007).

Recently Shan et al. (2015) tested 17 laboratory prepared fine-grained soil samples in a custom erosion flume and found that critical shear stress increased with increasing plasticity index. The empirical equation for critical shear stress, τ_c lb/ft^2 (Pa), was combined of several other soil parameters and is formulated as:

$$\tau_c = \alpha_d \left(\frac{w}{F}\right)^{-2.0} PI^{1.3} q_u^{0.4} \qquad \textbf{Equation 2.3}$$

Where:

w is the water content,

F is the percent of particles finer than 0.075 mm,

PI is the plasticity index,

q_u is the unconfined compressive strength of soil (lb/ft^2 [Pa]), and

α_d is a unit conversion constant, 0.007 in U.S. customary units and 0.07 in S.I.

The Shan equation was applied to the dataset herein and found to over-predict critical shear stress. Therefore, despite recent advances in predicting critical shear stress, erosion testing is still necessary for fine-grained soils.

2.2 Erosion Function Apparatus

Because no unifying equation exists based on measurable soil properties to predict soil erosion, researchers have developed devices to directly measure the erodibility of soils. These devices can be divided into four categories: rotating apparatus tests, JET erosion tests, flume

style erosion tests, and pinhole erosion tests. Each of these devices imparts a different hydraulic loading mechanism, that is, the way the water flows across the soil sample. The Erosion Function Apparatus (EFA) is a simple flume style test that was used exclusively in this research. In an EFA test, soil samples collected in ASTM Standard Shelby tubes are mounted in the flume as shown in Figure 2.1. Water is pumped at different velocities within a 4.4 ft (1.3 m) long rectangular flume that has a cross-sectional dimension of 4 inches × 2 inches (101.6 mm x 50.8 mm). A flow straightener is used at one end of the rectangular flume. The rectangular flume has a circular opening in its bottom to insert the top end of the Shelby tube containing the soil sample. The top of the Shelby tube (or the sample) is kept flush with the bottom of the rectangular flume. As erosion takes place, the sample is pushed from the other end of the sample with the aid of a piston. A leak-proof connection is established by a snug fit and an O-ring. The velocity of water flow in the rectangular flume is be maintained using a flow control pump. The average flow velocity range is 0.32 to 19.6 ft/s (0.1 to 6 m/s).

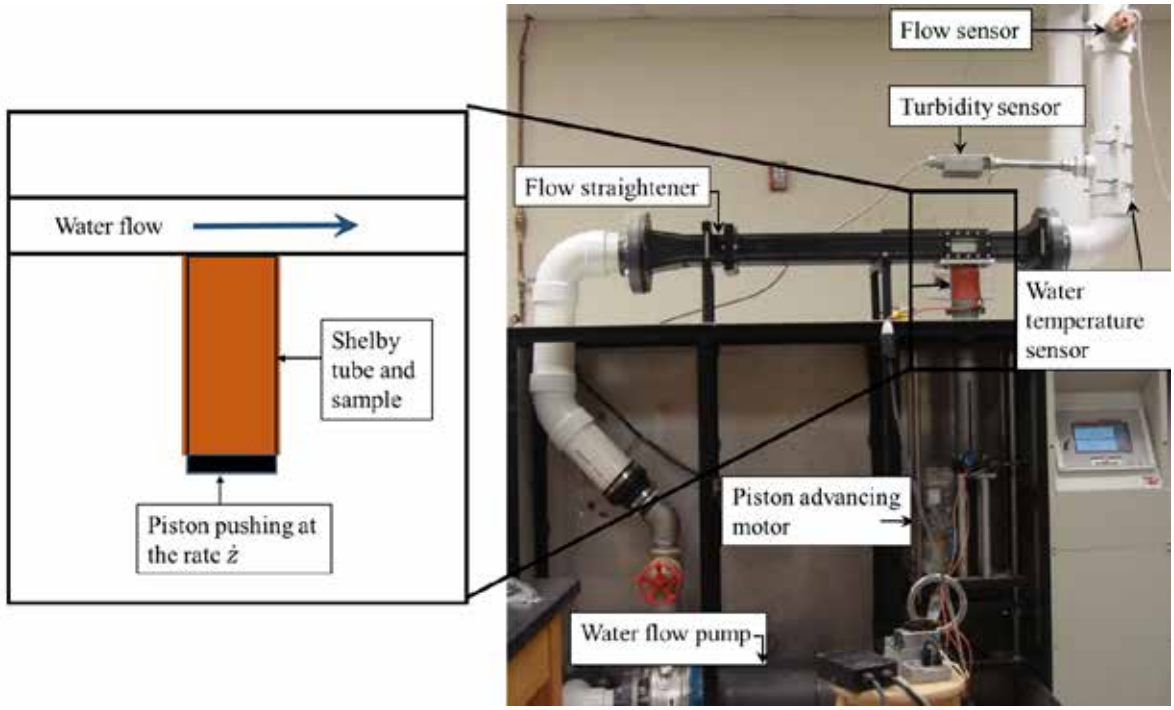

Figure 2.1: Erosion Function Apparatus at Kansas State University

EFA tests are conducted on soils at their in situ water content. During the test, the bottom of the sample is placed over the piston and the top is kept flush with the base of the rectangular flume. At first, the sample is eroded under the minimum velocity (typically 1.64 ft/s [0.5 m/s]) for 1 hour. When the sample erodes, the piston is pushed upward to keep the soil flush with the bottom of the flume. The sample is visually inspected during testing to determine when to extrude the sample and how much. The amount of sample eroded is equal to the length of sample lifted by the piston. This procedure is repeated for at least six different flow velocities so the erosion rate in inches per hour (mm/hr) is obtained for each velocity. The objective of erosion tests in an EFA is to obtain the plot of erosion rate, $\dot{z}$, in/hr (mm/hr) versus shear stress, τ, lb/ft^2 (N/m^2). The erosion rate, $\dot{z}$ for different velocities can be found by:

$$\dot{z} = \frac{h}{t} \qquad \textbf{Equation 2.4}$$

Where:
h is the length of sample eroded, inches (mm), and
t is the duration of the test.

The Moody (1944) chart is used to calculate the shear stress, τ, calculated by:

$$\boldsymbol{\tau = \frac{1}{8}\alpha f \rho V^2} \qquad \textbf{Equation 2.5}$$

Where:
f is the friction factor obtained from the Moody chart,
α is the unit conversion constant,
ρ is the density of water in slugs/ft^3 (kg/m^3), and
V is the mean velocity of flow in the pipe, ft/s (m/s).

Determining the friction factor is discussed further in Chapter 3.

2.3 Electrical Resistivity Imaging

Electrical resistivity (ER) imaging, one of the most widely used near surface geophysical methods, has gained more popularity since the mid-1900s due to advancements in data

acquisition systems (Loke, 1999; Dahlin, 2001; Zonge et al., 2005). An electric current I (measured in amperes) is injected into the ground through a current electrode and resulting voltage potential V (measured in volts) is measured across another pair of electrodes. The impedance of earth, $Z = \frac{V}{I}$ (measured in volts/ampere) is calculated, which is used to calculate resistivity, ρ (measured in Ω-m). The fundamentals of ER imaging were described in a previous KDOT study (Tucker-Kulesza, Snapp, & Koehn, 2016) and in Karim (2016). The information pertinent to this study is described herein.

2.3.1 Properties that Affect Electrical Resistivity Imaging

Many of the factors that affect soil erosion also determine a soil's ER. Subsurface characteristics such as water content and saturation, porosity, permeability, mineralogy, clay content, and temperature affect electrical resistivity measurements (Zonge et al., 2005). Electrical current in soil is dependent on the displacement of ions in pore-water; therefore, water content and saturation are the primary factors that influence the measured ER of soils (Kibria & Hossain, 2012; McCarter, 1984). Resistivity is also dependent on the electrical charge density at the surface of the solid constituents. The inherent higher electrical charges associated with clay particles result in lower resistivity than coarse-grained soils (Fukue, Minato, Horibe, & Taya, 1999). Moreover, coarse-grained soils are typically higher in ER due to the presence of larger voids where current dissipates. ER can also be related to the percentage of fines and coarse fraction. Abu-Hassanein, Benson, and Blotz (1996) used clay samples to correlate ER with percent fines and coarse fraction, shown in Figure 2.2. The measured ER values decreased with increasing percent fines. This was likely due to the increase in more conductive clay particles in the fines (Kwader, 1985). Figure 2.2b shows that ER values increased with increasing percent coarse fraction. The coarse fraction was primarily made of quartz and feldspar which have high ER (Keller & Frischknecht, 1966).

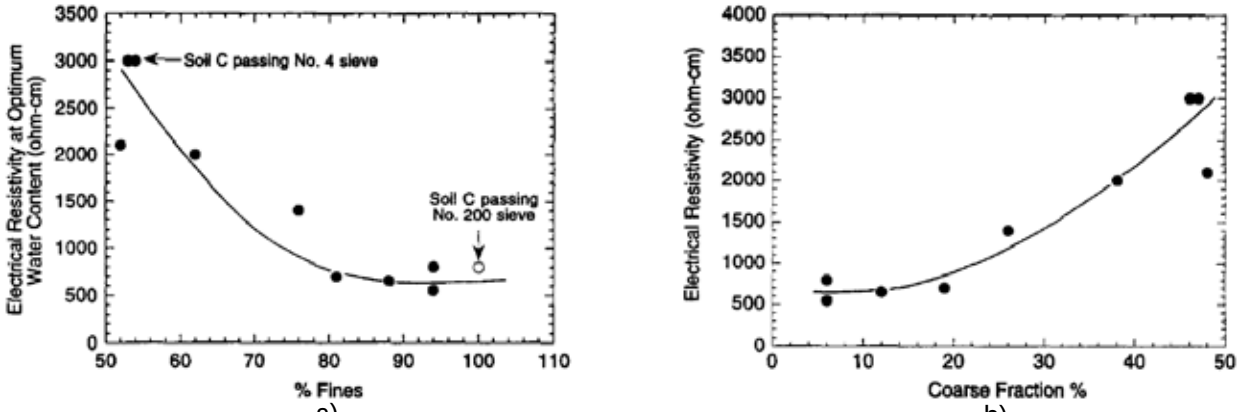

Figure 2.2: Relationship between ER and: (a) Percent Fines; (b) Percent Coarse Fraction
Source: Abu-Hassanein et al. (1996)

2.3.2 Electrical Resistivity Measurements

During an ER survey, two pairs of electrodes are used: the current pair (A, B) and voltage pair (P, Q). The electrode A (source) sends the current into the ground and electrode B (sink) receives it, and voltage difference is measured between electrodes P and Q. The resulting voltage difference between P and Q is:

$$V_{PQ} = V_p - V_Q = \frac{I\rho}{2\pi}\left(\frac{1}{r_{AP}} - \frac{1}{r_{AQ}} - \frac{1}{r_{BP}} + \frac{1}{r_{BQ}}\right)^{-1} \qquad \textbf{Equation 2.6}$$

Where:

r is the distance between electrodes and all other variables have previously been defined.

When running an ER survey, a known electric current (I) is injected into the subsurface and the corresponding voltage potential (V) is measured at known distances (r) so that the apparent resistivity can be calculated as:

$$r_a = \frac{2\pi V_{PQ}}{I}\left(\frac{1}{r_{AP}} - \frac{1}{r_{AQ}} - \frac{1}{r_{BP}} + \frac{1}{r_{BQ}}\right)^{-1} \qquad \textbf{Equation 2.7}$$

Where all variables have previously been defined.

The term apparent resistivity is used because initially the subsurface is assumed to be homogenous with uniform resistivity, ρ. An inversion process is required to determine the true resistivity of the subsurface.

Equation 2.7 assumed a four electrode system. Now, with the advancement of data acquisition systems, multiple 4-electrodes can be combined or modified to form different arrays to gather the needed data. Depth of penetration, signal-to-noise ratio, lateral resolution, and ease of deployment are some of the prime criteria upon which the choice of an electrode configuration depends (Everett, 2013). The Wenner, Schlumberger, and Dipole-Dipole configurations are the most common arrays. Although all arrays were investigated for optimal data collection, only the dipole-dipole array was used at the production sites in this research.

2.3.3 Dipole-Dipole Array

The dipole-dipole is one of the most popular arrays in electrical resistivity applications (Loke, 1999). The spacing between current electrodes AB is a, and is the same as the spacing between the voltage electrodes PQ (Figure 2.3). The electrode pairs are separated by na. The depth of penetration increases as n and/or a increases. The dipole-dipole provides good resolution with depth; effectively combining the benefits of each the Schlumberger and Wenner arrays. One of the drawbacks of the dipole-dipole array is the poor signal-to-noise ratio with increasing values of n. For this reason, n was limited to eight in this research.

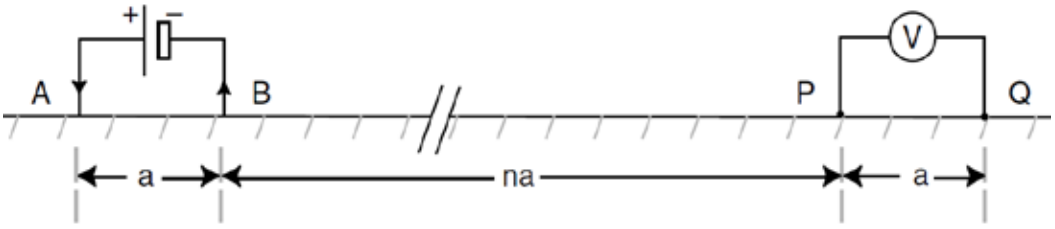

Figure 2.3: Dipole-Dipole Array Circuit Diagram
Source: Everett (2013)

The subsurface apparent resistivity data from the multi-electrode survey are expressed using the pseudosections. To plot the data from a 2-D imaging survey, the pseudosection contouring method is normally used (Loke, 1999). As shown in Figure 2.4, for a dipole-dipole

array, the apparent resistivity ρ_a corresponding to the current electrodes AB and voltage electrodes PQ is plotted at the intersection of the 45° lines (with horizon) drawn from the centers of the electrodes. The same procedure is repeated until all the current and potential electrode pairs are covered. In this way, a rough estimation of true subsurface resistivity is obtained because maximum sensitivity of the ground surface for a particular voltage measurement is found near the midpoint of the four-electrode configuration at a depth of one-half of the separation of the current-potential electrode pairs (Everett, 2013). However, the pseudosection gives a distorted picture of the subsurface because the shape of the contours depends on the type of array used as well as the true subsurface resistivity.

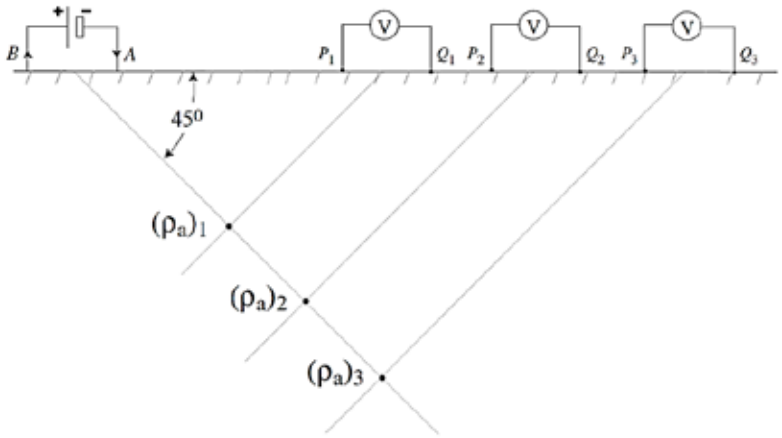

Figure 2.4: Apparent Electrical Resistivity Pseudosection of the Dipole-Dipole Array
Source: Tucker, Briaud, Hurlebaus, Everett, and Arjwech (2015)

2.3.4 Data Processing

The objective of conducting an ER survey is to estimate the subsurface electrical properties (resistivity or conductivity). The apparent resistivity (ρ_a) measured in the field can be converted to inverted resistivity though an iterative process that includes forward modeling and data inversion. Forward modeling mathematically models the apparent resistivity for given electrical properties and boundary condition using partial differential equations such as Poisson's equation (Binley & Kemna, 2005). Inversion, on the other hand, produces the subsurface distribution of electrical properties (model parameter) from a set of given measurements (data).

In a two-dimensional (2D) ER survey, the earth model is 2D but the electrical field due to a point source is 3D; hence, the problem is considered 2.5D and the domain of investigation is discretized for solving the 2.5D forward modeling problem (AGI, 2008). The commercial software AGI EarthImager 2D was used in this research (AGI, 2008). In order to find the forward solution, the 3D partial differential equation is Fourier transformed into a 2D partial differential equation:

$$\frac{d}{dx}\left(\sigma\frac{\partial V}{\partial x}\right)+\frac{d}{dz}\left(\sigma\frac{\partial V}{\partial z}\right)-k^2\sigma V=-I\delta(x)\delta(z) \qquad \textbf{Equation 2.8}$$

Where:

V and k are the scaler electrical potential and wavenumber in the Fourier transfer domain,

I is the injected electric current, and

σ is the electrical conductivity as function of (x, z).

The potential is calculated after solving linear system of equations derived from the discretized differential equation (such as Equation 2.8) and the boundary conditions (Binley & Kemna, 2005). Both finite element (FE) and finite difference (FD) methods can be used in EarthImager. Although FD is fast, FE method provides a more accurate solution to the forward modeling problem and was used in this research. EarthImager also offers both Cholesky decomposition (CD) and conjugate gradient (CG) methods as forward equation solver. For this research, CD was applied as this method is more accurate when more than 20 electrodes are used (AGI, 2008).

To formulate the inverse problem, a model vector **m** is constructed which comprises of electrical properties of the subsurface. This model vector contains the conductivities (σ; inverse of resistivity) of the individual elements or cell in the FE mesh used in the forward modeling such that:

$$m_j = \ln s_i$$ **Equation 2.9**

Where:

j = 1,2,…,M and the logarithm stands for probable large variation of earth conductivities.

Similarly, the measured apparent resistivities (ρ_a) can be stored in another vector **d** as:

$$d_i = - \ln r_{ai}$$ **Equation 2.10**

Where:

i = 1,2,…,N and logarithm stands for the same reason as in the previous vector.

The negative sign is used to convert measured apparent resistivity into conductivity and make the dimension constant with Equation 2.9. The inverse problem must now determine a model **m** so that it reproduces (using forward modeling) the data **d** with a certain level of uncertainty. To account for the non-uniqueness of inversion and the presence of error prone data, additional constraints are imposed in the inversion (Binley & Kemna, 2005). For this reason, inverse problem is solved as a regularized optimization problem (Tikhonov & Arsenin, 1977), in which the following objective function is minimized as:

$$y(\mathrm{m}) = y_d(\mathrm{m}) + a y_m(\mathrm{m})$$ **Equation 2.11**

Where:

$\psi_d(\mathbf{m}) = \|\mathbf{W}_\mathrm{d}[\mathbf{d} - \mathbf{f}(\mathbf{m})]\|^2$ is a measure of data misfit between measured and calculated (using forward modeling) resistivities, and

$\mathbf{W}_\mathrm{d}$ = diag($\frac{1}{\varepsilon_1}, \frac{1}{\varepsilon_2}, \ldots, \frac{1}{\varepsilon_N}$) is a data weighting matrix associated with the uncorrelated data errors ε_i (Binley & Kemna, 2005).

Again, $\psi_m(\mathbf{m})$ is a stabilizing model objective expressed as $\psi_m(\mathbf{m}) = \|\mathbf{W}_\mathrm{m}[\mathbf{m} - \mathbf{m}_\mathrm{ref}]\|^2$ that includes certain model constraints with respect to the reference model $\mathbf{m}_\mathrm{ref}$, and $\mathbf{W}_\mathrm{m}$ is the model weighting matrix similar to $\mathbf{W}_\mathrm{d}$. The regularization parameter, α controls the tradeoff between influence of data misfit and model objective function (Binley & Kemna, 2005). The reference model, $\mathbf{m}_\mathrm{ref}$, can have the value of expected model parameter and/or the result of

previous inversion. It can also be assigned to a homogenous half space or the null vector if sufficient information is not available.

Equation 2.11 can be simplified by applying gradient search method. Choosing Gauss-Newton approach iterations are continued, where at each step, k, the linear system equation:

$$\left(\mathbf{J}_k^{\mathrm{T}}\mathbf{W}_{\mathrm{d}}^{\mathrm{T}}\mathbf{W}_{\mathrm{d}}\mathbf{J}_k + a\,\mathbf{W}_{\mathrm{m}}^{\mathrm{T}}\mathbf{W}_{\mathrm{m}}\right)\Delta\mathbf{m}_k = \mathbf{J}_k^{\mathrm{T}}\mathbf{W}_{\mathrm{d}}^{\mathrm{T}}\mathbf{W}_{\mathrm{d}}\left[\mathbf{d} - \mathbf{f}\left(\mathbf{m}_k\right)\right] - a\,\mathbf{W}_{\mathrm{m}}^{\mathrm{T}}\mathbf{W}_{\mathrm{m}}\left(\mathbf{m}_k - \mathbf{m}_{\mathrm{ref}}\right)$$

Equation 2.12

is solved for a model update $\Delta\mathbf{m}_k$. Here, $\mathbf{J}_k$ is the Jacobian sensitivity matrix, and $J_{ij} = \frac{\partial d_i}{\partial m_j}$ is evaluated for the current model $\mathbf{m}_k$. The iteration process $\mathbf{m}_{k+1} = \mathbf{m}_k + \Delta\mathbf{m}_k$ continues until $\psi_d\ (m_k)$ matches the desired data misfit target value. For starting the iteration, initial model $\mathbf{m}_0$ is taken equal to $\mathbf{m}_{\mathrm{ref}}$, if available (Binley & Kemna, 2005).

There are four methods of inversion available in EarthImager; namely, forward modeling only, damped least squares inversion, smooth model inversion, and robust inversion. For this research, smooth model inversion or Occam's inversion was chosen. The smooth model inversion, which is based on Gaussian distribution of data errors, searches for the smoothest possible model that fits the data to an *a-priori* Chi-squared statistic. The whole inversion process can be summarized in the following few steps, shown in Figure 2.5.

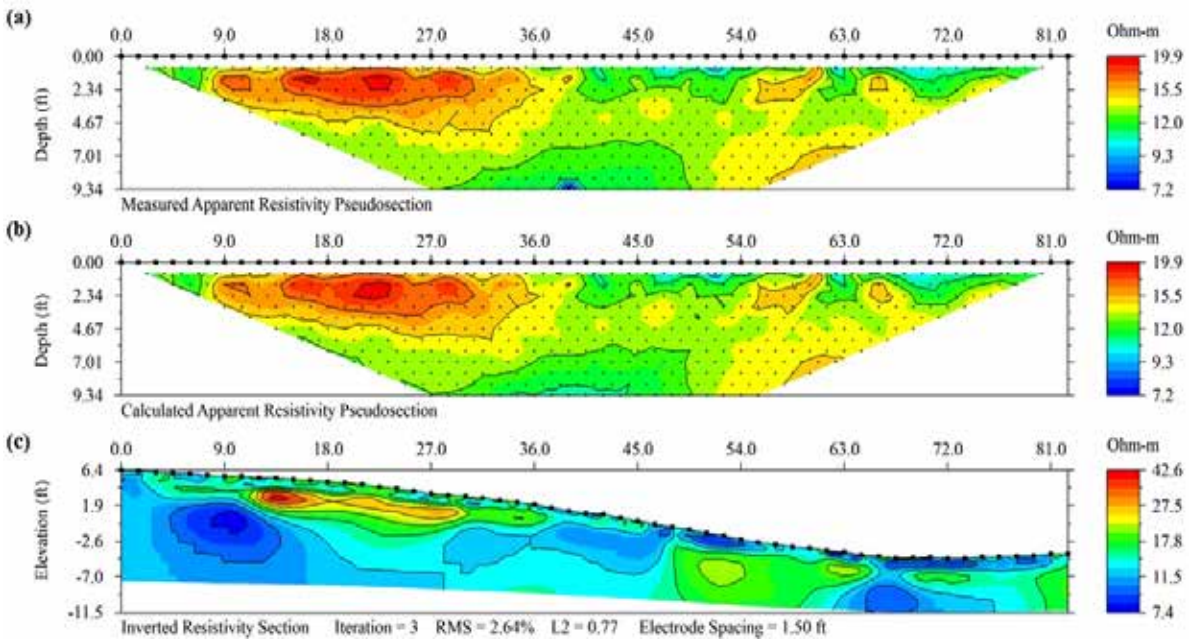

Figure 2.5: Results of an Electrical Resistivity Survey near a Kansas Highway 4 Bridge Abutment: (a) Measured Apparent Resistivity Pseudosection; (b) Calculated Apparent Resistivity Pseudosection; (c) Inverted Resistivity Section

After the ER survey and before starting the inversion process in EarthImager, only the distribution of measured apparent resistivity (ρ_a) is known (Figure 2.5a) based on the measured current (I), voltage difference (V), and electrode geometry (k). In the first iteration, the starting model is constructed based on the average apparent resistivity. Then, using the starting model, forward modeling is performed to predict the apparent resistivity distribution. At this stage, the root mean square (RMS) error between predicted (or calculated) and measured resistivity is determined using:

$$RMS = \sqrt{\frac{\sum_{i=1}^{N}\left(\frac{d_i^{Pred} - d_i^{Meas}}{d_i^{Meas}}\right)^2}{N}} \times 100\% \qquad \textbf{Equation 2.13}$$

Where:

N = total number of measurements,

d_i^{Pred} = predicted data at ith iteration, and

d_i^{Meas} = measured data at ith iteration.

Based on the data misfit, a linearized inversion is performed for a model update ($\Delta \mathbf{m}_k$). The resistivity model is updated and the new inverted resistivity distribution (Figure 2.5c) is obtained. Forward modeling using the updated model is performed in the next iteration to obtain calculated resistivity (Figure 2.5b). If the new RMS error (between measured and calculated resistivity) at this stage meets the desired criteria, then inversion stops; otherwise the process is repeated. The algorithm of forward modeling and inversion based on the measured apparent resistivity and initial resistivity model is given in Figure 2.6.

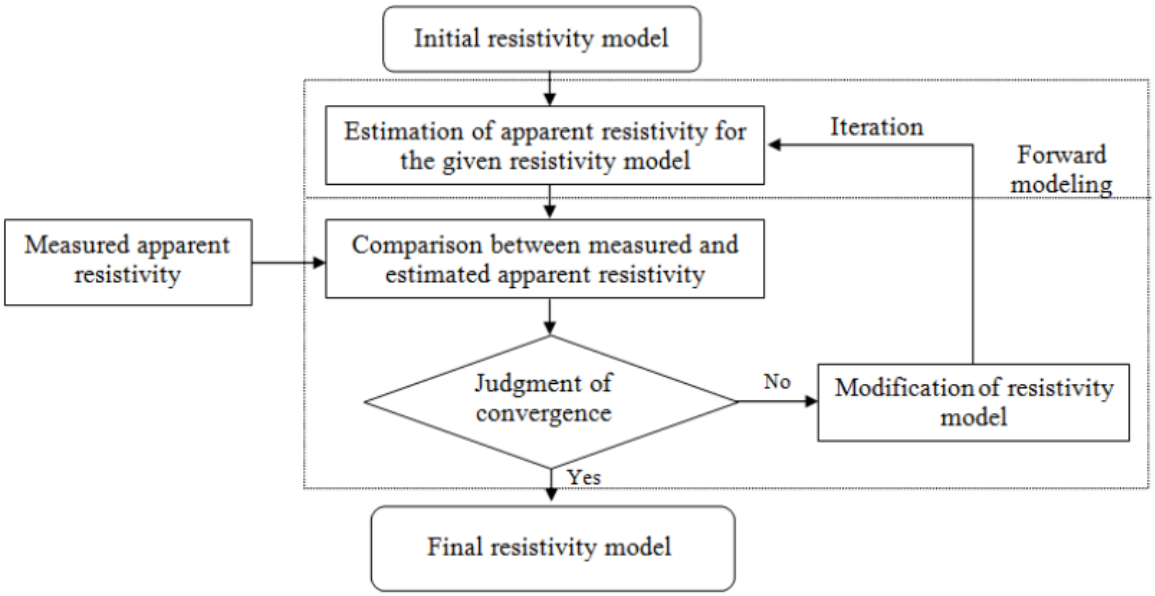

Figure 2.6: Algorithm of Forward Modeling and Data Inversion
Source: Arjwech (2011)

This chapter highlighted that there are many mutual factors such as: soil type, water content, plasticity index, unit weight of soil, and temperature that affect both erosion and electrical resistivity of soils. Despite this no direct attempts were found in the literature to correlate erosion rate with the electrical resistivity of soil, which is the main objective for this research.

Chapter 3: Methodology

To correlate the erosion potential of soil with electrical resistivity, samples were collected from 15 bridge sites that were selected by KDOT. Electrical resistivity (ER) surveys were also conducted at the bridge sites. Erosion tests, soil classification, and analysis of the ER survey were done in the KSU Geotechnical Laboratory. The overall methodology is shown in the following diagram in Figure 3.1.

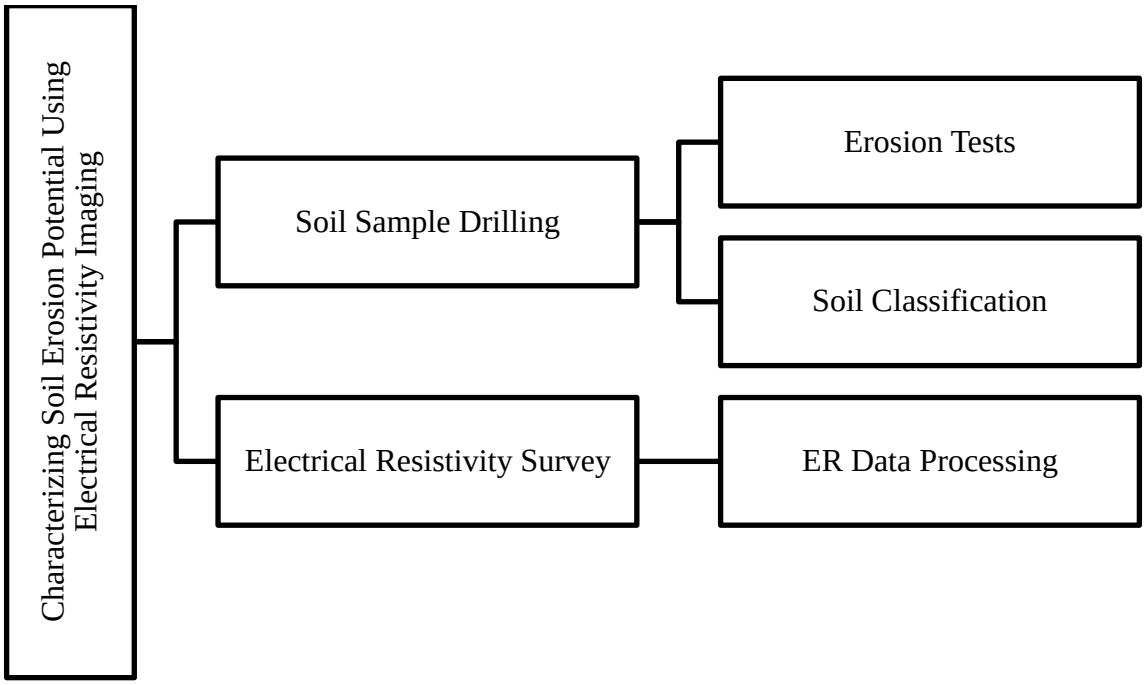

Figure 3.1: Flow Diagram of the Research Methodology

3.1 Experimental Sites

KDOT selected 15 sites around Kansas for this study. Depending on the accessibility, soil samples were collected as close to the stream as possible. ER surveys were conducted so that the borehole was in the center of the array; this also affected the sample drilling position. A short description of these sites is given in Table 3.1, and a map containing all the sites is presented in Figure 3.2 (Google Maps, 2016).

Table 3.1: Selected Sites for the Research

No.	Bridge ID**	County	KDOT District	KDOT Area Office	Highway	Scour Critical*	Crossing
1	043-0030	43-Jackson	1	4-Topeka	US-75	8	Straight Creek
2	058-0008	58-Marshall	1	1-Horton	US-36	3	NF Black Vermillion River Drg.
3	058-0025	58-Marshall	1	5-Wamego	K-9	3	Robidoux Creek
4	007-0013	7-Brown	1	1-Horton	US-73 (US-159)	3	Walnut Creek
5	015-0005	15-Cloud	2	2-Mankato	US-24	3	Cris Creek
6	085-0108	85-Saline	2	4-Ellsworth	K-4	3	Dry Creek
7	085-0146	85-Saline	2	4-Ellsworth	K-4	3	East Dry Creek
8	011-0025	11-Cherokee	4	4-Pittsburg	US-166	3	Neosho River Drainage
9	011-0027	11-Cherokee	4	4-Pittsburg	US-166	3	Neosho River Drainage
10	016-0041	16-Coffey	4	1-Iola	K-58	3	Neosho River Drainage
11	019-0056	19-Crawford	4	4-Pittsburg	K-126	3	East Cow Creek
12	050-0067	50-Labette	4	4-Pittsburg	US-400	3	Hickory creek
13	050-0048	50-Labette	4	4-Pittsburg	US-160	3	Neosho River Drainage
14	054-0030	54-Linn	4	2-Garnett	US-69 Northbound	3	Big Sugar Creek
15	006-0005	6-Bourbon	4	1-Iola	US-54 (US-69)	3	Marmaton Creek

Notes:

*A value of 4 or less indicates a scour critical bridge

**Bridge ID = County Number-Bridge Serial Number

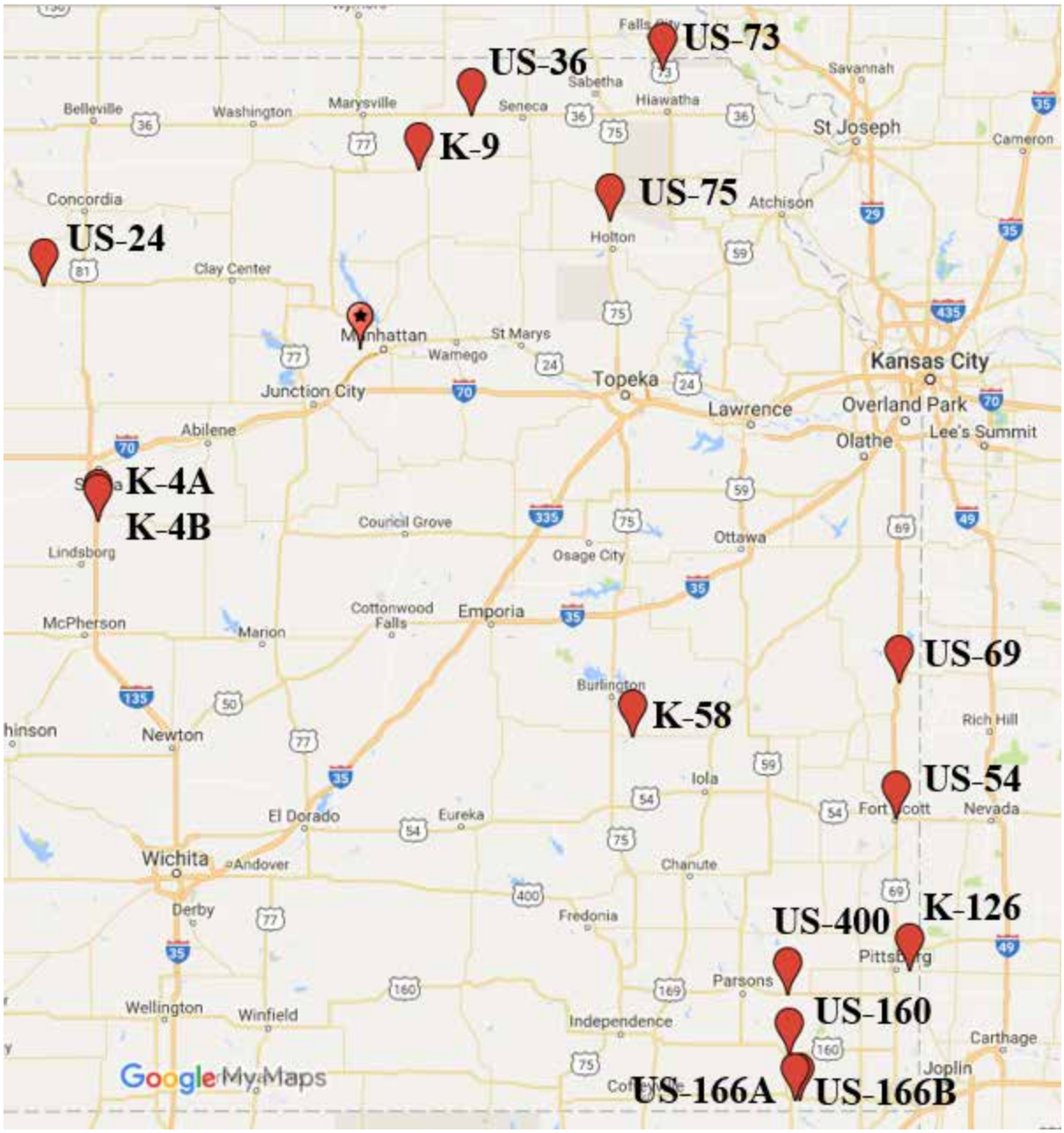

Figure 3.2: Map Containing Research Sites
Source: Google Maps (2016)

3.1.1 Soil Sampling

Thin-walled Shelby tubes were used following ASTM Standard D1587 (2015) to collect undisturbed soil samples at each bridge site. The tubes were 3.5 inches (88.9 mm) in diameter and 36 inches (914.4 mm) long. Five 2 ft (609.6 mm) long samples were collected at each of the

15 sites at a fixed drilling position. As a result, the total drilling depth was approximately 10 ft (3.1 m) at every site. The drilling operations were conducted by KDOT. Prior to drilling, one of the constraints was to find the optimal location for the borehole using the following criteria:

1. Engineered fills are often used to construct embankments near bridge abutments and pavement. Therefore, drilling was not performed close to the pavement or bridge abutment so that the collected samples represented the native geology of the site.
2. Approximately 41 ft (12.5 m) of accessible land was required on either side of the potential borehole. This length was required for half of the ER survey line so the borehole could be in the middle.
3. Prior investigations were required to verify there were no utility lines or fiber optic cables underneath the soil.

Once these criteria were met, the drill rig was moved to the selected drilling position (Figure 3.3). Loose material and vegetative cover were removed from the center of the casing to avoid sample disturbance. The expected sample recovery was marked on the Shelby tube and the sampler was advanced without rotation by pushing the tube to the marked point. To increase the sample recovery, a minimum 10-minute delay was applied before withdrawing the tube. This delay ensured enough skin friction was achieved between the soil and tube. Special care was taken to minimize sample disturbance. For example, especially for highly plastic soils, the Shelby tube was slowly rotated to shear the sample at the bottom and maximize recovery.

Sample recovery and compressive soil strength of the sample were measured using a measuring tape and pocket penetrometer respectively. A field log was also recorded at the time of the subsurface exploration which included the name of the project, location, sampling equipment, name of KDOT drillers and engineers, sample number, the depth of the retained sample, and the length of the push and recovery. ASTM Standard D4220 (2014) was followed for preserving and transporting soil samples to maintain the in situ conditions for erosion testing. After sampling and measuring the sample recovery, both ends of the Shelby tube were sealed using plastic end-caps. To provide for more protection to preserve the in-situ moisture content, duct tape was used at both ends and the whole tube was wrapped using plastic wrap. Samples

were labeled with the bridge number and sampling depth. If the ER survey was not conducted on the same day due to the limitations of the drilling schedule, the borehole location was marked with respect to at least two permanent objects. Samples were stored in a 100% humidity-controlled room at Kansas State University until they were taken to the lab for erosion tests. The samples were designated according to their highway name and the order of sampling. For example, the top sample from US-400 site was designated as US-400 #1. Moreover, if there was more than one bridge site on a single highway, the sites were differentiated using letters ‘A’ and ‘B.’

Figure 3.3: (a) Sample Drilling with the Drill Rig; (b) Close View of Drilling

3.1.2 Erosion Testing

The soil erosion rate was measured in an Erosion Function Apparatus (EFA). The length of the piston rod in the EFA is such that it allows a maximum length of 16 inches (406.4 mm) of sample to be tested. For this reason, Shelby tubes containing the sample were cut and approximately 15 inches (381 mm) was used for the erosion test. The rest of the sample was used for soil water content and classification. The water temperature during each EFA test was maintained between 59±4°F (15±2 °C) by continuous filling and sump pumping of the water reservoir with cold tap water. Soil samples were tested at room temperature, 68 °F (20 °C).

The goal was to test each sample under six different velocities in the EFA. The range of velocities chosen for each sample varied depending on the sample type. The range of velocities

for samples that had a large amount of fines and high plasticity was typically 3.3 to 19.7 ft/s (1.00 to 6.00 m/s; i.e., 3.3, 6.6, 9.8, 13.1, 16.4, and 19.7 ft/s [1.00, 2.00, 3.00, 4.00, 5.00, and 6.00 m/s]). Samples with a large amount of coarse particles were tested from 1.3 to 4.3 ft/s (0.30 to 1.30 m/s; i.e., 1.3, 1.6, 2.5, 3.0, 3.6, and 9.8 ft/s [0.30, 0.50, 0.75, 0.90, 1.10, 1.30 m/s]). The lower velocities of coarse samples ensured enough data points could be measured under different velocities before running out of sample.

The soil moisture content was measured before the EFA test according to ASTM Standard D2216 (2010). Initially the sample was placed on the platform over the piston head and the outside of the tube was tightened with a bracket attached to the platform. This ensured that only the soil moved when the piston was pushed to extrude the sample (Figure 3.4a). The platform was lifted so that the top of the tube (and sample) were flush with the bottom of the flume (Figure 3.4b). Temperature and velocity of water were measured by a temperature sensor and a flowmeter respectively and recorded with time. When erosion occurred, the sample was extruded using the motor controlled piston so that the soil sample remained flush with the bottom of the flume.

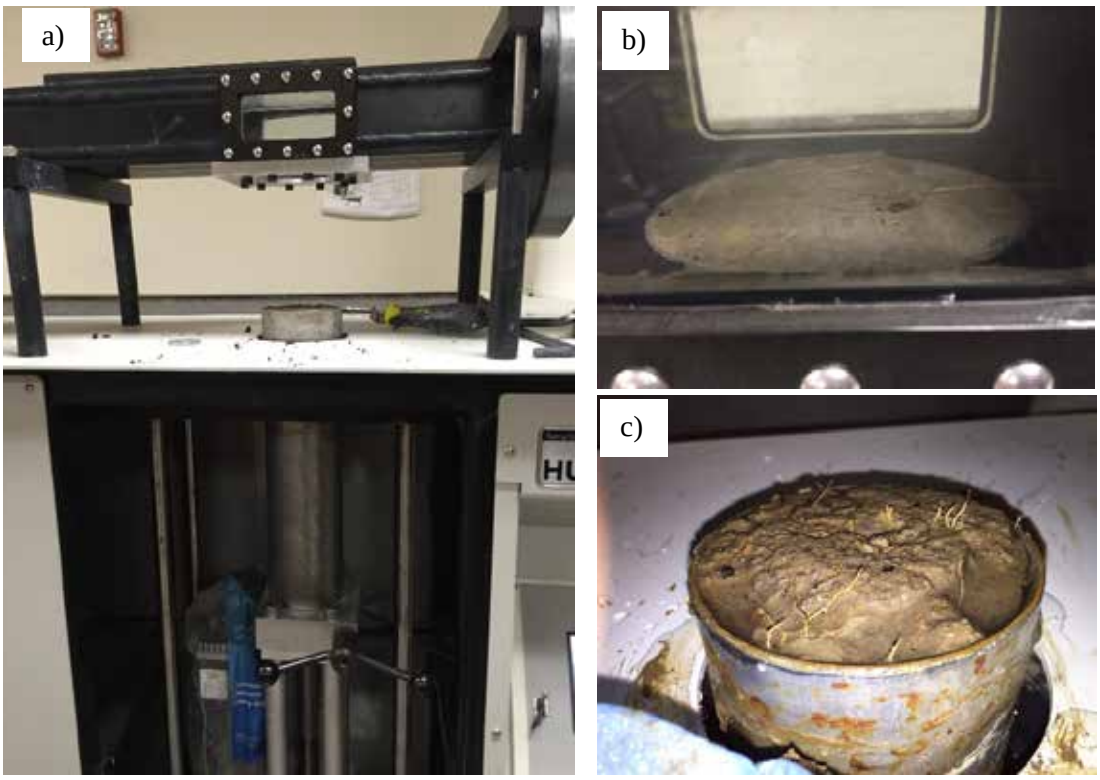

Figure 3.4: EFA Testing: (a) Placement of the Sample on Piston Head; (b) Trimmed Sample in Flush with Flume Bottom (Before the Test); (c) Sample with Rough Surface (After the Test)

Ideally, each test was conducted for 60 mins under each velocity. However, for highly erodible soils, the duration of test under each velocity was reduced to 30 mins or less to ensure enough sample remained for testing at additional velocities. The rate of erosion was obtained by dividing the total amount of erosion by the duration of the test. This process was repeated for each velocity. As mentioned in Chapter 2, in the equation for calculating shear stress τ (lb/ft^2 [N/m^2]; Equation 2.5), there is a term called the friction factor f which is obtained from the Moody chart (Munson, Young, & Okiishi, 1990), shown in Figure 3.5. The friction factor f is a function of pipe Reynolds number and relative roughness. Reynold's number, R is calculated using:

$$R = \frac{VD}{\nu}$$ **Equation 3.1**

Where:

V is the water velocity,

D is the pipe diameter,

υ is the kinematic viscosity of water (1.1 x 10^{-5} ft^2/s at 68°F [10^{-6} m^2/s at 20 °C]).

Again, relative roughness is calculated from the ratio, ε/d; where, ε is the average height of roughness elements of the eroding surface of the sample, and d is diameter of the sample. For the rectangular cross section of the flume, D is taken as the hydraulic diameter $D = 4A/P$; where, A is the cross-sectional area; P is the wetted perimeter; and 4 is a factor to convert the hydraulic diameter of the flume to the diameter of a circular pipe.

The accuracy of the shear stress calculation depends on the accurate measurement of the relative roughness of the eroding surface. After testing under each velocity, the plain eroding surface becomes irregular and rough (Figure 3.4c) because erosion does not occur homogeneously along the surface. For calculating the average height of the roughness, ϵ, several measurements of the height of the individual roughness elements and their corresponding areas were taken so that:

$$\tau_0 = \sum_{i=1}^{n} \frac{h_i A_i}{A}$$ **Equation 3.2**

Where:

h_i , A_i are the height and corresponding area of i-th roughness element measured by calipers;

n is the number of roughness elements; and

A is the cross-sectional area of the sample.

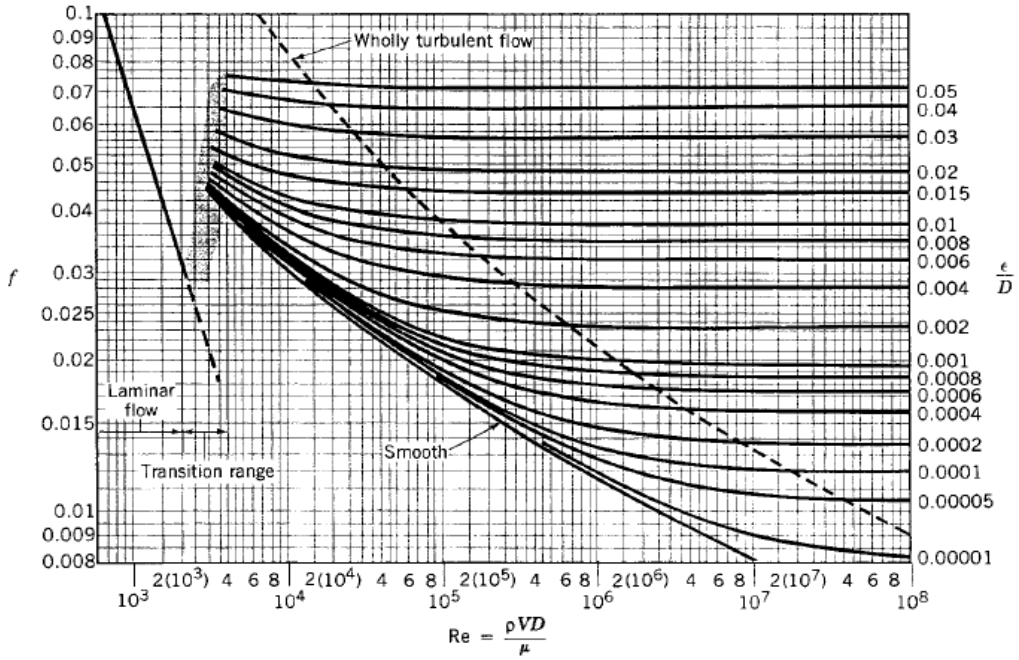

Figure 3.5: Moody Chart
Source: Munson et al. (1990)

3.1.3 Soil Classification

The EFA test samples were classified using Unified Soil Classification System (USCS). ASTM Standards C117 (2013) and C136 (2014) were followed for wet and dry sieving respectively; while ASTM D422 (2007) was followed for the hydrometer analysis. The soil samples were dried in the oven at approximately 220°F (105 °C) for 24 hours. The aggregation of the dried sample was broken by grinding it with a rubber covered pestle in a mortar. Approximately 500 g of each sample was used for sieve analysis. At first, the sample was washed through a #200 sieve. Then, the portion retained on #200 were left for drying in the oven at 220°F (105 °C) for 24 hours; after drying they were dry sieved using the sieves recommended by ASTM Standard C136. The hydrometer analysis was conducted using the sample that passed through the #200 sieve. The mass retained on each sieve and hydrometer data were used to prepare grain size distribution curve. Although not needed for classification according to the USCS, the hydrometer analysis was conducted to obtain median grain size, d_{50}. Atterberg limits tests were conducted according to ASTM Standard D4318 (2010).

3.1.4 Electrical Resistivity Survey

ER data were collected using the 'SuperSting with Wi-Fi Eight-Channel Earth Resistivity, Induced Polarization and Self Potential Instrument for Geo-Electrical Tomography' (SuperSting) meter, manufactured by Advanced Geosciences Inc. (AGI). Powered by two 12V deep-cycle marine batteries, the SuperSting can take up to eight simultaneous voltage readings per single current injection, speeding up data acquisition. Each connecting cable has four electrodes on it and Kansas State has 14 cables allowing for 56 electrodes per survey. The electrodes were connected to metal stakes that were hammered into the ground to couple the electrodes to the subsurface. The metal stakes were 1.5 ft (46 cm) in length and 0.87 inches (2.2 cm) in diameter. The stakes were hammered as deep as possible into the ground to ensure contact for the injected current and measured voltage potential.

A command file was created in the computer and uploaded to the SuperSting prior to the ER survey. The command file provided all directions to the SuperSting regarding the sequence in which different electrodes should be used for current injection or measurement of voltage difference following the dipole-dipole array. The array type was selected considering vertical and lateral resolution, depth of investigation, and test duration. As mentioned previously, the total drilling length was approximately 10 ft (3.1 m) and the diameter of drilling was 3.5 inches (88.9 mm). As such, the primary intention of the ER investigation was to achieve higher vertical resolution than lateral resolution around the borehole. The dipole-dipole array was selected because it provided highest vertical and lateral resolution simultaneously. The command file was created for the dipole-dipole array and loaded on the SuperSting before going to each site. Simulation of the command file showed that approximate depth of investigation was $10ES$ for the dipole-dipole array, where ES is the electrode spacing. Therefore, 1.5 ft (0.46 m) was chosen as the electrode spacing in the site, so the intended depth of 10 ft (3.1 m) was imaged with optimum resolution.

With 56 electrodes and a spacing of 1.5 ft (0.46 m), the length of survey line was 82.5 ft (25.2 m). The survey line was selected in such a way that the position of the borehole was in the center of the ER survey line (between the 28^{th} and 29^{th} electrode). This was also selected because, in the ER survey, more data points are in the central region of the survey line and

consequently the highest resolution is obtained in that region. The cables adjacent to the 28th and 29th electrodes were connected to the SuperSting for data acquisition (Figure 3.6b).

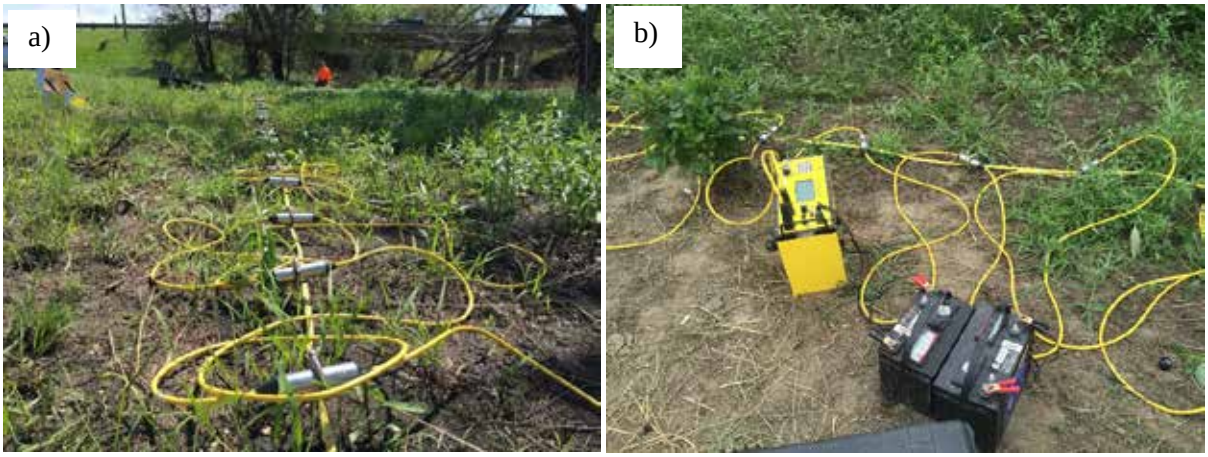

Figure 3.6: (a) ER Survey Line; (b) 28th and 29th Electrodes Connected to the SuperSting

Once the setup was complete, the contact resistance test was performed before the actual ER survey. The contact resistance test indicated if the surface area of the stakes was getting enough contact into the ground. A higher value indicated that current was not flowing into the ground with ease, and this may produce noisy data. The contact resistance test also verified that all cables were connected to each other and that the electrodes were attached to the steel stakes. If the LCD screen of the SuperSting shows an error "HVOVL," that indicated poor contact between the stake and the ground. Since most of the sites were fine-grained soils, contact with the ground was not an issue. The second error, "INOV" indicated that there was improper connection of the electrode cables. The values of contact resistances found in all sites were in the range of 1 to 500 Ω. Contact resistance values less than 40,000 Ω ensures good contact between electrode and ground, meaning the maximum electric current could be injected into the ground, reducing noise in the survey.

The actual ER survey was conducted following the contact resistance test. In this research, the runtime of each ER survey using dipole-dipole array was around 32 minutes. This time was utilized for measuring the relative elevations of each electrodes using a total station and a survey rod. This information was required to produce the terrain file. All data were downloaded from the SuperSting and processed at Kansas State University.

Chapter 4: Results and Analysis

ER surveys were conducted as close to the stream as possible depending on the site conditions for all 15 sites. Five 2 ft (0.6 m) long soil samples were collected at each site with a drill rig continuously pushing from the surface to 10 ft (3.1 m) using 3.5 inch (88.9 mm) diameter thin-walled Shelby tubes. Since five samples were collected from each site, a total of 75 samples were available for running erosion tests in the EFA. However, six of the Shelby tubes from different sites were bent during sampling and could not be used for erosion tests. Also one of the samples from the K-9 site had minimal recovery which only allowed for two erosion tests from a single sample. Ultimately, 70 samples were used for the erosion tests. After conducting the erosion tests, the remaining soil of each sample was classified. Although all test results from 15 sites are used for analysis, only test results of K-58 site are shown below as a typical site. All ER, EFA, and soil property data for each site are presented in Appendix A with GPS location.

4.1 Kansas Highway 58 Results

The K-58 site is located in Coffee County of eastern Kansas. The K-58 bridge crosses one of the Neosho river drainages; no water-flow was observed during the ER survey on October 22, 2015. The dipole-dipole array with 56 electrodes and 1.5 ft (0.46 m) center-to-center spacing was used, shown in Figure 4.1.

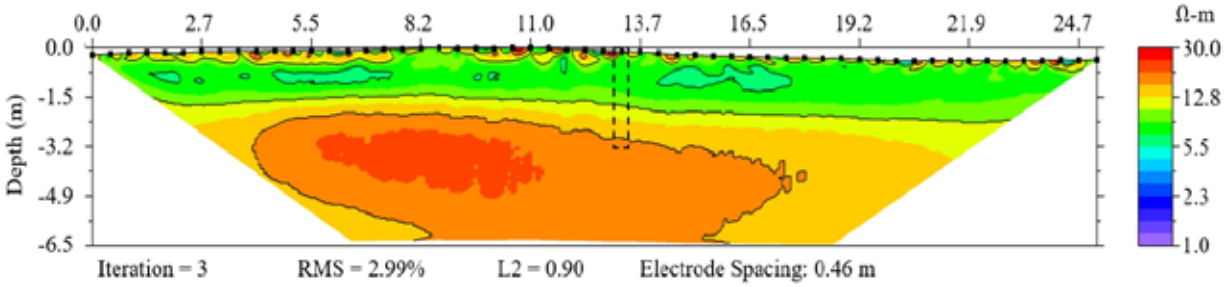

Figure 4.1: Subsurface Inverted ER Distribution of K-58 Site

The RMS error for the inversion was 2.99% and L2 norm was 0.90, which indicate good agreement of the measured and calculated resistivity. All inversion statistics in this research had an RMS error below 3% and L2 norm less than one. These boundaries were set for data quality

specifications to ensure minimum error in the inversion process. The dashed line rectangle in Figure 4.1 shows the location of borehole corresponding to the five samples from K-58. This two-dimensional distribution of ER is a contour diagram of ER constructed of thousands of elements in the subsurface. Each sample was 2 ft (0.6 m) long and 3.5 inches (88.9 mm) in diameter. In the ER profile, this area corresponded to 16 elements of resistivity. The average ER from these 16 elements was used to calculate the ER of each sample. The ER measurements of the five samples from K-58 were between 8.7 to 18.5 Ω-m and are shown versus the mid-depth of the samples in Figure 4.2b.

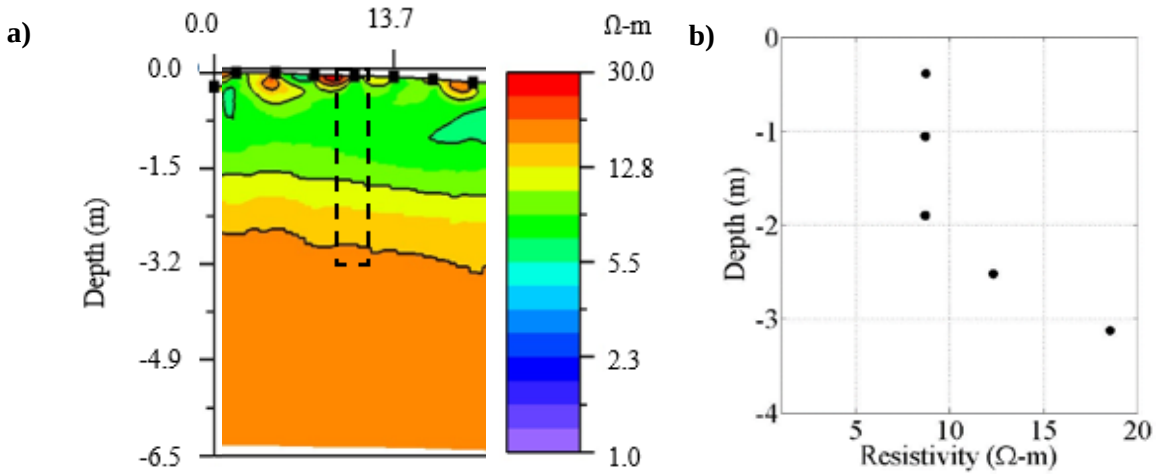

Figure 4.2: (a) Cropped ER Distribution near Sampling Location of K-58, (b) Average ER for Each Sample

Each erosion test was performed under six different water velocities and samples were allowed to erode for 1 hour under each velocity. Equation 2.5 was used to calculate the shear stress. The erosion results of K-58 are shown in Table 4.1.

Table 4.1: K-58 Erosion Test Results

Sample	Erosion Test Results							Critical Shear Stress, lb/ft^2 (N/m^2)
K-58 #1	Water Velocity, ft/s (m/s)	3.28 (1.00)	6.56 (2.00)	9.84 (3.00)	11.5 (3.50)	13.1 (4.00)	-	0.34 (16.3)
	Shear Stress, lb/ft^2 (N/m^2)	0.06 (2.90)	0.42 (20.0)	0.85 (40.5)	1.05 (50.5)	1.36 (65.0)	-	
	Erosion Rate, in/hr (mm/hr)	0.00 (0.00)	0.07 (1.80)	0.37 (9.30)	0.43 (10.8)	0.51 (12.9)	-	
K-58 #2	Water Velocity, ft/s (m/s)	3.28 (1.00)	6.56 (2.00)	9.84 (3.00)	13.1 (4.00)	16.4 (5.00)	19.7 (6.00)	1.00 (46.3)
	Shear Stress, lb/ft^2 (N/m^2)	0.06 (3.00)	0.24 (11.3)	0.55 (26.4)	0.99 (47.6)	2.02 (96.9)	4.04 (194)	
	Erosion Rate, in/hr (mm/hr)	0.00 (0.00)	0.00 (0.00)	0.00 (0.00)	0.02 (0.50)	0.63 (16.0)	5.31 (135)	
K-58 #3	Water Velocity, ft/s (m/s)	3.28 (1.00)	6.56 (2.00)	9.84 (3.00)	13.1 (4.00)	16.4 (5.00)	19.7 (6.00)	0.44 (21.2)
	Shear Stress, lb/ft^2 (N/m^2)	0.08 (3.7)	0.28 (13.3)	0.48 (23.1)	1.07 (51.0)	2.50 (120.0)	2.91 (140.0)	
	Erosion Rate, in/hr (mm/hr)	0.00 (0.00)	0.00 (0.00)	0.02 (0.50)	0.30 (7.50)	0.75 (19.0)	1.14 (29.0)	
K-58 #4	Water Velocity, ft/s (m/s)	3.28 (1.00)	6.56 (2.00)	9.84 (3.00)	13.1 (4.00)	16.4 (5.00)	19.7 (6.00)	0.85 (40.8)
	Shear Stress, lb/ft^2 (N/m^2)	0.07 (3.30)	0.25 (12.2)	0.49 (23.6)	0.96 (46.0)	2.05 (98.1)	2.60 (125)	
	Erosion Rate, in/hr (mm/hr)	0.00 (0.00)	0.00 (0.00)	0.00 (0.00)	0.02 (0.50)	0.04 (1.00)	0.12 (3.00)	
K-58 #5	Water Velocity, ft/s (m/s)	3.28 (1.00)	6.56 (2.00)	9.84 (3.00)	13.1 (4.00)	16.4 (5.00)	19.7 (6.00)	0.64 (30.6)
	Shear Stress, lb/ft^2 (N/m^2)	0.07 (3.30)	0.25 (11.9)	0.53 (25.3)	0.84 (40.0)	2.28 (109)	3.01 (144)	
	Erosion Rate, in/hr (mm/hr)	0.00 (0.00)	0.00 (0.00)	0.00 (0.00)	0.02 (0.50)	0.08 (2.00)	0.22 (5.50)	

Table 4.1 shows that, Sample #2 through #5 were tested under a maximum velocity of 19.7 ft/s (6 m/s). However, Sample #1 was comparatively more erodible, hence it was tested up to 13.1 ft/s (4 m/s). The high erodibility of Sample #1 is also evident by its lower critical shear stress, 0.34 lb/ft^2 (16.3 N/m^2). These results were compiled using HEC-18 (Arneson, Zevenbergen, Lagasse, & Clopper, 2012) erodibility categorizing plot in Figure 4.3. Note that

this a logarithmic plot. Points below critical shear stress have zero erosion rate and therefore are not visible in this plot.

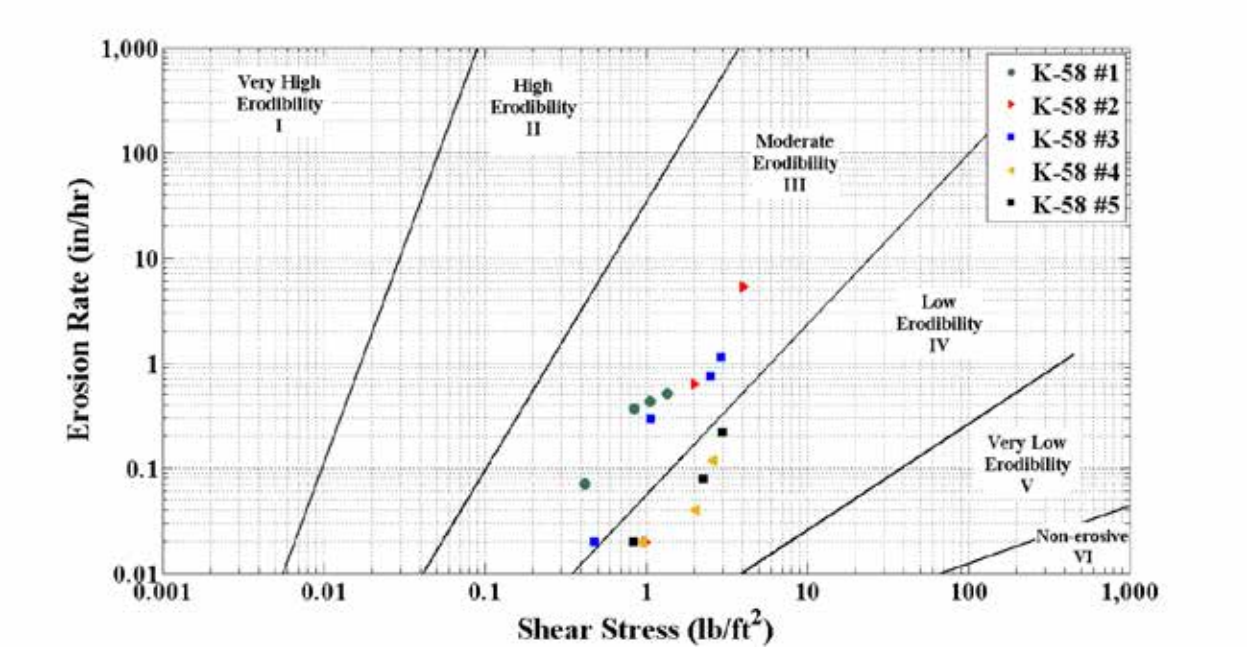

Figure 4.3: Erosion Rate versus Shear Stress for Five Samples of K-58

Figure 4.3 shows that Sample #1 was comparatively more erodible than the rest of the samples at the site. Note that all points from these samples were in the low to moderate erodibility zones according to HEC-18 erodibility categorization. The remaining samples were used for soil classification and determining soil parameters. Table 4.2 shows the soil parameters and the USCS classification of the five samples from K-58.

Table 4.2: Soil Parameters and Classification of K-58 Samples

Sample Designation	Water Content (%)	Percent Finer than 0.075 mm (%)	Median Grain Size (mm)	LL	PL	PI	USCS Classification
K-58 #1	33	99	0.0012	80	28	52	CH
K-58 #2	32	99	0.0014	72	22	50	CH
K-58 #3	26	99	0.0102	43	16	27	CL
K-58 #4	28	99	0.0070	44	14	30	CL
K-58 #5	30	98	0.0145	41	15	26	CL

Table 4.2 shows the water content (prior to erosion tests), w; percent finer than 0.075 mm, F; median grain size, d_{50} (mm); liquid limit (LL); plastic limit (PL); plasticity index (PI); and USCS classifications of the five samples of K-58. The samples classified as low and high plasticity clays. The median grain size ranged between 0.0012 to 0.0145 mm and the plasticity indexes ranged between 26 and 52. These results were in agreement with their low ER values (8.7 to 18.5 Ω-m).

4.2 Analysis of the Erosion Characteristics Integrating All Sites

All of the sites in this study were distributed throughout eastern Kansas. As previously mentioned, although 75 samples were collected from 15 sites (five from each), six of them were damaged and one extra sample was collected at a site. Results of erosion tests of 70 samples from the 15 sites are shown in Figure 4.4.

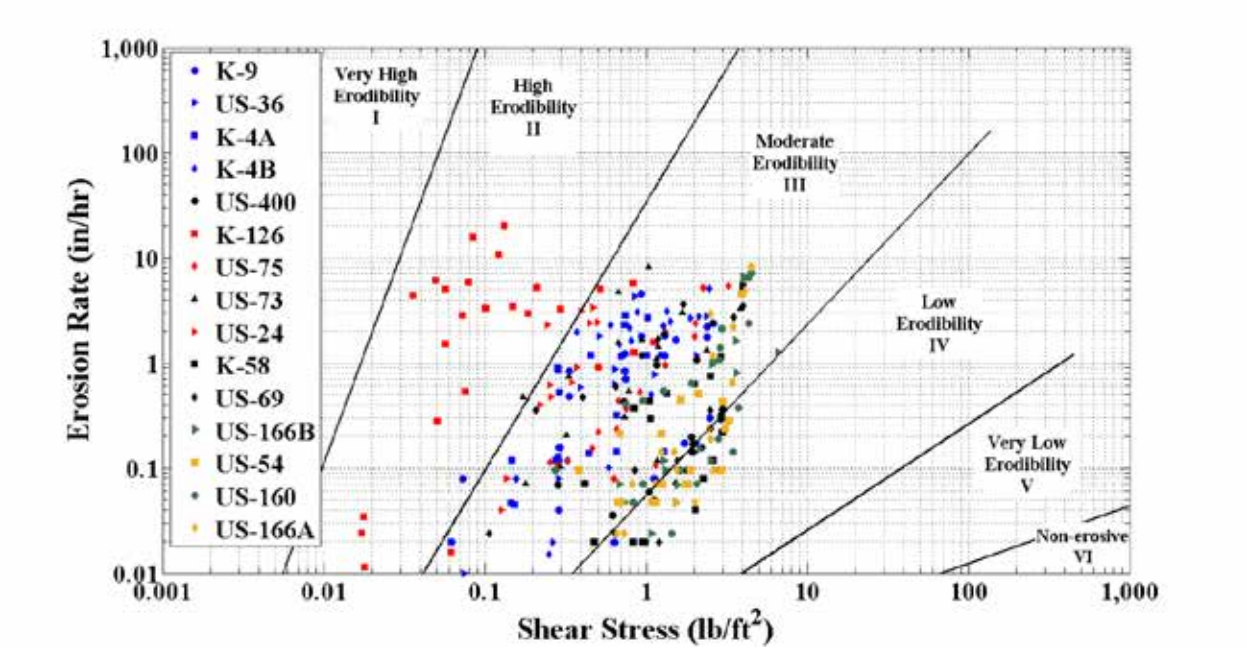

Figure 4.4: Erosion Rate versus Shear Stress for 15 Sites

Most of the soil samples (74%) in this study were classified as moderate erodibility. Points falling in the low erodibility zones were mostly from US-400, US-58, US-69, US-166B, US-54, and US-166A. K-126 samples alone contributed to the most of the points falling in the

high erodibility zone. The lowest erodibility sites (US-400, US-58, US-69, US-166B, US-54, and US-166A) and the highest erodibility site (K-126) were all in southeast Kansas. A site such as K-126 may be given priority in any further bridge-scour monitoring by KDOT because it was highly erodible compared to the other sites.

4.2.1 Effects of Index Properties on Erodibility

The plasticity indexes of all the samples were divided into five categories and plotted on the erodibility graph as shown in Figure 4.5. A total of 22 points fell in the high erodibility zone; of them, 19 points had plasticity indexes below 10. Again, among the points falling in the moderate erodibility zone, those having PI of 10 to 19 (shown with green dots) were more erosive (plotting closer to moderate-high erodibility boundary) than the other points corresponding to comparatively higher plasticity indexes. Bernhardt et al. (2011) also performed a similar analysis using plasticity indexes of the Mississippi River levee soils.

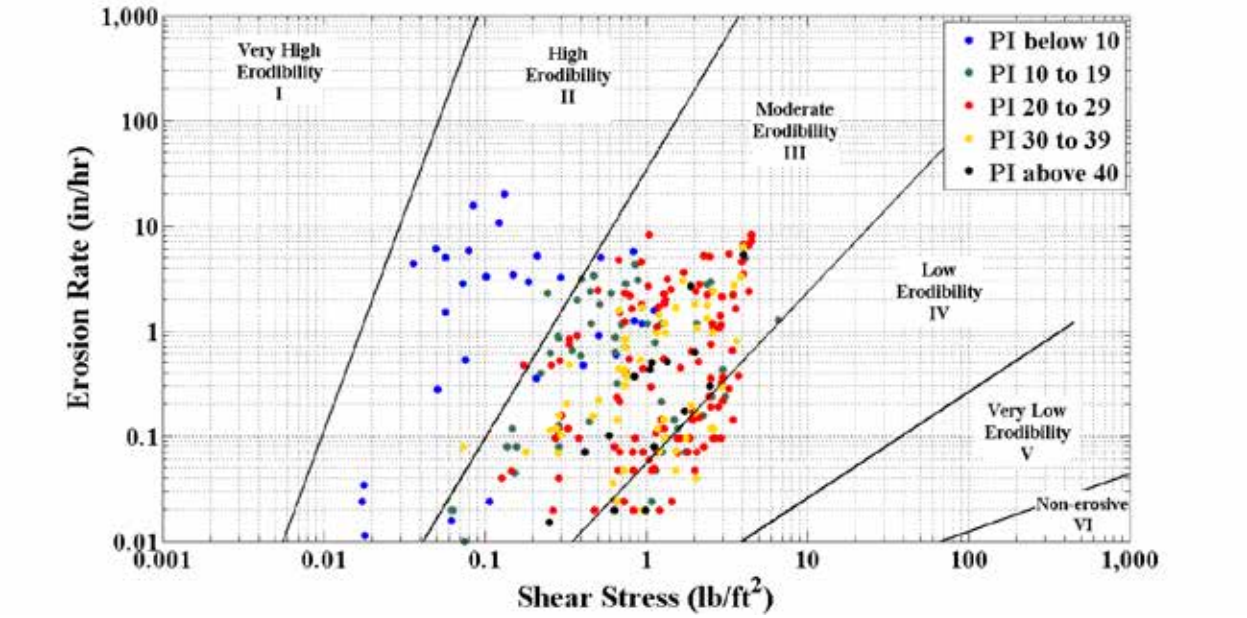

Figure 4.5: Erosion Rate versus Shear Stress for Varying Plasticity Index

4.2.2 Effects of Particle Size on Erodibility

Median grain size was calculated from each sample using the grain size distribution curve. Note that the samples from the first three sites of this project (K-9, US-36, and K-4B) were not sieved using the wet sieve method. The values of percent finer than #200 sieve were in the range of 50% to 60% for the samples from these three sites (using dry sieving only). Index properties of these samples were not in agreement with the previously obtained median grain sizes. As the samples were discarded after sieving, corrections could not be made to the median grain sizes of the samples from these three sites. Samples from the remaining 12 sites were sieved using both dry and wet sieving methods. Among the remaining 12 sites, only K-126 had coarse gained samples, with particles up to 1.9200 mm. The median grain sizes of the remaining sites' samples were between 0.0012 mm and 0.0310 mm. The median grain sizes of the 12 sites were divided into four categories to analyze the effect of grain size on erosion performance shown in Figure 4.6. Particles with larger median grain size were more erodible. Most of the points (19 out of 21) that showed high erodibility had median grain size above 0.025 mm. Moreover, the higher density of red dots near the moderate-high erodibility boundary indicates that the samples corresponding to median grain size of 0.017 to 0.024 mm were more erodible than the smaller particles.

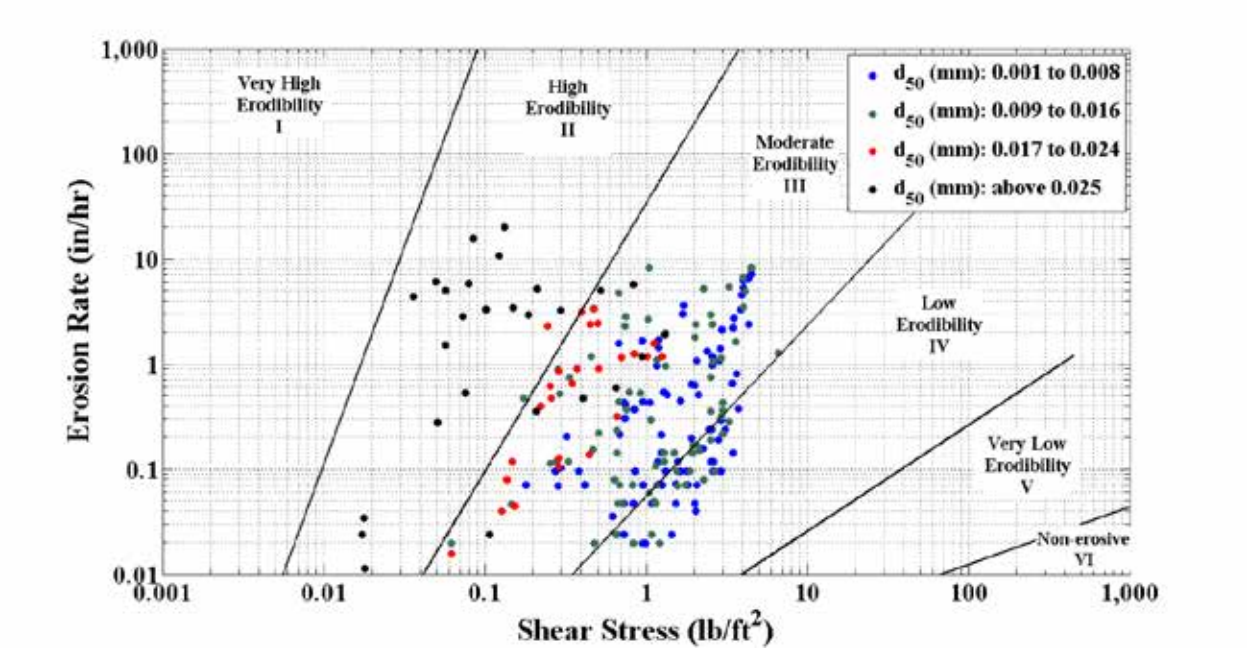

Figure 4.6: Erosion Rate versus Shear Stress for Varying Median Grain Size

4.2.3 Effects of Soil Classification on Erodibility

Erodibility categorizing graph was also utilized in terms of the USCS soil types of the samples. Soil classification gave six different types of soils for the samples collected from 15 sites. The results of the erosion tests with varying soil type are presented in Figure 4.7.

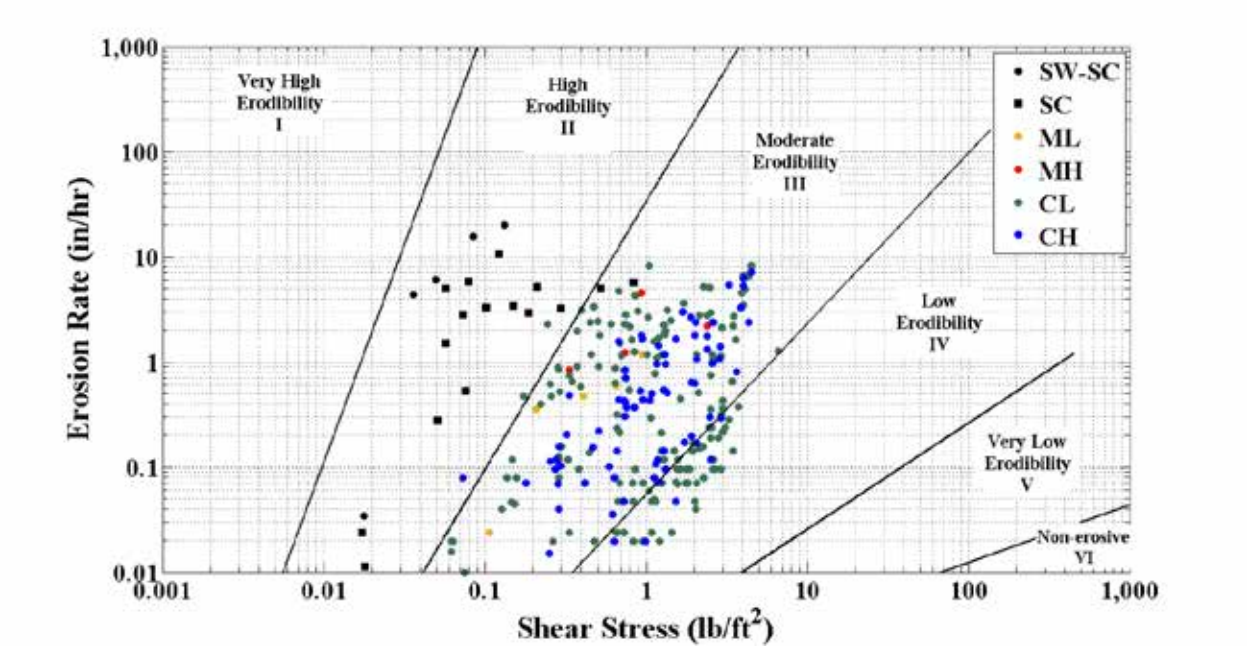

Figure 4.7: Erosion Rate versus Shear Stress for Varying Soil Type

It is evident from Figure 4.7 that soils classified as sand (SW-SC and SC) have mainly contributed to the points showing high erodibility. Two samples of K-9 were classified as highly plastic silts (MH) and one sample from US-69 was classified as low plastic silt (ML); all of these showed moderate erodibility (represented by the red and yellow dots). The remaining samples were classified either as low or high plastic clays (CL or CH) and were moderate and low erodibility. The density of the green dots (representing the CL) was more in the moderate-high erodibility boundary. This may indicate that CL samples were more erodible than CH samples (blue dots). The classification in Figure 4.7 highlights the need for more silty soils and sandy clays for a more robust analysis of fine-grained soils in Kansas. Briaud et al. (2011) included the corresponding soil types into the erodibility categorizing graph based on their previous erosion test results in EFA as shown in Figure 4.8. The classification results of this study were similar to those in Figure 4.8.

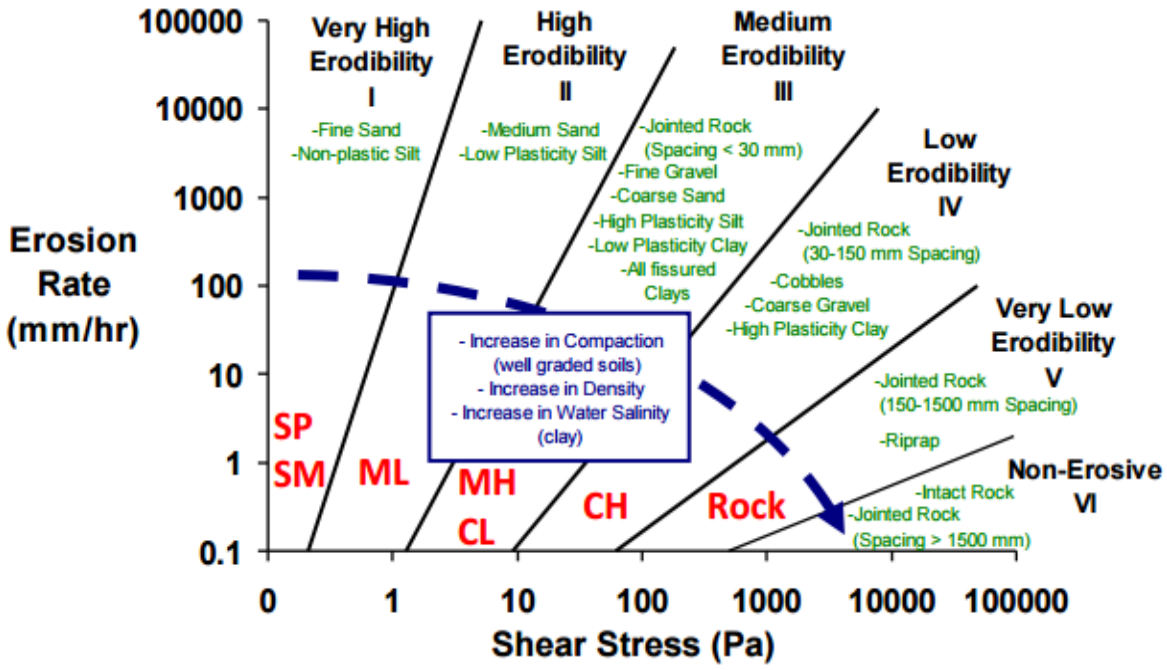

Figure 4.8: Erodibility Categories of Different Soil Types Based on Shear Stress
Source: Briaud et al. (2011)

4.2.4 Effects of Electrical Resistivity on Erodibility

Soil parameters such as median grain size, plasticity index, percent of fines, and water content have been used to characterize the erosion by previous researchers such as Hanson and Temple (2002), Clark and Wynn (2007), and Bernhardt et al. (2011). However, no evidence of using geophysical methods such as ER to describe soil erosion was found in literature. In this project, ER values of different samples varied from 6 Ω-m (K-9 #4, US-73 #1) to 328 Ω-m (K-126 #2). Erosion rate versus shear stress for varying ER is shown in Figure 4.9.

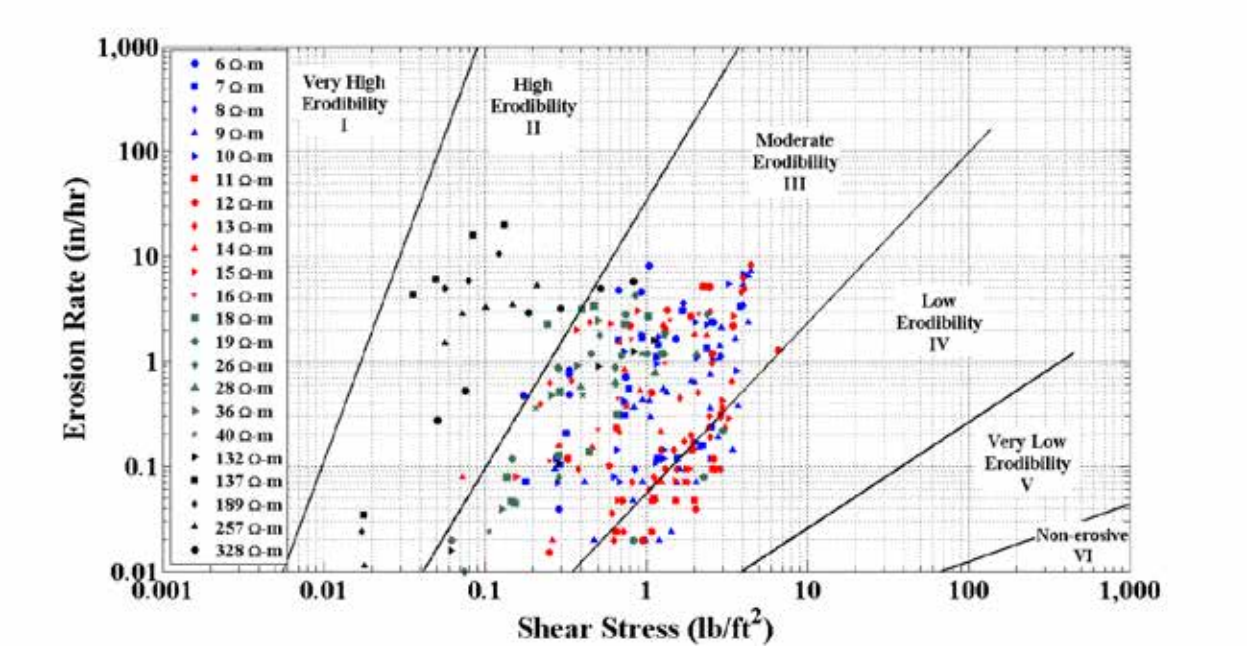

Figure 4.9: Erosion Rate versus Shear Stress for Varying ER

There were 22 different measured ERs from the 70 samples. A trend showing samples with higher ER values tended to be in the high erodibility category is shown in Figure 4.9. As such, ER values were divided in two ranges: below and above 100 Ω-m as shown in Figure 4.10 to improve the visualization of the effect of ER on erosion. In this study, 243 out of 269 of the points in the erodibility graph corresponded to ER of less than 100 Ω-m. When ER values were below 100 Ω-m, 98.8% (240 out of 243) points showed low to moderate erodibility. Again, when ER values were above 100 Ω-m, 73.1% (19 out of 26) points showed high erodibility. Figure 4.10 shows that ER survey can be used as a preliminary tool to prioritize scour critical bridges and eliminate time consuming erosion tests. In fact, only one site from this study, K-126, provided samples that had ER values over 100 Ω-m. Most of the samples from this site, although classified as sands, contained both fines and gravel. Visually it looked like a fine-grained soil but the ER survey identified the presence of gravel (as ER was more than 100 Ω-m) entrapped within the fines in the subsurface and later it showed high erodibility when tested. This highlights how ER can be used to predict the erodibility.

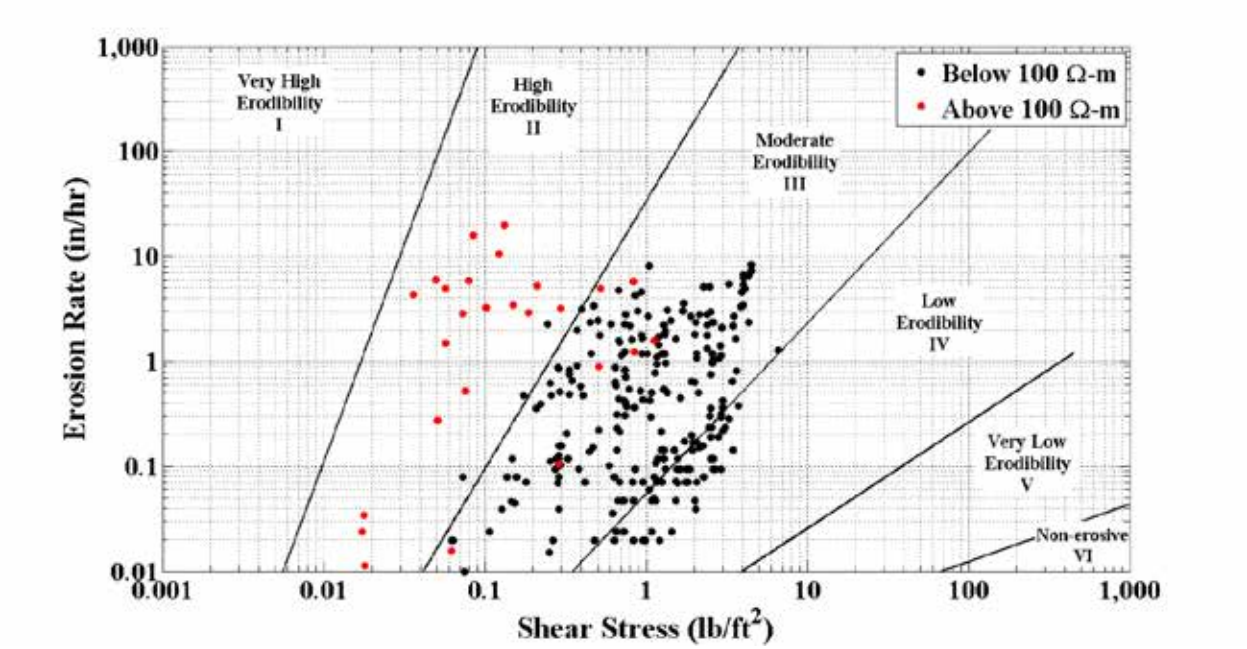

Figure 4.10: Erosion Rate versus Shear Stress for Two Ranges of ER

4.3 Predicting Critical Erosion

All 70 samples from 15 sites showed various erosion patterns. The majority of the samples started eroding in small particles at lower velocity (and corresponding shear stress) and as velocity was increased they eroded in soil blocks. Samples #2 through #5 from K-126 and #1 from US-69 had considerable amount of gravels and very low plasticity indexes. These samples started to erode at very low velocities (such as 1.3 ft/s [0.3 m/s]) and all soils finished eroding at very low maximum velocity (below 9.8 ft/s [3.0 m/s]). Furthermore, some samples (such as from K-58) with very high plasticity indices had very low erosion rates (less than 0.4 in/hr [10.0 mm/hr]) at a flow velocity as high as 19.7 ft/s (6 m/s). Although all the tests were velocity controlled, the corresponding shear stress was used for any analytical development. It is the shear stress exerted by the water on soil surface that actually causes the erosion. Different samples tested under the same velocity have different shear stress depending on the roughness of the erosion surface. The relationship between erosion rate and shear stress as shown in Figures 4.3 through 4.10 can take various shapes when plotted. For describing this relationship, critical shear stress is an important curve fitting parameter.

4.3.1 Predicting Critical Shear Stress Using Electrical Resistivity

For predicting critical shear stress, 65 samples from 14 sites were used for regression analysis and five samples from one site were used for validation. This research identified that ER may be used as a rapid tool for determining whether a bridge-site is vulnerable by using the HEC-18 erodibility categorizing graph to evaluate erosion potential. For analytical development, measured critical shear stresses of the 65 samples were plotted against the corresponding in-situ ER. When data were plotted, critical shear stress did not appear to vary linearly with ER and the linear relationship provided R^2 = 0.11. Various mathematical functions such as exponential, logarithmic, power, and polynomial relationship between the independent and dependent variables were iterated. Ultimately a power relationship provided the best fit to the data with R^2 = 0.52, and therefore, was selected. The relationship is presented in logarithmic scale in Figure 4.11.

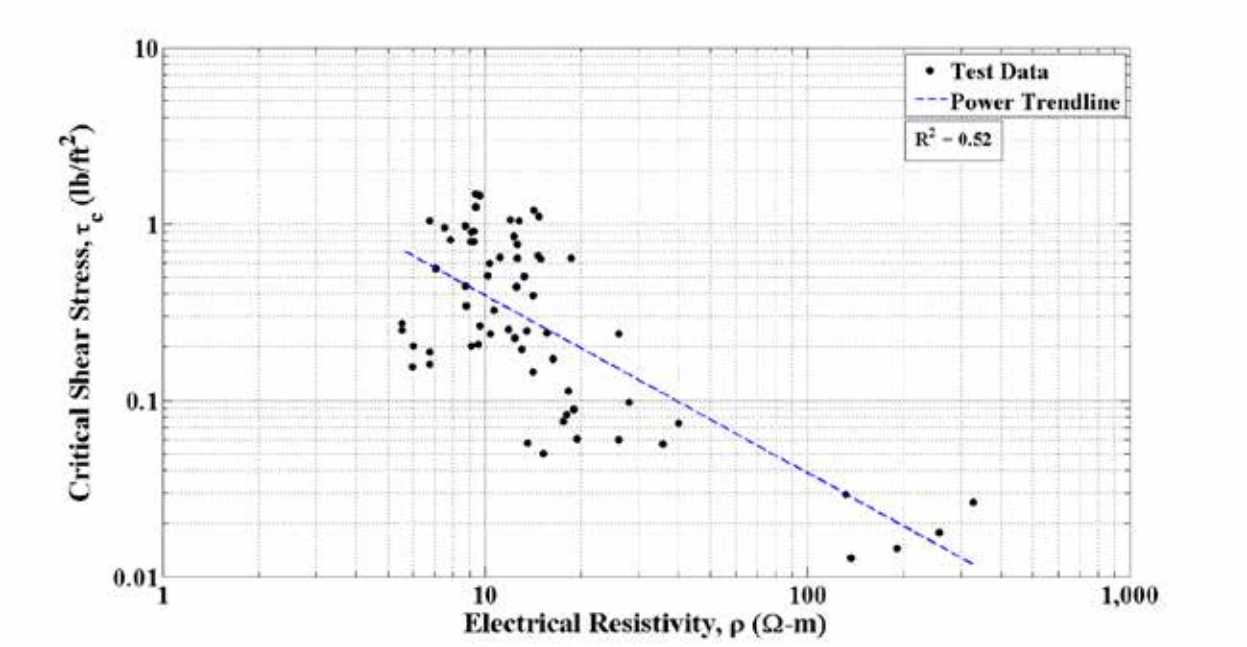

Figure 4.11: Critical Shear Stress versus Electrical Resistivity

As seen from Figure 4.11, critical shear stress decreased with increasing ER. The regression was performed in SAS™ software (SAS Institute Inc., 2014) and the equation to predict critical shear stress, τ_c (lb/ft^2 [Pa]) using ER is given as:

$$\tau_c = a\,\rho^{-1.007}$$ **Equation 4.1**

Where:

ρ is the ER of soil in Ω-m,

and a is the unit conversion constant, 3.998 in U.S. customary units and 191.435 in S.I.

Prior to this study, no evidence of predicting critical shear stress using ER was found in the literature. Although examples of predicting critical shear stress using other soil parameters can be found in the literature, the R^2 were very low and the datasets were small for those experiments. Per this research, an R^2 of 0.52 for 65 data sets shows that ER alone may be used to predict the critical shear stress.

4.3.2 Predicting Critical Shear Stress Using Median Grain Size

One advantage of this project was, although soil samples were predominantly fine-grained, a wide range of grain sizes were observed. This helped to obtain a relationship between critical shear stress and median grain size. Previous researchers have attempted to correlate critical shear stress and median grain size; however, they did not find a good correlation between these two parameters. For example, Kimiaghalam, Clark, and Ahmari (2016) obtained an R^2 of 0.11 when critical shear stresses were plotted against median grain sizes of 17 fine-grained samples in a linear scale. In this project, a linear relationship provided $R^2 = 0.10$. Several other models were investigated (such as exponential, logarithmic, and polynomial), but the power model provided the best fit among the data and R^2 was found 0.56.

Figure 4.12 shows that critical shear stress for erosion decreases with increasing median grain size. The predictive equation for critical shear stress, τ_c (lb/ft^2 [Pa]) from this power model was:

$$\tau_c = b\,d_{50}^{-0.676}$$ **Equation 4.2**

Where:

d_{50} is median grain size in mm, and

b is the unit conversion constant, 0.016 in U.S. customary units and 0.756 in S.I.

Note that this correlation does not include the median grain sizes of the samples from first three sites (K-9, US-36, and K-4B); so there were total 51 observations from remaining 11 sites used in the regression.

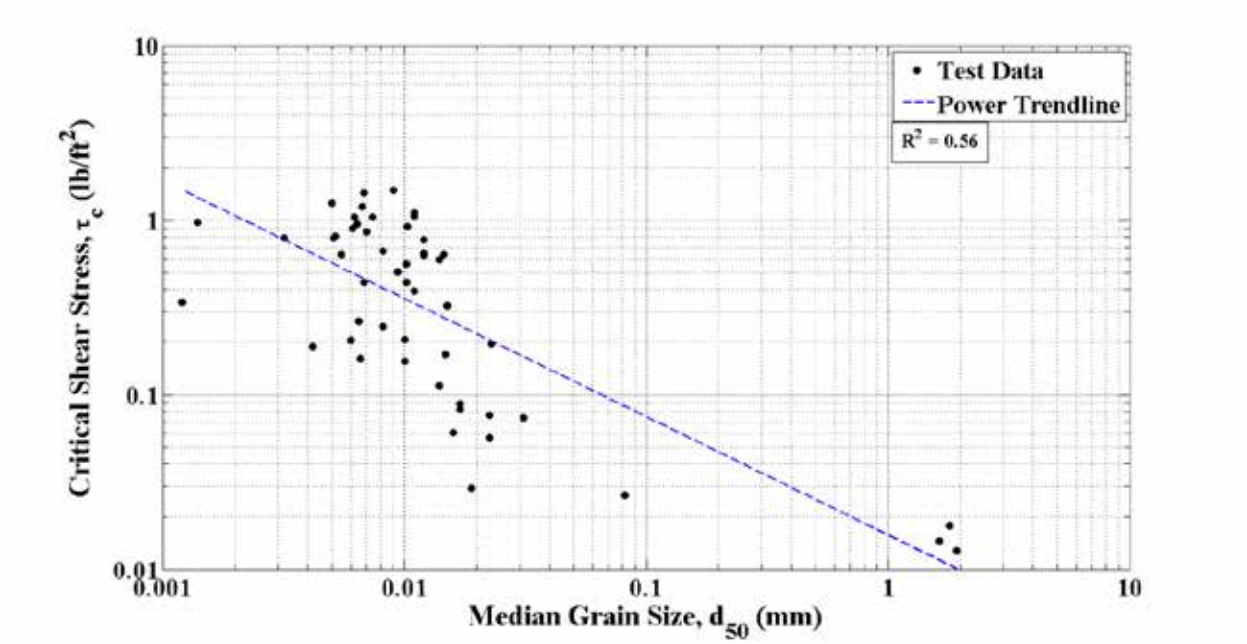

Figure 4.12: Critical Shear Stress versus Median Grain Size

4.3.3 Predicting Critical Shear Stress Using Plasticity Index

Previously, researchers have tried to correlate critical shear stress using plasticity index. Moreover, Figure 4.5 showed that plasticity index can categorize the erodibility. For this reason, critical shear stress was correlated with plasticity index. Kimiaghalam et al. (2016) used 17 fine-grained soil samples for predicting critical shear stress using plasticity index and obtained a linear upward (critical shear stress increases with increasing plasticity index) trend with an R^2 of 0.20. Interestingly, on the contrary, Briaud et al. (2001) obtained a linear downward trend with a R^2 as low as 0.01 for 11 fine-grained soil samples.

In this project, when critical shear stresses were plotted against the corresponding plasticity indexes from 65 samples in a linear scale, an R^2 of 0.05 was obtained. Like previous equations, several other models were investigated and again the power model gave the best fit to

the dataset with R^2 = 0.33. Figure 4.13 shows that critical shear stress increases with increasing plasticity index. The equation to predict critical shear stress, τ_c (lb/ft^2 [Pa]) using plasticity index is:

$$\tau_c = c\, PI^{1.342} \qquad \textbf{Equation 4.3}$$

Where:

PI is the plasticity index, and

c is the is the unit conversion constant, 0.004 in U.S. customary units and 0.202 in S.I.

In total, 65 observations were used in the regression. There are a few outliers in this correlation; for example, one of the US-69 sample (#1; classified as ML) provided a plasticity index of three.

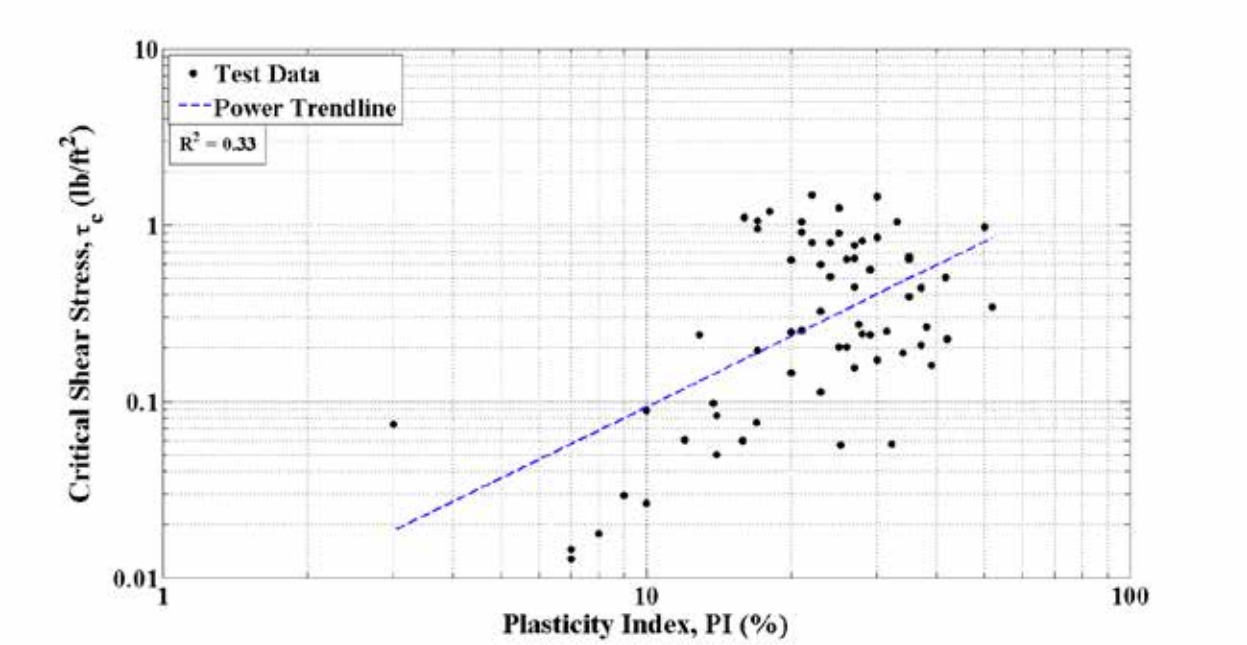

Figure 4.13: Critical Shear Stress versus Plasticity Index

Among the other soil parameters, percent finer than 0.075 mm and water content were obtained and may influence critical shear stress as discussed in the literature review. However, when these properties were analyzed for a correlation, no relationship was found.

4.4 Variable Screening and Preliminary Model Building

The previous sections showed the influence of ER, median grain size, and plasticity index on critical shear stress. Previous researchers have not correlated ER with critical shear stress. Several researchers have established that median grain size (Briaud et al., 2011; Smerdon & Beasley, 1961) and plasticity index (Shan et al., 2015; Smerdon & Beasley, 1961) are correlated with critical shear stress. As such, the objective was to combine ER with median grain size and plasticity index to determine if the resulting model predicting critical shear stress would be more accurate. This was done through a statistical analysis of the data. There are several model selection criteria in statistics, such as coefficient of determination (R^2), adjusted coefficient of determination (R^2_{adj}), Mallow's C_p, and Akaike's Information Criteria (AIC). One of the important conditions to use these analyses is to have at least 10 observations for each independent variable. As mentioned before, among the 65 samples of known ER and PI, there were 51 known data points for median grain size. The results of these analyses as obtained from SAS software are presented in Table 4.3.

Table 4.3: Variable Screening Results Output from SAS Software

Model #	No. of Variables	R^2_{adj}	R^2	C_p	AIC	Model Variables
Model #1	3	0.6171	**0.6401**	4.0000	-104.1135	log (ρ), log (d_{50}), log (PI)
Model #2	2	0.5101	0.5254	3.0000	-127.2215	log (ρ), log (PI)
Model #3	2	**0.6247**	0.6397	2.0522	-106.0569	log (ρ), log (d_{50})
Model #4	2	0.5518	0.5697	11.1900	-97.0054	log (d_{50}), log (PI)
Model #5	1	0.5101	0.5178	**1.9879**	**-128.1939**	log (ρ)
Model #6	1	0.5472	0.5563	10.9468	-97.4353	log (d_{50})
Model #7	1	0.3188	0.3294	26.5919	-106.7605	log (PI)

Table 4.3 shows the values of coefficients for four different model selection criteria: R^2_{adj}, R^2, C_p, and AIC. Mendenhall and Sincich (2012) provide a detailed derivation of these coefficients. There were seven models possible with various combinations of the independent variables. Note that variables were in logarithmic scales as all the models were power models. The criterion for the coefficients R^2_{adj}, and R^2 was, among the competing models, whichever had

the highest value. Therefore, Models #1 and #3 were selected using criteria for R^2_{adj}, and R^2. The criterion for C_p and AIC was the model corresponding to the lowest value; therefore, Model #5 was selected for these two methods. The governing coefficient value among the seven different models for each model selection criteria are shown in bold in Table 4.3.

No criteria were satisfied for Models #2, #4, #6, and #7; hence, these were discarded from further consideration. To select the best model for predicting critical shear stress, Models #1, #3, and #5 were compared. The variables for Model#1 were log(ρ), log(d_{50}), and log(PI); the variables for Model #3 were log(ρ) and log(d_{50}); and Model #5 had only log(ρ) as variable. The calculation of plasticity index is dependent on determining the Liquid Limit (LL) and Plastic Limit (PL) of the respective soil sample. Determination of LL and PL are user dependent, which may result in error. On the other hand, the median grain size is a unique soil property that does not require any visual judgement and is less operator dependent. Therefore, Model #1 was discarded. With the presence of ER, log(ρ), and median grain size, log(d_{50}), as variables, Model #3 (R^2_{adj} = 0.6247, R^2 = 0.6397) was more robust and selected as the final model. The model parameters were obtained after regression analysis and the model equation was:

$$\log \tau_c = \log \alpha - 0.727 \log \rho - 0.278 \log d_{50} \qquad \textbf{Equation 4.4}$$

Where:

ρ is the ER of soil in Ω-m,

d_{50} is median grain size in mm, and

α is the unit conversion constant, 0.654 in U.S. customary units and 31.304 in S.I.

When Equation 4.4 was solved for critical shear stress, τ_c (lb/ft^2 [Pa]), the final model equation was:

$$\tau_c = \alpha \, \rho^{-0.727} \, d_{50}^{-0.278} \qquad \textbf{Equation 4.5}$$

Where all variables have been defined.

However, the developed model for predicting critical shear stress in Equation 4.5 must be validated using additional data. ***Due to the limited dataset of primarily moderately erodible soils, this model should only be considered a preliminary model at this time.***

4.5 Preliminary Model Validation

As shown in Table 4.3, seven different models were possible with combination of the three variables, namely, ER, d_{50}, and PI. On the basis of four variable screening criteria, Model #3 was chosen as the best model. The model was constructed based on the regression analysis of 65 samples from 14 sites. Predicted values of critical shear stress using Model #3 (Equation 4.5) were evaluated with respect to the measured values using the five samples of the remaining site (US-166A). The inverted resistivity section of US-166A is shown in Figure 4.14. The location of drilling for the five samples is shown with the dashed rectangle. The ER values of the five samples varied between 11 to 13 Ω-m, therefore the predicted erodibility was *low to moderate* based on the data in this study.

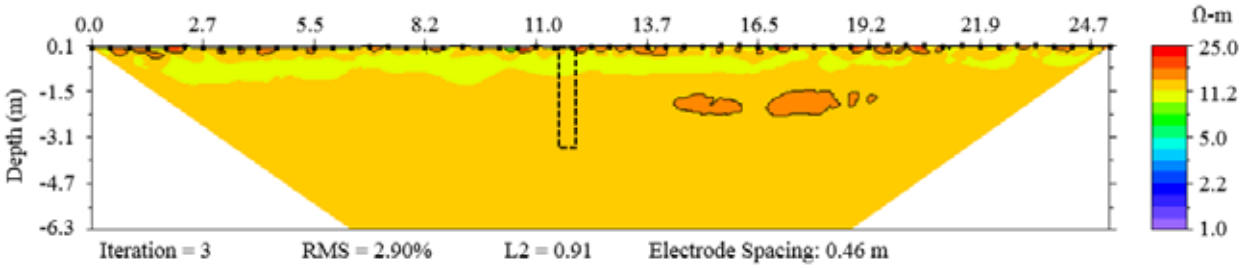

Figure 4.14: Subsurface Inverted ER Distribution of US166A Site

All the five samples were tested under six different velocities (and corresponding shear stresses). The results of the soil classifications and erosion tests are shown in Table 4.4 and Table 4.5, respectively. All samples from US-166A were classified as CL with median grain size (d_{50}) varying between 0.0038 to 0.015 mm.

Table 4.4: Soil Parameters and Classification of K-58 Samples

Sample	Electrical Resistivity (Ω-m)	Water Content (%)	Percent Finer than 0.075 mm (%)	Median Grain Size (mm)	LL	PL	PI	USCS Classification
US-166A #1	11.2	24	98	0.0038	46	26	20	CL
US-166A #2	12.4	26	99	0.0042	45	21	24	CL
US-166A #3	13.0	27	99	0.0182	41	21	20	CL
US-166A #4	13.0	28	99	0.0100	39	19	20	CL
US-166A #5	13.0	30	90	0.0150	33	18	15	CL

Table 4.5: Erosion Test Results of K-58 Samples

Sample	Erosion Test Results							Critical Shear Stress, lb/ft^2 (N/m^2)
US-166A #1	Water Velocity, ft/s (m/s)	3.28 (1.00)	6.56 (2.00)	9.84 (3.00)	13.1 (4.00)	16.4 (5.00)	19.7 (6.00)	1.95 (93.4)
	Shear Stress, lb/ft^2 (N/m^2)	0.07 (3.30)	0.42 (20.0)	0.68 (32.6)	1.29 (61.6)	2.02 (96.9)	2.60 (125)	
	Erosion Rate, in/hr (mm/hr)	0.00 (0.00)	0.00 (0.00)	0.00 (0.00)	0.00 (0.00)	0.05 (1.20)	0.09 (2.40)	
US-166A #2	Water Velocity, ft/s (m/s)	3.28 (1.00)	6.56 (2.00)	9.84 (3.00)	13.1 (4.00)	16.4 (5.00)	19.7 (6.00)	0.56 (26.9)
	Shear Stress, lb/ft^2 (N/m^2)	0.06 (3.0)	0.28 (13.2)	0.66 (31.5)	1.53 (73.4)	2.59 (124)	3.48 (167)	
	Erosion Rate, in/hr (mm/hr)	0.00 (0.00)	0.00 (0.00)	0.02 (0.60)	0.05 (1.20)	1.18 (30.0)	2.19 (55.7)	
US-166A #3	Water Velocity, ft/s (m/s)	3.28 (1.00)	6.56 (2.00)	9.84 (3.00)	13.1 (4.00)	16.4 (5.00)	19.7 (6.00)	0.67 (31.9)
	Shear Stress, lb/ft^2 (N/m^2)	0.09 (4.10)	0.29 (14.0)	0.73 (34.9)	1.24 (59.4)	2.46 (118)	3.44 (165)	
	Erosion Rate, in/hr (mm/hr)	0.00 (0.00)	0.00 (0.00)	0.02 (0.60)	0.14 (3.60)	0.24 (6.00)	0.65 (16.4)	
US-166A #4	Water Velocity, ft/s (m/s)	3.28 (1.00)	6.56 (2.00)	9.84 (3.00)	13.1 (4.00)	16.4 (5.00)	19.7 (6.00)	0.68 (32.7)
	Shear Stress, lb/ft^2 (N/m^2)	0.07 (3.30)	0.26 (12.5)	0.82 (39.4)	1.55 (74.0)	2.50 (120.0)	4.48 (215)	
	Erosion Rate, in/hr (mm/hr)	0.00 (0.00)	0.00 (0.00)	0.07 (1.8)	0.09 (2.4)	0.19 (4.8)	8.20 (208)	
US-166A #5	Water Velocity, ft/s (m/s)	3.28 (1.00)	6.56 (2.00)	9.84 (3.00)	13.1 (4.00)	16.4 (5.00)	19.7 (6.00)	0.61 (29.2)
	Shear Stress, lb/ft^2 (N/m^2)	0.06 (2.90)	0.29 (14.0)	0.71 (34.2)	1.50 (72.0)	2.50 (120)	4.12 (197)	
	Erosion Rate, in/hr (mm/hr)	0.00 (0.00)	0.00 (0.00)	0.05 (1.20)	0.14 (3.60)	2.95 (75.0)	4.91 (125)	

As shown in Table 4.5, Sample #2 through Sample #4 showed critical shear stress between 0.56 and 0.68 lb/ft^2 (26.9 and 32.7 N/m^2). However, Sample #1 showed very high critical shear stress of 1.95 lb/ft^2 (93.4 N/m^2), which was the maximum among all the sites of this

project. As mentioned before, Model #3, which uses ER (ρ) and median grain size (d_{50}) as variables, was selected as the preliminary model to predict critical shear stress. Table 4.6 shows the preliminary model of this study under-predicted the shear stress for all the samples of US-166A. Therefore, for bridge scour monitoring, the model can provide conservative estimate of critical shear stress at this time.

Table 4.6: Predicted versus Actual for US-166A

Sample	Electrical Resistivity (Ω-m)	Predicted Erodibility	Measured Erodibility	Predicted Critical Shear Stress lb/ft^2 (N/m^2)	Measured Critical Shear Stress lb/ft^2 (N/m^2)	Variation (%)
US-166A #1	11.2	Low/Moderate	Low	0.53 (25.5)	1.95 (93.4)	73
US-166A #2	12.4	Low/Moderate	Low/Moderate	0.48 (23.0)	0.56 (26.9)	15
US-166A #3	13.0	Low/Moderate	Low/Moderate	0.39 (18.5)	0.67 (31.9)	42
US-166A #4	13.0	Low/Moderate	Low/Moderate	0.36 (17.4)	0.68 (32.7)	47
US-166A #5	13.0	Low/Moderate	Moderate	0.32 (15.5)	0.61 (29.2)	47

Figure 4.15 verifies that for such low values of resistivity (11 to 13 Ω-m), the erodibility was low to moderate as predicted. The validation showed how ER can be used as a primary tool (with the aid of HEC-18 erodibility categorizing graph) for prioritizing bridge monitoring schedule by predicting if a site is likely high or low-to-moderate erodibility. The preliminary model to predict critical shear stress based on 14 sites in this study was showed to be conservative using one additional site for validation.

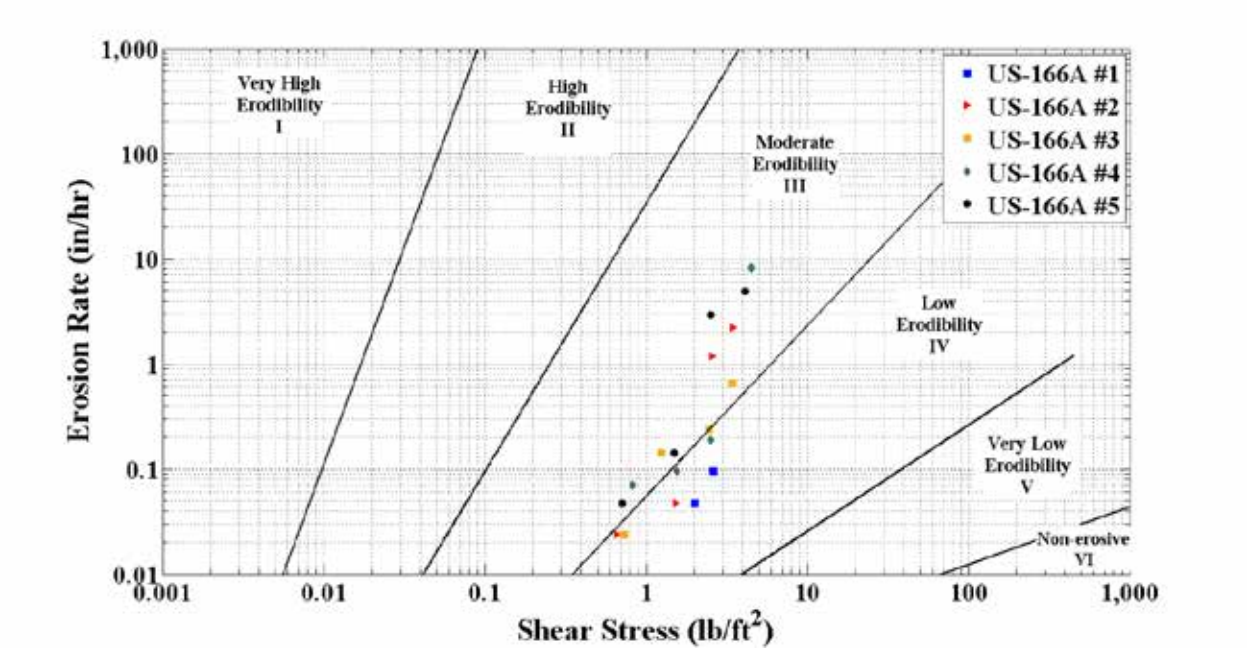

Figure 4.15: Erosion Rate versus Shear Stress for US-166A Samples

Chapter 5: Conclusions

The current FHWA methodology for predicting soil erosion potential is based on the analysis of coarse-grained soils. When this methodology is applied to fine-grained soils, the scour design is typically over-conservative. Therefore, site-specific testing is currently needed. Although a recent method (Shan et al., 2015) to predict the erosion potential of fine-grained soils has been published by the FHWA, it was shown to over-predict critical shear stress of the soils in this study. While site-specific testing is a valuable tool, it is time consuming and costly. In this study, the data obtained from Electrical Resistivity (ER) surveys were used to predict erodibility for bridge scour monitoring and design. Fifteen sites were selected by KDOT around Kansas and used to determine the correlation between ER and soil erodibility.

ER surveys were conducted at each site and soil samples were collected for erosion testing using an Erosion Function Apparatus (EFA). Geotechnical parameters such as median grain size, plasticity index, percent finer, and water content were also measured and each sample was classified according to the Unified Soil Classification System (USCS). With the aid of the erodibility categorizing graphs (Arneson et al., 2012), it was shown that soils were more erosive when median grain size increased and plasticity index decreased. According to the USCS, 63 out of 70 samples from 15 sites were classified as high or low plastic clays (CH or CL). Of the other seven samples, three were clayey sands (SC) from K-126, one was well-graded sand with clay (SW-SC) also from K-126, two were elastic silts (MH) from K-9, and one was silt (ML) from US-69. Using the erodibility categorizing graph, it was shown that SC and SW-SC were highly erodible. The other soil types had low to moderate erodibility.

The objective of this research was to characterize erodibility based solely on bulk ER measurements. The ER values corresponding to all 269 points in the erodibility categorizing graph were divided into two ranges (i.e., above and below 100 Ω-m). It was shown that 73.1% of the samples that had an ER over 100 Ω-m were classified as high erodibility. When ER values were below 100 Ω-m, 98.8% of the samples were low-to-moderate erodibility. Erodibility levels with respect to ER for all the samples are shown in Table 5.1. Based on these findings shown, KDOT can utilize ER to prioritize bridge sites for additional sampling and erosion testing as part

of scour monitoring procedures. This methodology has the potential to reduce a large number of erosion tests during the primary stage of the FHWA required scour monitoring procedures.

Table 5.1: Categorizing Erodibility using ER

	ER below 100 Ω-m	ER above 100 Ω-m	Percentage (When below 100 Ω-m)	Percentage (When above 100 Ω-m)
High Erodibility	3	19	1.23%	73.08%
Low/Moderate Erodibility	240	7	98.77%	26.92%
Total	243	26	100.00%	100.00%

Additionally, seven models were developed to predict critical shear stress, τ_c (lb/ft^2 [Pa]), using 65 samples from 14 sites. Variable screening criteria were used to select the best model among these and the following model was selected:

$$\boldsymbol{\tau_c = \alpha\, \rho^{-0.727}\, d_{50}^{-0.278}} \qquad \textbf{Equation 5.1}$$

Where:

ρ is the ER of soil in Ω-m,

d_{50} is median grain size in mm, and

α is the unit conversion constant, 0.654 in U.S. customary units and 31.304 in S.I.

This equation was developed primarily using clayey soils and is likely not appropriate when the median grain size is greater than 4.76 mm, the nominal size of a standard No. 4 sieve. The R^2 of this equation was 0.64. Moreover, in one of the other models, critical shear stress, τ_c (lb/ft^2 [Pa]), was predicted using only ER as independent variable such that:

$$\boldsymbol{\tau_c = a\, \rho^{-1.007}} \qquad \textbf{Equation 5.2}$$

Where:

ρ is the ER of soil in Ω-m, and

a is the unit conversion constant, 3.998 in U.S. customary units and 191.435 in S.I.

The corresponding R^2 of 0.52 of the model in Equation 5.2 indicates that ER itself can predict the critical erosion with an acceptable accuracy if laboratory tests to determine other soil parameters are not possible. Again, due to the limited variability of test sites in this study, Equation 5.2 is likely not appropriate where the measured ER is over 500 Ω-m. ***Both Equation 5.1 and 5.2 should only be considered preliminary equations at this time and should not be used for design purposes.***

5.1 Recommendations

This study showed that electrical resistivity can be used as a preliminary screening tool to identifying if a bridge site has highly erodible soils. It is recommended that ER surveys conducted by KDOT at bridge stream crossings follow the methodology described in this study. If the measured ER is over 100 Ω-m, soil samples should be collected for laboratory erosion tests as these soils are likely highly erodible. If d_{50} data are available, the preliminary equations can be used to predict critical shear stress; however, the equation is currently very conservative.

5.2 Future Work

The preliminary critical shear stress model was developed using measured soil properties; however, the current model is limited. Among the 15 sites used in this study, only one site was highly erodible and six sites (including the validation site) had some measured low erodible points. The remaining sites were moderately erodible. Also, all but three sites were either high or low plastic clays. Therefore, additional testing is needed to encompass a wider variety of erodibility and fine-grained soil types. This study focused on predicting erosion using electrical resistivity, therefore no strength tests were conducted other than a pocket penetrometer in the field. Because the soil index properties showed correlation with erosion potential, it is very likely that measured strength parameters such as cohesion can be used to predict erosion potential in fine-grained soils as well. Additional samples are needed to incorporate soil strength parameters in the predictive model. Samples can be collected for strength tests from the sites in this study to add this needed data. Finally, some of the available soil parameters such as water content, percent finer, and liquid limit were not considered for critical shear stress model development

because these parameters did not show good relationship with critical shear stress individually. A more robust statistical analysis is needed where interactions between parameters are included. Additional samples, strength tests, and studying the interactions between soil properties will help to build a more robust model applicable to a wide range of fine-grained soil erosion in Kansas.

Future studies can also investigate a different approach to quantify the amount of erosion across a stream. One of the advantages of electrical resistivity surveys is that they capture a continuous profile (as opposed to discrete data) across the measured subsurface. In fact, ER data are collected for thousands of points to create a contour map of the bulk resistivity. For example, in this study, ER values were measured across as many as 46,480 elements for a two-dimensional plane of 82.3 ft × 21.7 ft (25.1 m × 6.6 m). It was shown ER alone can predict critical shear stress with an R^2 of 0.52 (Equation 5.2). Therefore, all of these subsurface elements can be transformed to critical shear stress to characterize the entire site.

References

Abu-Hassanein, Z. S., Benson, C. H., & Blotz, L. R. (1996). Electrical resistivity of compacted clays. *Journal of Geotechnical Engineering*, *122*(5), 397–406.

Advanced Geosciences, Inc. (AGI). (2008). *Instruction manual for EarthImager 2D Version 2.4.0 Resistivity and IP Inversion Software*. Austin, TX: Author.

Amaryan, L. S. (1993). *Soft soil properties and testing methods*. Netherlands: CRC Press.

Amos, C. L., Bergamasco, A., Umgiesser, G., Cappucci, S., Cloutier, D., DeNat, L.,… Cristante, S. (2004). The stability of tidal flats in Venice Lagoon---the results of in-situ measurements using two benthic, annular flumes. *Journal of Marine Systems*, *51*(1–4), 211–241.

Arjwech, R. (2011). *Electrical resistivity imaging for unknown bridge foundation depth determination* (Doctoral dissertation). Texas A&M University, College Station, TX.

Arjwech, R., Everett, M. E., Briaud, J.-L., Hurlebaus, S., Medina-Cetina, Z., Tucker, S., & Yousefpour, N. (2013). Electrical resistivity imaging of unknown bridge foundations. *Near Surface Geophysics*, *11*(6), 591–598.

Arneson, L. A., Zevenbergen, L. W., Lagasse, P. F., & Clopper, P. E. (2012). Evaluating scour at bridges, Fifth edition (Report No. FHWA-HIF-12-003). Retrieved from https://www.fhwa.dot.gov/engineering/hydraulics/pubs/hif12003.pdf

ASTM C117-13. (2013). *Standard test method for materials finer than 75-μm (No. 200) sieve in mineral aggregates by washing*. West Conshohocken, PA: ASTM International. doi: 10.1520/C0117-13, www.astm.org

ASTM C136 / C136M-14. (2014). Standard test method for sieve analysis of fine and coarse aggregates. West Conshohocken, PA: ASTM International. doi: 10.1520/C0136_C0136M-14, www.astm.org

ASTM D422-63. (2007). *Standard test method for particle-size analysis of soils*. West Conshohocken, PA: ASTM International. doi: 10.1520/D0422-63R07E02, www.astm.org

ASTM D1587 / D1587M-15. (2015). *Standard practice for thin-walled tube sampling of fine-grained soils for geotechnical purposes*. West Conshohocken, PA: ASTM International. doi: 10.1520/D1587_D1587M-15, www.astm.org

ASTM D2216-10. (2010). *Standard test methods for laboratory determination of water (moisture) content of soil and rock by mass*. West Conshohocken, PA: ASTM International. doi: 10.1520/D2216-10, www.astm.org

ASTM D4220 / D4220M-14. (2014). *Standard practices for preserving and transporting soil samples*. West Conshohocken, PA: ASTM International. doi: 10.1520/D4220_D4220M, www.astm.org

ASTM D4318-10. (2010). *Standard test methods for liquid limit, plastic limit, and plasticity index of soils*. West Conshohocken, PA: ASTM International. doi: 10.1520/D4318-10, www.astm.org

Bale, A. J., Stephens, J. A., & Harris, C. B. (2007). Critical erosion profiles in macro-tidal estuary sediments: Implications for the stability of intertidal mud and the slope of mud banks. *Continental Shelf Research, 27*(18), 2303–2312.

Bernhardt, M., Briaud, J.-L., Kim, D., Leclair, M., Storesund, R., Lim, S.-G.,…Rogers, J. D. (2011). Mississippi River levee failures: June 2008 flood. *International Journal of Geoengineering Case Histories, 2*(3), 127–162.

Binley, A., & Kemna, A. (2005). DC resistivity and induced polarization methods. In Y. Rubin & S. Hubbard (Eds.), *Hydrogeophysics* (pp. 129–156). Dordrecht: Springer Netherlands.

Bloomquist, D., & Crowley, R. (2010). *Enhancement of FDOT's SERF device and a study of erosion rates of rock, sand, and clay mixtures using FDOT's RETA and SERF equipment* (Report No. BDK-75-977-09). Tallahassee, FL: Florida Department of Transportation.

Briaud, J.-L., Chen, H.-C., Chang, K.-A., Oh, S. J., Chen, S., Wang, J.,…Ting, F. (2011). *The SRICOS–EFA method*. College Station, TX: Texas A&M University.

Briaud, J. L., Ting, F. C., Chen, H. C., Cao, Y., Han, S. W., & Kwak, K. W. (2001). Erosion function apparatus for scour rate predictions. *Journal of Geotechnical and Geoenvironmental Engineering, 127*(2), 105–113.

Briaud, J.-L., Ting, F. C. K., Chen, H. C., Gudavalli, R., Perugu, S., & Wei, G. (1999). SRICOS: Prediction of scour rate in cohesive soils at bridge piers. *Journal of Geotechnical and Geoenvironmental Engineering, 125*(4), 237–246.

Calappi, T., Miller, C. J., & Carpenter, D. (2010). Revisiting the HEC-18 scour equation. In *Scour and erosion* (pp. 1102–1109). Reston, VA: American Society of Civil Engineers.

Chambers, J. E., Wilkinson, P. B., Penn, S., Meldrum, P. I., Kuras, O., Loke, M. H., & Gunn, D. A. (2013). River terrace sand and gravel deposit reserve estimation using three-dimensional electrical resistivity tomography for bedrock surface detection. *Journal of Applied Geophysics, 93*, 25–32.

Clark, L. A., & Wynn, T. M. (2007). Methods for determining streambank critical shear stress and soil erodibility: Implications for erosion rate predictions. *Transactions of the ASABE, 50*(1), 95–106.

Dahlin, T. (2001). The development of DC resistivity imaging techniques. *Computers & Geosciences, 27*(9), 1019–1029.

Debnath, K., Nikora, V., Aberle, J., Westrich, B., & Muste, M. (2007). Erosion of cohesive sediments: Resuspension, bed load, and erosion patterns from field experiments. *Journal of Hydraulic Engineering, 133*(5), 508–520.

Dickhudt, P. J., Friedrichs, C. T., & Sanford, L. P. (2011). Mud matrix solids fraction and bed erodibility in the York River estuary, USA, and other muddy environments. *Continental Shelf Research, 31*(10), S3–S13.

Droppo, I. G., Lau, Y. L., & Mitchell, C. (2001). The effect of depositional history on contaminated bed sediment stability. *Science of the Total Environment, 266*(1–3), 7–13.

Dunn, I. S. (1959). Tractive resistance of cohesive channels. *Journal of the Soil Mechanics and Foundations Division, 85*(3), 1–24.

Everett, M. E. (2013). Electrical resistivity method. In *Near-surface applied geophysics* (pp. 70-103). New York, NY: Cambridge University Press.

Fukue, M., Minato, T., Horibe, H., & Taya, N. (1999). The micro-structures of clay given by resistivity measurements. *Engineering Geology, 54*(1), 43–53.

Google Maps. (2016). [Kansas] [Street map]. Retrieved from https://www.google.com/maps/@38.8580219,-97.5989946,8.53z/data=!4m2!6m1!1s1TSszfwP27a3s5mQ-oy5yqrME9Z0 .

Grabowski, R. C., Droppo, I. G., & Wharton, G. (2011). Erodibility of cohesive sediment: The importance of sediment properties. *Earth-Science Reviews, 105*(3), 101–120.

Grissinger, E. H. (1982). Bank erosion of cohesive materials. In R. Hey, J. Bathurst, & C. Thorne (Eds.), *Gravel-bed rivers* (pp. 273-287). Chichester, UK: Wiley.

Hanson, G. J. (1990). Surface erodibility of earthen channels at high stresses. Part I - Open channel testing. *Transactions of the ASAE, 33*(1), 127–131.

Hanson, G. J., & Cook, K. R. (2004). Apparatus, test procedures, and analytical methods to measure soil erodibility in situ. *Applied Engineering in Agriculture, 20*(4), 455−462.

Hanson, G. J., Cook, K. R., & Simon, A. (1999). Determining erosion resistance of cohesive materials. In *American Society of Civil Engineers Water Resources Conference proceedings*.

Hanson, G. J., & Simon, A. (2001). Erodibility of cohesive streambeds in the loess area of the midwestern USA. *Hydrological Processes, 15*(1), 23–38.

Hanson, G. J., & Temple, D. M. (2002). Performance of bare-earth and vegetated steep channels under long-duration flows. *Transactions of the ASAE, 45*(3), 695–701.

Heinzen, R. T. (1976). *Erodibility criteria for soil* (Master's thesis). University of California, Davis, CA.

Houwing, E. J. (1999). Determination of the critical erosion threshold of cohesive sediments on intertidal mudflats along the Dutch Wadden Sea coast. *Estuarine, Coastal and Shelf Science, 49*(4), 545–555.

Jepsen, R., Roberts, J., & Lick, W. (1997). Effects of bulk density on sediment erosion rates. In R. Evans, J. Wisniewski, & J. Wisniewski (Eds.), *The interactions between sediments and water* (pp. 21–31). Dordrecht: Springer Netherlands.

Johnson, B. D., Kranck, K., & Muschenheim, D. K. (1994). Physicochemical factors in particle aggregation. In R. Wotton (Ed.), *The biology of particles in aquatic systems* (pp. 75–96). Boca Raton, FL: Lewis Publishers.

Karim, M. Z. (2016). *Characterizing soil erosion potential using electrical resistivity imaging* (Master's thesis). Kansas State University, Manhattan, KS. Retrieved from http://krex.k-state.edu/dspace/bitstream/handle/2097/32899/MdZahidulKarim2016.pdf?sequence=1

Keller, G. V., & Frischknecht, F. C. (1966). *Electrical methods in geophysical prospecting*. Oxford, UK: Pergamon Press.

Kibria, G., & Hossain, M. S. (2012). Investigation of geotechnical parameters affecting electrical resistivity of compacted clays. *Journal of Geotechnical and Geoenvironmental Engineering*, *138*(12), 1520–1529.

Kimiaghalam, N., Clark, S. P., & Ahmari, H. (2016). An experimental study on the effects of physical, mechanical, and electrochemical properties of natural cohesive soils on critical shear stress and erosion rate. *International Journal of Sediment Research, 31*(1), 1–15.

Knapen, A., Poesen, J., Govers, G., Gyssels, G., & Nachtergaele, J. (2007). Resistance of soils to concentrated flow erosion: A review. *Earth-Science Reviews, 80*(1), 75–109.

Knight, R. J., & Endres, A. L. (2005). 3. An introduction to rock physics principles for near-surface geophysics. In *Near-Surface Geophysics* (pp. 31–70). Tulsa, OK: Society of Exploration Geophysicists.

Kwader, T. (1985). Estimating aquifer permeability from formation resistivity factors. *Ground Water, 23*(6), 762–766.

Lau, Y. L., & Droppo, I. G. (2000). Influence of antecedent conditions on critical shear stress of bed sediments. *Water Research, 34*(2), 663–667.

Leeder, M. R. (1999). *Sedimentology and sedimentary basins: From turbulence to tectonics*. Oxford, UK: Blackwell Science.

Lick, W., Jin, L., & Gailani, J. (2004). Initiation of movement of quartz particles. *Journal of Hydraulic Engineering, 130*(8), 755–761.

Lick, W., & McNeil, J. (2001). Effects of sediment bulk properties on erosion rates. *Science of the Total Environment, 266*(1), 41–48.

Loke, M. H. (1999). *Electrical imaging surveys for environmental and engineering studies: A practical guide to 2-D and 3-D surveys*.

Lucius, J. E., Langer, W. H., & Ellefsen, K. J. (2006). *An introduction to using surface geophysics to characterize sand and gravel deposits*. Reston, VA: U.S. Geological Survey.

McCarter, W. J. (1984). The electrical resistivity characteristics of compacted clays. *Geotechnique, 34*(2), 263–267.

Mendenhall, W., & Sincich, T. (2012). *A second course in statistics: Regression analysis* (7th ed.). Boston, MA: Prentice Hall.

Moody, L. F. (1944). Friction factors for pipe flow. *Transactions of the ASME, 66*(8), 671–684

Munson, B. R., Young, D. F., & Okiishi, T. H. (1990). *Fundamentals of fluid mechanics*. New York, NY: Wiley.

Nassif, H., Ertekin, A. O., & Davis, J. (2002). *Evaluation of bridge scour monitoring methods* (Report No. FHWA-NJ-2003-009). Washington, DC: Federal Highway Administration.

Panagiotopoulos, I., Voulgaris, G., & Collins, M. B. (1997). The influence of clay on the threshold of movement of fine sandy beds. *Coastal Engineering, 32*(1), 19–43.

Partheniades, E. (1965). Erosion and deposition of cohesive soils. *Journal of the Hydraulics Division, 91*(1), 105–139.

Richardson, E. V., & Davis, S. R. (2001). *Evaluating scour at bridges* (Hydraulic Engineering Circular No. 18, Report No. FHWA-NHI-01-001, 4th ed.). Washington, DC: Federal Highway Administration.

Richardson, E. V., Harrison, L. J., Richardson, J. R., & Davis, S. R. (1993). *Evaluating scour at bridges* (Hydraulic Engineering Circular No. 18, 2nd ed.). McLean, VA: Federal Highway Administration.

Richardson, E. V., Pagan-Ortiz, J. E., Schall, J. D., & Price, G. R. (2003). Monitoring and plans for action for bridge scour: Instruments and State Departments of Transportation experiences. *Transportation Research E-Circular, E-C049*, 292–305.

SAS Institute Inc. (2014). SAS™ [Computer software]. Cary, NC: SAS Institute Inc.

Shan, H., Shen, J., Kilgore, R., & Kerenyi, K. (2015). *Scour in cohesive soils* (Report No. FHWA-HRT-15-033). McLean, VA: Federal Highway Administration. Retrieved from https://www.fhwa.dot.gov/publications/research/infrastructure/structures/bridge/15033/15033.pdf

Smerdon, E. T., & Beasley, R. P. (1961). Critical tractive forces in cohesive soils. *Agricultural Engineering, 42*(1), 26–29.

Thomsen, L., & Gust, G. (2000). Sediment erosion thresholds and characteristics of resuspended aggregates on the western European continental margin. *Deep Sea Research Part I: Oceanographic Research Papers, 47*(10), 1881–1897.

Tikhonov, A. N., & Arsenin, V. Y. (1977). Solutions of ill-posed problems. *SIAM Review, 21*(2), 266–267.

Tucker, S. E., Briaud, J.-L., Hurlebaus, S., Everett, M. E., & Arjwech, R. (2015). Electrical resistivity and induced polarization imaging for unknown bridge foundations. *Journal of Geotechnical and Geoenvironmental Engineering, 141*(5). doi: 10.1061/(ASCE)GT.1943-5606.0001268

Tucker-Kulesza, S., Snapp, M., & Koehn, W. (2016). *Electrical resistivity measurement of mechanically stabilized earth wall backfill* (Report No. K-TRAN: KSU-15-6). Topeka, KS: Kansas Department of Transportation.

Van Klaveren, R. W., & McCool, D. K. (1998). Erodibility and critical shear of a previously frozen soil. *Transactions of the ASAE, 41*(5), 1315–1321

Van Ledden, M., Van Kesteren, W. G. M., & Winterwerp, J. C. (2004). A conceptual framework for the erosion behaviour of sand–mud mixtures. *Continental Shelf Research, 24*(1), 1–11.

Vaudelet, P., Schmutz, M., Pessel, M., Franceschi, M., Guérin, R., Atteia, O.,…P. Bégassat. (2011). Mapping of contaminant plumes with geoelectrical methods. A case study in urban context. *Journal of Applied Geophysics, 75*(4), 738–751.

Winterwerp, J. C., & Van Kesteren, W. G. M. (2004). *Introduction to the physics of cohesive sediment dynamics in the marine environment* (Developments in Sedimentology, Volume 56). Amsterdam, Netherlands: Elsevier.

Zhou, Q. Y., Shimada, J., & Sato, A. (2001). Three-dimensional spatial and temporal monitoring of soil water content using electrical resistivity tomography. *Water Resources Research, 37*(2), 273–285.

Zonge, K., Wynn, J., & Urquhart, S. (2005). 9. Resistivity, induced polarization, and complex resistivity. In *Near-surface geophysics* (pp. 265–300). Tulsa, OK: Society of Exploration Geophysicists.

Appendix: Inverted Resistivity, Erosion Test and Soil Classification Results of Thirteen Sites

Bridge 058-0025 on K-9 Highway
(GPS Co-ordinate: 39.6915,-96.4445)

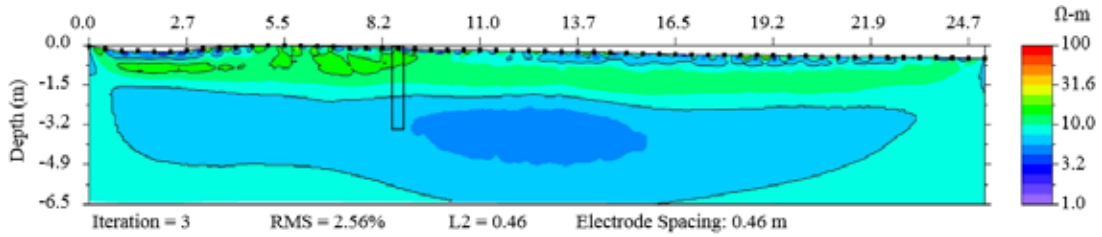

Figure A.1: Inverted Resistivity of K-9

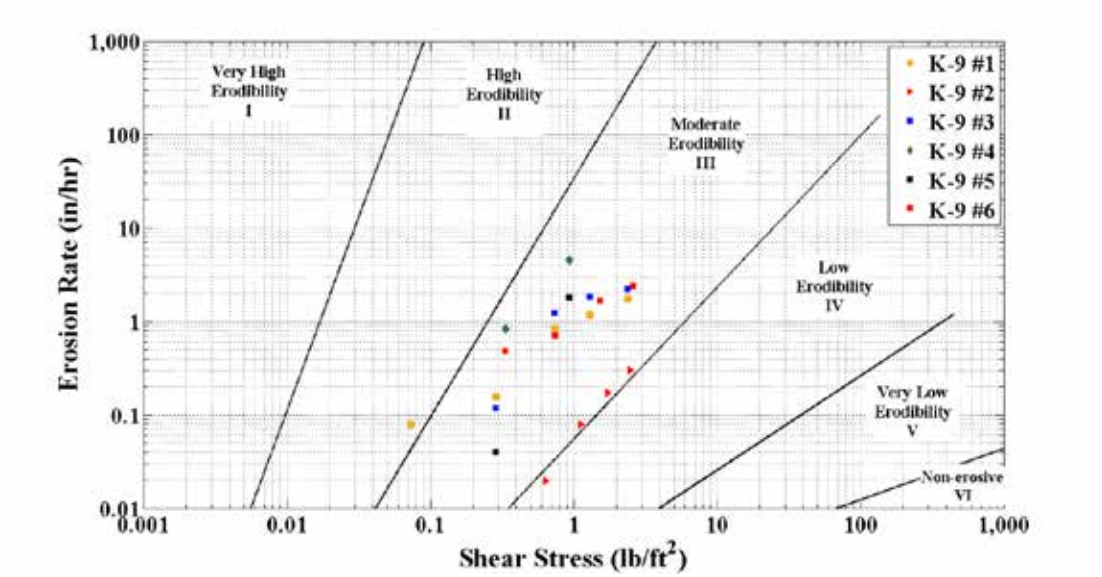

Figure A.2: Erosion Rate versus Shear Stress for K-9 Samples

Table A.1: Classification of K-9 Samples

Sample Designation	Water Content (%)	Percent Finer than 0.075 mm (%)	Median Grain Size (mm)	LL	PL	PI	USCS Classification
K-9 #1	31	-	-	59	27	32	CH
K-9 #2	30	-	-	70	28	42	CH
K-9 #3	32	-	-	61	32	29	MH
K-9 #4	30	-	-	55	30	25	MH
K-9 #5	35	-	-	58	31	28	CH
K-9 #6	25	-	-	60	29	31	CH

Table A.2: Erosion Test Results of K-9 Samples

Sample	Erosion Test Results							Critical Shear Stress, lb/ft^2 (N/m^2)
K-9 #1	Water Velocity, ft/s (m/s)	1.64 (0.50)	3.28 (1.00)	6.56 (2.00)	9.84 (3.00)	13.1 (4.00)	16.4 (5.00)	0.06 (2.70)
	Shear Stress, lb/ft^2 (N/m^2)	0.02 (0.90)	0.07 (3.50)	0.29 (13.8)	0.74 (35.4)	1.31 (62.8)	2.38 (114)	
	Erosion Rate, in/hr (mm/hr)	0.00 (0.00)	0.08 (2.00)	0.16 (4.00)	0.83 (21.0)	1.18 (30.0)	1.76 (44.7)	
K-9 #2	Water Velocity, ft/s (m/s)	3.28 (1.00)	6.56 (2.00)	9.84 (3.00)	13.1 (4.00)	16.4 (5.00)	19.7 (6.00)	0.50 (24.1)
	Shear Stress, lb/ft^2 (N/m^2)	0.07 (3.50)	0.29 (13.8)	0.63 (30.4)	1.12 (53.6)	1.74 (83.1)	2.48 (119)	
	Erosion Rate, in/hr (mm/hr)	0.00 (0.00)	0.00 (0.00)	0.02 (0.50)	0.08 (2.00)	0.17 (4.40)	0.30 (7.60)	
K-9 #3	Water Velocity, ft/s (m/s)	1.64 (0.50)	3.28 (1.00)	6.56 (2.00)	9.84 (3.00)	13.1 (4.00)	16.4 (5.00)	0.24 (11.4)
	Shear Stress, lb/ft^2 (N/m^2)	0.02 (0.90)	0.07 (3.50)	0.29 (13.8)	0.74 (35.4)	1.31 (62.8)	2.38 (114)	
	Erosion Rate, in/hr (mm/hr)	0.00 (0.00)	0.00 (0.00)	0.11 (3.00)	1.22 (31.0)	1.81 (46.0)	2.20 (55.9)	
K-9 #4	Water Velocity, ft/s (m/s)	1.64 (0.50)	3.28 (1.00)	6.56 (2.00)	9.84 (3.00)	-	-	0.20 (9.70)
	Shear Stress, lb/ft^2 (N/m^2)	0.02 (0.90)	0.07 (3.50)	0.33 (16.0)	0.93 (44.6)	-	-	
	Erosion Rate, in/hr (mm/hr)	0.00 (0.00)	0.00 (0.00)	0.83 (21.0)	4.56 (116)	-	-	
K-9 #5	Water Velocity, ft/s (m/s)	1.64 (0.50)	3.28 (1.00)	6.56 (2.00)	9.84 (3.00)	-	-	0.27 (13.1)
	Shear Stress, lb/ft^2 (N/m^2)	0.02 (0.90)	0.07 (3.50)	0.29 (13.8)	0.94 (45.0)	-	-	
	Erosion Rate, in/hr (mm/hr)	0.00 (0.00)	0.00 (0.00)	0.04 (1.00)	1.77 (45.0)	-	-	
K-9 #6	Water Velocity, ft/s (m/s)	1.64 (0.50)	3.28 (1.00)	6.56 (2.00)	9.84 (3.00)	13.1 (4.00)	16.4 (5.00)	0.25 (12.0)
	Shear Stress, lb/ft^2 (N/m^2)	0.02 (0.90)	0.07 (3.50)	0.33 (16.0)	0.75 (35.7)	1.54 (73.6)	2.61 (125)	
	Erosion Rate, in/hr (mm/hr)	0.00 (0.00)	0.00 (0.00)	0.48 (12.2)	0.71 (18.0)	1.65 (42.0)	2.36 (60.0)	

Bridge 058-0008 on US-36 Highway
(GPS Co-ordinate: 39.8416,-96.2500)

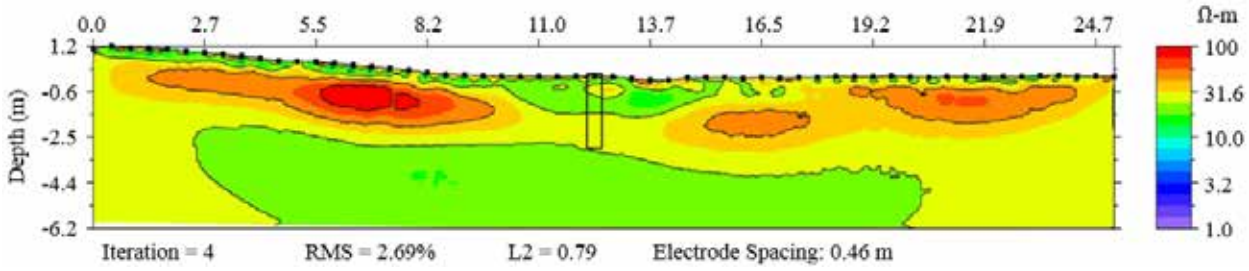

Figure A.3: Inverted Resistivity of US-36

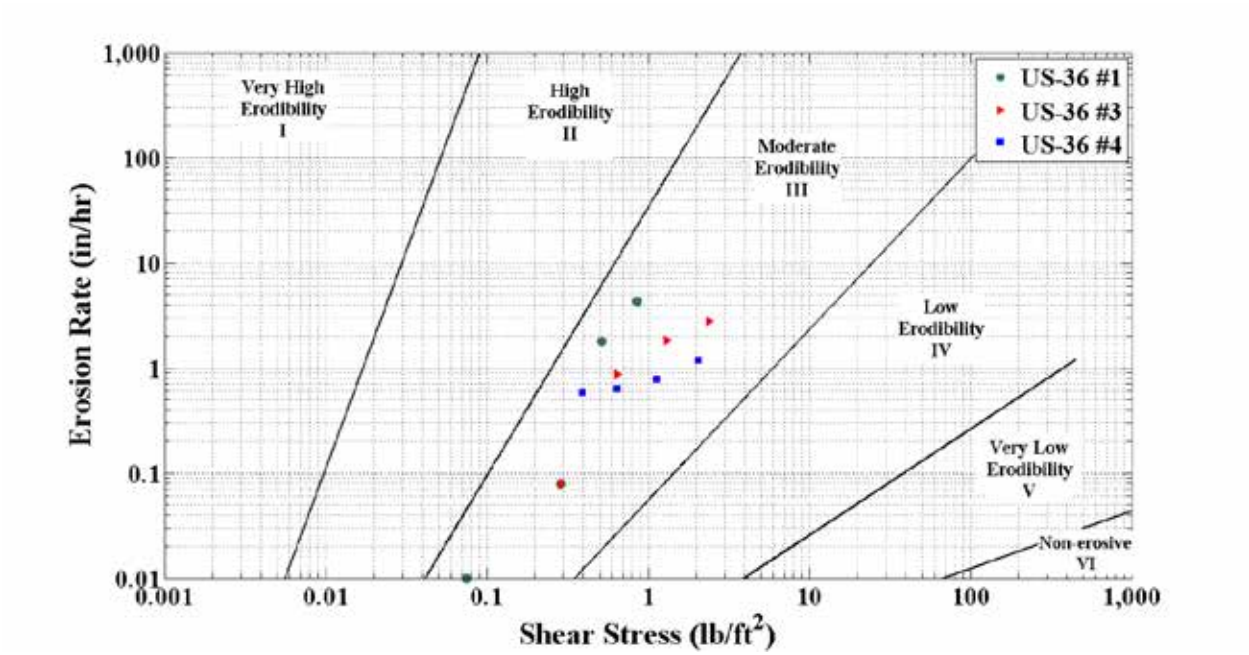

Figure A.4: Erosion Rate versus Shear Stress for US-36 Samples

Table A.3: Classification of US-36 Samples

Sample Designation	Water Content (%)	Percent Finer than 0.075 mm (%)	Median Grain Size (mm)	LL	PL	PI	USCS Classification
US-36 #1	25	-	-	37	21	16	CL
US-36 #3	28	-	-	35	22	13	CL
US-36 #4	22	-	-	36	22	14	CL

Table A.4: Erosion Test Results of US-36 Samples

Sample	Erosion Test Results							Critical Shear Stress, lb/ft^2 (N/m^2)
US-36 #1	Water Velocity, ft/s (m/s)	1.64 (0.50)	3.28 (1.00)	6.56 (2.00)	8.20 (2.50)	9.84 (3.00)	-	0.06 (2.90)
	Shear Stress, lb/ft^2 (N/m^2)	0.02 (0.90)	0.08 (3.60)	0.29 (13.8)	0.52 (24.8)	0.86 (41.1)	-	
	Erosion Rate, in/hr (mm/hr)	0.00 (0.00)	0.01 (0.30)	0.08 (2.00)	1.77 (45.0)	4.25 (108)	-	
US-36 #3	Water Velocity, ft/s (m/s)	1.64 (0.50)	3.28 (1.00)	6.56 (2.00)	9.84 (3.00)	13.1 (4.00)	16.4 (5.00)	0.24 (11.4)
	Shear Stress, lb/ft^2 (N/m^2)	0.02 (0.90)	0.067 (3.20)	0.29 (13.8)	0.65 (30.9)	1.31 (62.6)	2.40 (115)	
	Erosion Rate, in/hr (mm/hr)	0.00 (0.00)	0.00 (0.00)	0.08 (2.00)	0.87 (22.0)	1.81 (46.0)	2.78 (70.7)	
US-36 #4	Water Velocity, ft/s (m/s)	1.64 (0.50)	3.28 (1.00)	6.56 (2.00)	9.84 (3.00)	13.1 (4.00)	16.4 (5.00)	0.10 (4.60)
	Shear Stress, lb/ft^2 (N/m^2)	0.02 (0.90)	0.08 (3.60)	0.39 (18.8)	0.65 (30.9)	1.14 (54.4)	2.07 (99.1)	
	Erosion Rate, in/hr (mm/hr)	0.00 (0.00)	0.00 (0.00)	0.58 (14.7)	0.63 (16.0)	0.78 (19.7)	1.18 (30.0)	

Bridge 085-0146 on K-4 Highway
(GPS Co-ordinate: 38.7001,-97.6130)

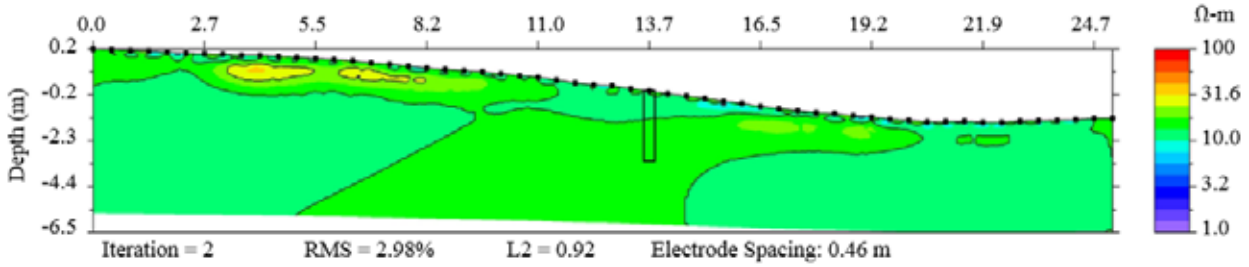

Figure A.5: Inverted Resistivity of K-4B

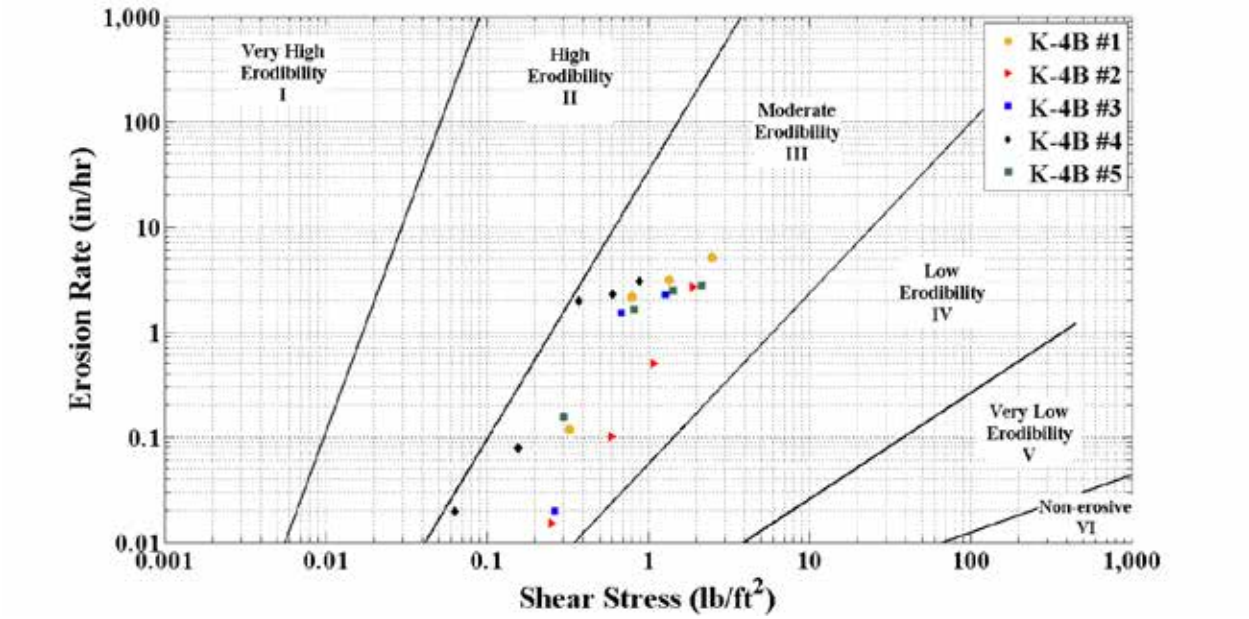

Figure A.6: Erosion Rate versus Shear Stress for K-4B Samples

Table A.5: Classification of K-4B Samples

Sample designation	Water content (%)	Percent finer than 0.075 mm (%)	Mean grain size (mm)	LL	PL	PI	USCS classification
K-4B #1	23	-	-	39	18	21	CL
K-4B #2	31	-	-	63	21	42	CH
K-4B #3	29	-	-	37	17	20	CL
K-4B #4	28	-	-	33	19	14	CL
K-4B #5	26	-	-	26	17	28	CL

Table A.6: Erosion Test Results of K-4B Samples

Sample	Erosion Test Results							Critical Shear Stress, lb/ft^2 (N/m^2)
K-4B #1	Water Velocity, ft/s (m/s)	1.64 (0.50)	3.28 (1.00)	6.56 (2.00)	9.84 (3.00)	13.1 (4.00)	16.4 (5.00)	0.25 (12.1)
	Shear Stress, lb/ft^2 (N/m^2)	0.02 (0.80)	0.06 (3.00)	0.33 (15.6)	0.79 (38.0)	1.36 (65.0)	2.51 (120.0)	
	Erosion Rate, in/hr (mm/hr)	0.00 (0.00)	0.00 (0.00)	0.12 (3.00)	2.17 (55.0)	3.08 (78.2)	5.12 (130.0)	
K-4B #2	Water Velocity, ft/s (m/s)	1.64 (0.50)	3.28 (1.00)	6.56 (2.00)	9.84 (3.00)	13.1 (4.00)	16.4 (5.00)	0.26 (10.8)
	Shear Stress, lb/ft^2 (N/m^2)	0.02 (0.80)	0.06 (3.10)	0.25 (12.1)	0.59 (28.1)	1.08 (51.6)	1.89 (90.6)	
	Erosion Rate, in/hr (mm/hr)	0.00 (0.00)	0.00 (0.00)	0.02 (0.40)	0.10 (2.60)	0.50 (12.7)	2.68 (68.0)	
K-4B #3	Water Velocity, ft/s (m/s)	1.64 (0.50)	3.28 (1.00)	6.56 (2.00)	9.84 (3.00)	13.1 (4.00)	-	0.15 (7.00)
	Shear Stress, lb/ft^2 (N/m^2)	0.02 (0.80)	0.06 (3.10)	0.27 (12.7)	0.68 (32.7)	1.29 (62.0)	-	
	Erosion Rate, in/hr (mm/hr)	0.00 (0.00)	0.00 (0.00)	0.20 (0.50)	1.52 (38.6)	2.24 (56.9)	-	
K-4B #4	Water Velocity, ft/s (m/s)	1.64 (0.50)	3.28 (1.00)	4.92 (1.50)	6.56 (2.00)	8.20 (2.50)	9.84 (3.00)	0.05 (2.30)
	Shear Stress, lb/ft^2 (N/m^2)	0.02 (0.80)	0.06 (3.10)	0.16 (7.60)	0.38 (18.0)	0.61 (29.0)	0.89 (42.6)	
	Erosion Rate, in/hr (mm/hr)	0.00 (0.00)	0.20 (0.50)	0.08 (2.00)	1.97 (50.0)	2.28 (58.0)	3.03 (76.9)	
K-4B #5	Water Velocity, ft/s (m/s)	1.64 (0.50)	3.28 (1.00)	6.56 (2.00)	9.84 (3.00)	13.1 (4.00)	16.4 (5.00)	0.24 (11.6)
	Shear Stress, lb/ft^2 (N/m^2)	0.02 (0.80)	0.08 (3.60)	0.30 (14.4)	0.81 (38.8)	1.43 (68.4)	2.15 (103)	
	Erosion Rate, in/hr (mm/hr)	0.00 (0.00)	0.00 (0.00)	0.16 (4.00)	1.62 (41.2)	2.45 (62.2)	2.79 (70.9)	

Bridge 085-0108 on K-4 Highway
(GPS Co-ordinate: 38.7109,-97.6119)

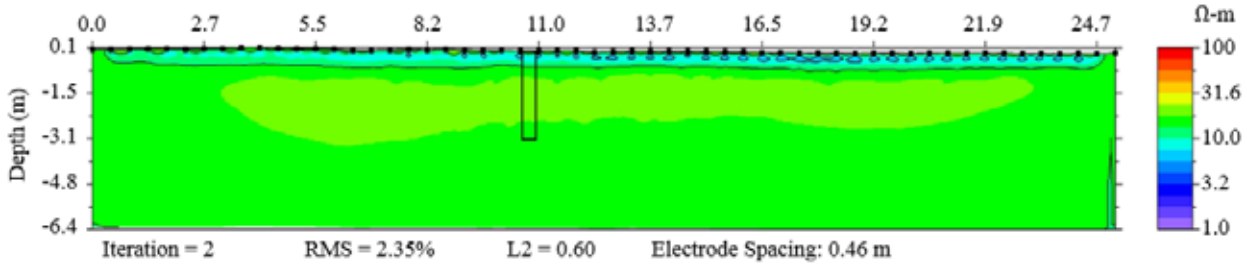

Figure A.7: Inverted Resistivity of K-4A

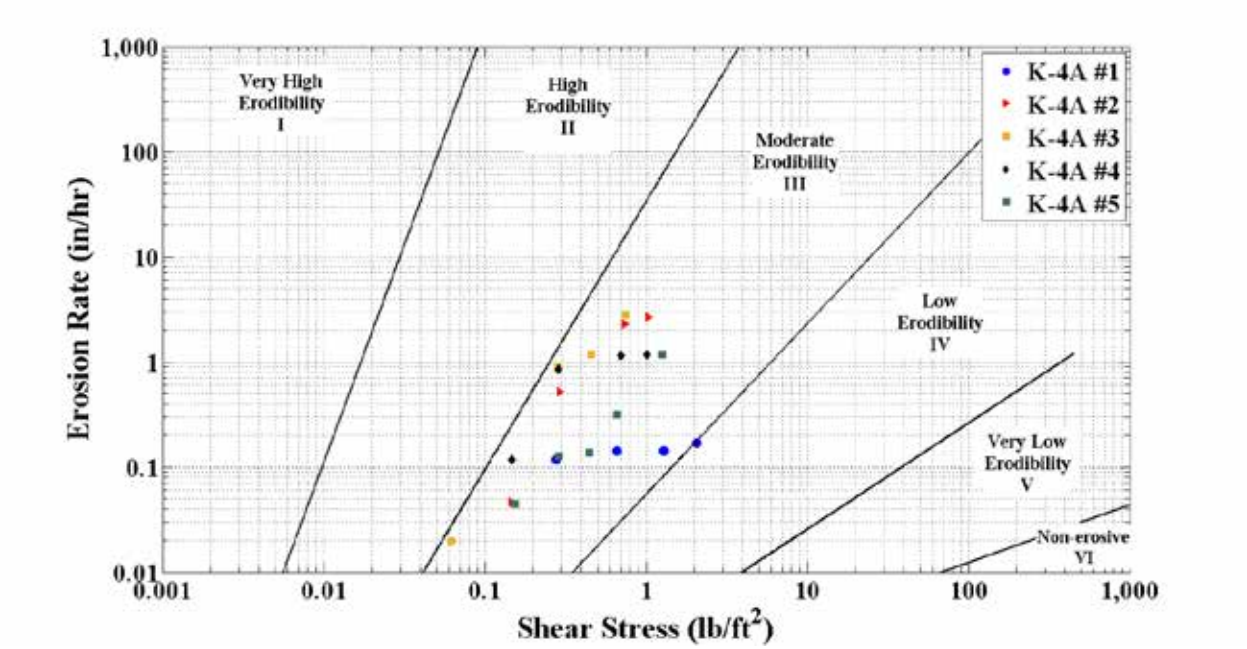

Figure A.8: Erosion Rate versus Shear Stress for K-4A Samples

Table A.7: Classification of K-4A Samples

Sample designation	Water content (%)	Percent finer than 0.075 mm (%)	Mean grain size (mm)	LL	PL	PI	USCS Classification
K-4A #1	40	97	0.010	55	18	37	CH
K-4A #2	30	92	0.014	40	17	23	CL
K-4A #3	23	90	0.016	31	19	12	CL
K-4A #4	24	91	0.017	30	20	10	CL
K-4A #5	27	92	0.017	31	17	14	CL

Table A.8: Erosion Test Results of K-4A Samples

Sample	Erosion Test Results							Critical Shear Stress, lb/ft^2 (N/m^2)
K-4A #1	Water Velocity, ft/s (m/s)	1.64 (0.50)	3.28 (1.00)	6.56 (2.00)	9.84 (3.00)	13.1 (4.00)	16.4 (5.00)	0.21 (9.90)
	Shear Stress, lb/ft^2 (N/m^2)	0.02 (0.80)	0.06 (3.00)	0.28 (13.4)	0.66 (31.6)	1.29 (61.8)	2.07 (99.1)	
	Erosion Rate, in/hr (mm/hr)	0.00 (0.00)	0.00 (0.00)	0.12 (3.00)	0.14 (3.60)	0.14 (3.60)	0.17 (4.30)	
K-4A #2	Water Velocity, ft/s (m/s)	1.64 (0.50)	3.28 (1.00)	4.92 (1.50)	6.56 (2.00)	9.84 (3.00)	11.5 (3.50)	0.11 (5.40)
	Shear Stress, lb/ft^2 (N/m^2)	0.02 (0.80)	0.06 (3.10)	0.14 (6.90)	0.29 (13.9)	0.74 (35.2)	1.03 (49.2)	
	Erosion Rate, in/hr (mm/hr)	0.00 (0.00)	0.00 (0.00)	0.05 (1.20)	0.52 (13.1)	2.28 (57.9)	2.69 (68.3)	
K-4A #3	Water Velocity, ft/s (m/s)	1.64 (0.50)	3.28 (1.00)	6.56 (2.00)	8.20 (2.50)	9.84 (3.00)	-	0.06 (2.90)
	Shear Stress, lb/ft^2 (N/m^2)	0.02 (0.80)	0.06 (3.00)	0.28 (13.6)	0.46 (21.9)	0.75 (35.8)	-	
	Erosion Rate, in/hr (mm/hr)	0.00 (0.00)	0.20 (0.50)	0.88 (22.4)	1.18 (30.0)	2.81 (71.4)	-	
K-4A #4	Water Velocity, ft/s (m/s)	1.64 (0.50)	3.28 (1.00)	4.92 (1.50)	6.56 (2.00)	9.84 (3.00)	11.5 (3.50)	0.09 (4.20)
	Shear Stress, lb/ft^2 (N/m^2)	0.02 (0.80)	0.06 (3.00)	0.15 (7.00)	0.29 (13.8)	0.71 (33.8)	48.7	
	Erosion Rate, in/hr (mm/hr)	0.00 (0.00)	0.00 (0.00)	0.12 (3.00)	0.85 (21.6)	1.14 (29.0)	1.18 (30.0)	
K-4A #5	Water Velocity, ft/s (m/s)	3.28 (1.00)	4.92 (1.50)	6.56 (2.00)	8.20 (2.50)	9.84 (3.00)	13.1 (4.00)	0.08 (4.00)
	Shear Stress, lb/ft^2 (N/m^2)	0.06 (3.00)	0.15 (7.30)	0.29 (13.8)	0.45 (21.4)	0.66 (31.6)	1.26 (60.4)	
	Erosion Rate, in/hr (mm/hr)	0.00 (0.00)	0.04 (1.10)	0.13 (3.20)	0.14 (3.50)	0.31 (8.00)	1.18 (30.0)	

Bridge 050-0067 on US-400 Highway
(GPS Co-ordinate: 37.3402,-95.0983)

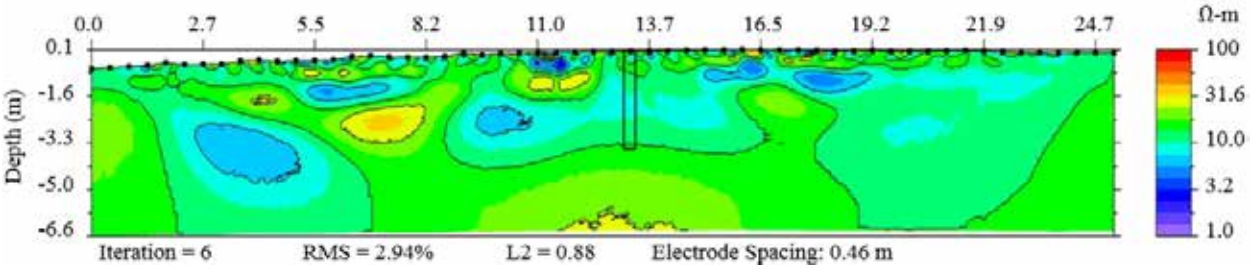

Figure A.9: Inverted Resistivity of US-400

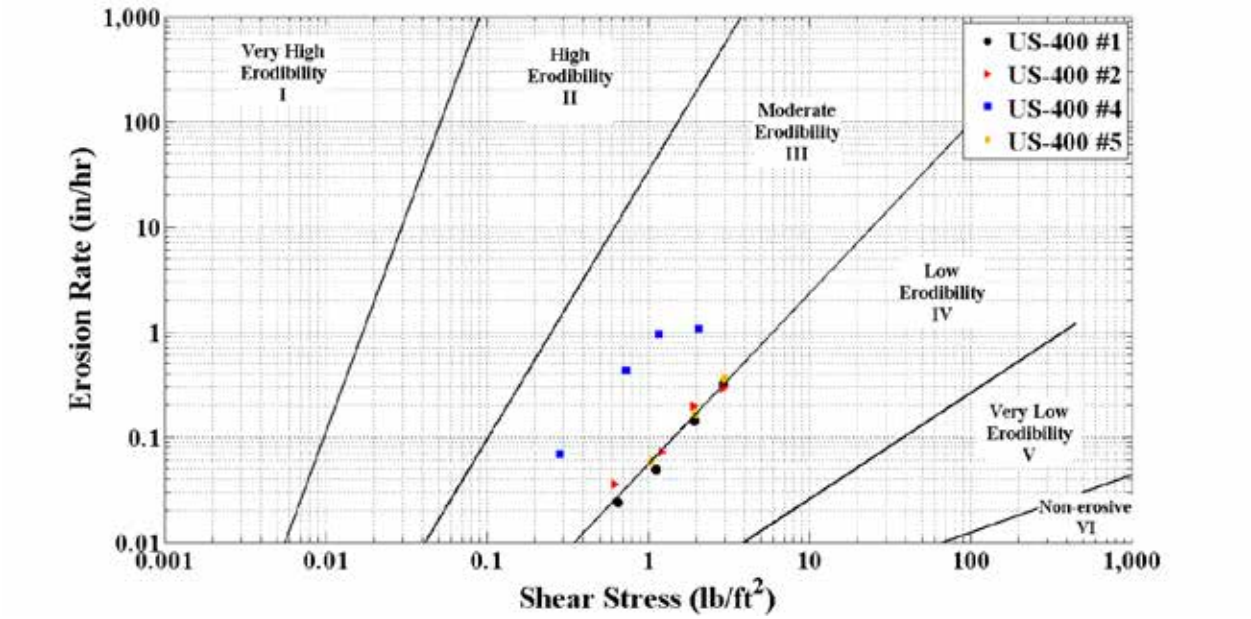

Figure A.10: Erosion Rate versus Shear Stress for US-400 Samples

Table A.9: Classification of US-400 Samples

Sample designation	Water content (%)	Percent finer than 0.075 mm (%)	Mean grain size (mm)	LL	PL	PI	USCS classification
US-400 #1	21	89	0.012	41	14	27	CL
US-400 #2	21	97	0.007	53	16	37	CH
US-400 #4	23	96	0.007	53	15	38	CH
US-400 #5	25	95	0.012	41	14	27	CL

Table A.10: Erosion Test Results of US-400 Samples

Sample	Erosion Test Results							Critical Shear Stress, lb/ft^2 (N/m^2)
US400 #1	Water Velocity, ft/s (m/s)	3.28 (1.00)	6.56 (2.00)	9.84 (3.00)	13.12 (4.00)	16.40 (5.00)	19.69 (6.00)	0.52 (25.10)
	Shear Stress, lb/ft^2 (N/m^2)	0.06 (2.90)	0.26 (12.5)	0.65 (31.1)	1.12 (53.80)	1.94 (92.8)	2.91 (139.5)	
	Erosion Rate, in/hr (mm/hr)	0.00 (0.00)	0.00 (0.00)	0.02 (0.60)	0.05 (1.30)	0.14 (3.60)	0.31 (8.00)	
US400 #2	Water Velocity, ft/s (m/s)	3.28 (1.00)	6.56 (2.00)	9.84 (3.00)	13.12 (4.00)	16.40 (5.00)	19.69 (6.00)	0.44 (21.10)
	Shear Stress, lb/ft^2 (N/m^2)	0.06 (2.90)	0.25 (11.9)	0.62 (29.6)	1.22 (58.20)	1.91 (91.6)	2.92 (140.0)	
	Erosion Rate, in/hr (mm/hr)	0.00 (0.00)	0.00 (0.00)	0.04 (0.90)	0.07 (1.80)	0.20 (5.00)	0.30 (7.50)	
US400 #4	Water Velocity, ft/s (m/s)	1.64 (0.50)	3.28 (1.00)	6.56 (2.00)	9.84 (3.00)	13.12 (4.00)	16.40 (5.00)	0.27 (12.70)
	Shear Stress, lb/ft^2 (N/m^2)	0.02 (0.80)	0.06 (3.00)	0.28 (13.6)	0.73 (35.1)	1.16 (55.6)	2.06 (98.80)	
	Erosion Rate, in/hr (mm/hr)	0.00 (0.00)	0.00 (0.00)	0.07 (1.80)	0.43 (10.80)	0.94 (24.0)	1.08 (27.4)	
US400 #5	Water Velocity, ft/s (m/s)	3.28 (1.00)	6.56 (2.00)	9.84 (3.00)	13.12 (4.00)	16.40 (5.00)	19.69 (6.00)	0.77 (36.80)
	Shear Stress, lb/ft^2 (N/m^2)	0.06 (2.70)	0.21 (9.90)	0.51 (24.6)	1.05 (50.20)	1.96 (93.8)	1.99 (143.1)	
	Erosion Rate, in/hr (mm/hr)	0.00 (0.00)	0.00 (0.00)	0.00 (0.00)	0.06 (1.05)	0.17 (4.30)	0.36 (9.20)	

Bridge 019-0056 on K-126 Highway
(GPS Co-ordinate: 37.4110,-94.6545)

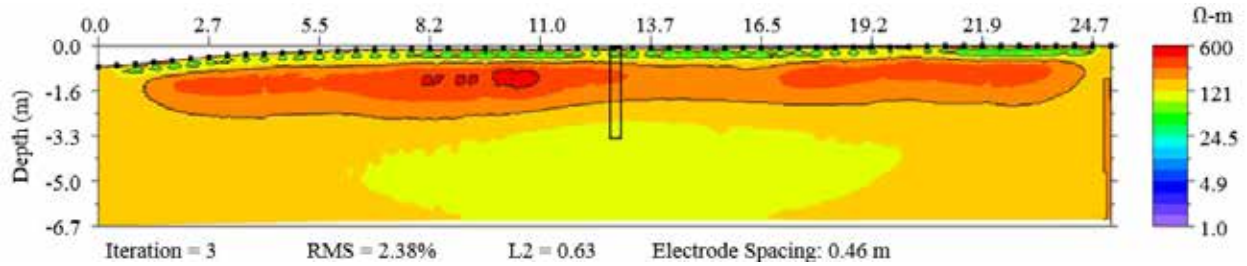

Figure A.11: Inverted Resistivity of K-126

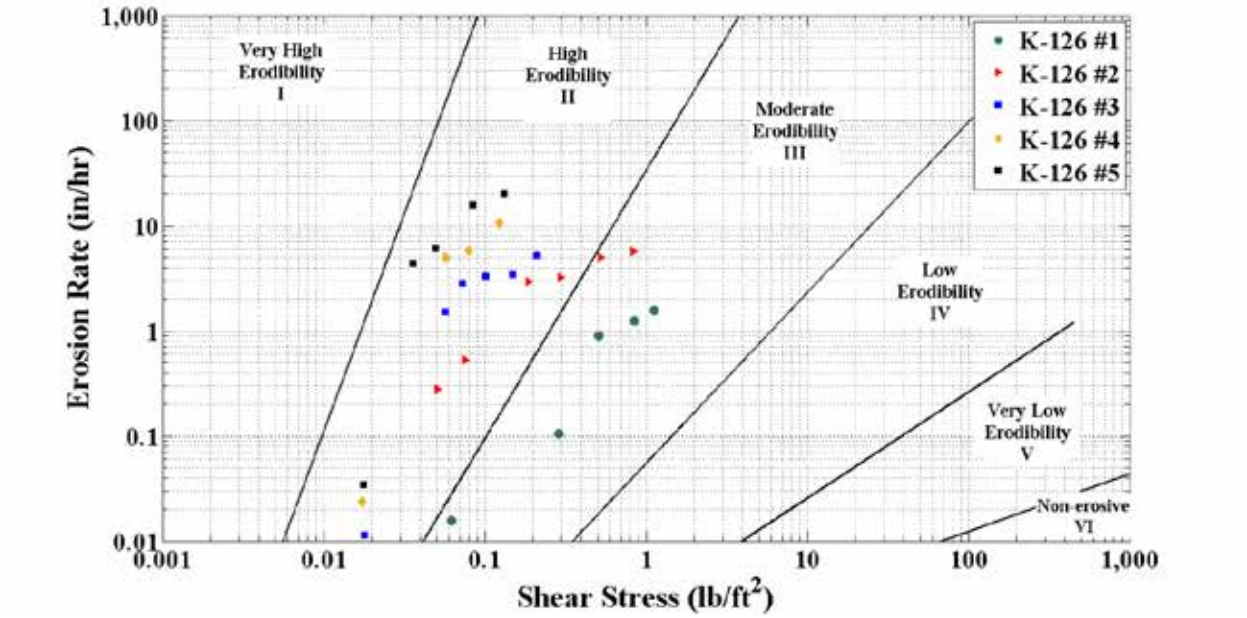

Figure A.12: Erosion Rate versus Shear Stress for K-126 Samples

Table A.11: Classification of K-126 Samples

Sample designation	Water content (%)	Percent finer than 0.075 mm (%)	Mean grain size (mm)	LL	PL	PI	USCS Classification
K-126 #1	21	73	0.019	31	22	9	CL
K-126 #2	18	49	0.082	28	18	10	SC
K-126 #3	25	12	1.800	26	18	8	SC
K-126 #4	17	12	1.640	27	20	7	SC
K-126 #5	24	6	1.920	26	19	7	SW-SC

Table A.12: Erosion Test Results of K-126 Samples

Sample	Erosion Test Results							Critical Shear Stress, lb/ft^2 (N/m^2)
K-126 #1	Water Velocity, ft/s (m/s)	1.64 (0.50)	3.28 (1.0)	6.56 (2.00)	8.20 (2.50)	9.84 (3.00)	11.48 (3.50)	0.03 (1.40)
	Shear Stress, lb/ft^2 (N/m^2)	0.02 (0.80)	0.06 (3.00)	0.29 (13.90)	0.51 (24.50)	0.84 (40.30)	1.13 (53.90)	
	Erosion Rate, in/hr (mm/hr)	0.00 (0.00)	0.02 (0.40)	0.11 (2.70)	0.90 (22.80)	1.24 (31.50)	1.57 (40.00)	
K-126 #2	Water Velocity, ft/s (m/s)	2.62 (0.80)	3.28 (1.0)	4.92 (1.50)	6.56 (2.00)	8.20 (2.50)	9.84 (3.00)	0.03 (1.30)
	Shear Stress, lb/ft^2 (N/m^2)	0.05 (2.40)	0.08 (3.60)	0.19 (9.00)	0.29 (14.10)	0.52 (25.00)	0.83 (39.80)	
	Erosion Rate, in/hr (mm/hr)	0.28 (7.00)	0.52 (13.3)	2.91 (74.00)	3.20 (81.30)	4.97 (126.3)	5.74 (145.70)	
K-126 #3	Water Velocity, ft/s (m/s)	1.64 (0.50)	2.62 (0.80)	2.96 (0.90)	3.28 (1.0)	4.27 (1.30)	4.92 (1.50)	0.02 (0.90)
	Shear Stress, lb/ft^2 (N/m^2)	0.02 (0.90)	0.06 (2.70)	0.07 (3.50)	0.10 (4.90)	0.15 (7.20)	0.21 (10.20)	
	Erosion Rate, in/hr (mm/hr)	0.01 (0.30)	1.50 (38.2)	2.85 (72.30)	3.27 (83.10)	3.42 (86.80)	5.20 (132.00)	
K-126 #4	Water Velocity, ft/s (m/s)	0.98 (0.30)	1.64 (0.50)	2.62 (0.80)	2.96 (0.90)	3.60 (1.10)	-	0.01 (0.70)
	Shear Stress, lb/ft^2 (N/m^2)	0.01 (0.30)	0.02 (0.80)	0.06 (2.70)	0.08 (3.80)	0.12 (5.90)	-	
	Erosion Rate, in/hr (mm/hr)	0.00 (0.00)	0.02 (0.60)	4.96 (126.0)	5.86 (148.8)	10.63 (270.0)	-	
K-126 #5	Water Velocity, ft/s (m/s)	0.98 (0.30)	1.64 (0.50)	1.97 (0.60)	2.62 (0.80)	2.96 (0.90)	3.60 (1.10)	0.01 (0.60)
	Shear Stress, lb/ft^2 (N/m^2)	0.01 (0.30)	0.02 (0.90)	0.04 (1.70)	0.05 (2.40)	0.09 (4.10)	0.13 (6.30)	
	Erosion Rate, in/hr (mm/hr)	0.00 (0.00)	0.04 (0.90)	4.36 (110.8)	6.02 (153.0)	15.75 (400.0)	19.87 (504.70)	

Bridge 043-0030 on US-75 Highway
(GPS Co-ordinate: 39.5459,-95.7483)

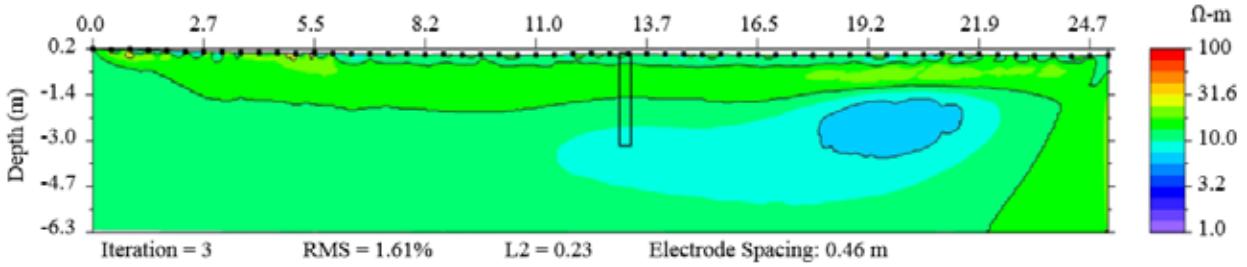

Figure A.13: Inverted Resistivity of US-75

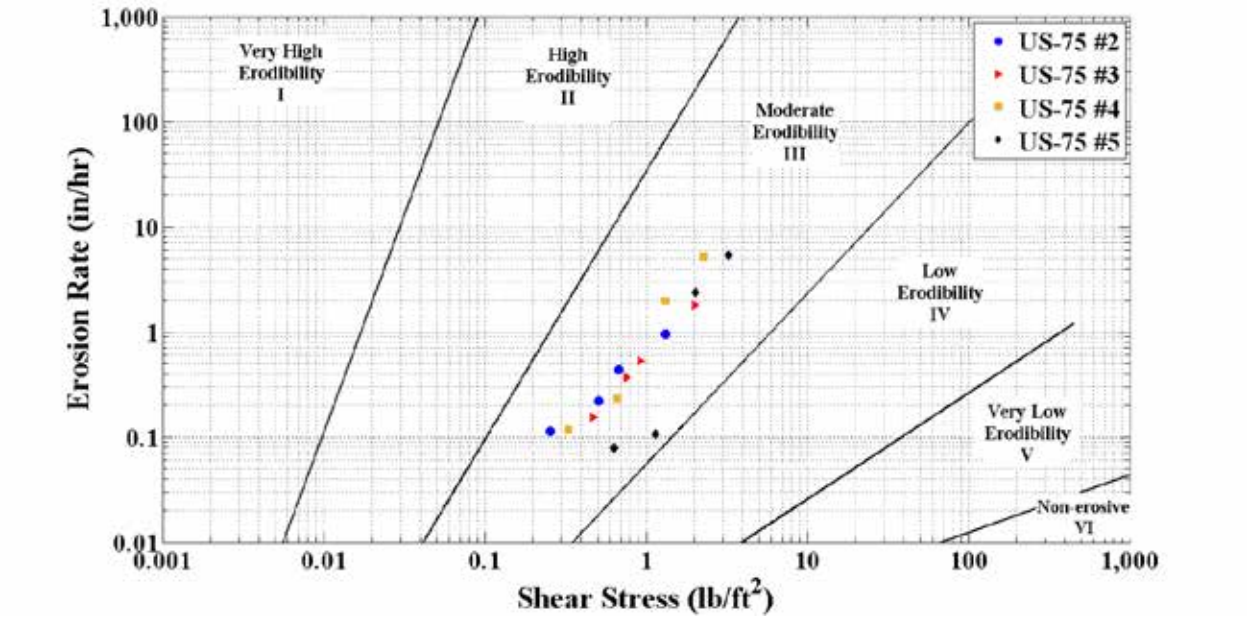

Figure A.14: Erosion Rate versus Shear Stress for US-75 Samples

Table A.13: Classification of US-75 Samples

Sample designation	Water content (%)	Percent finer than 0.075 mm (%)	Mean grain size (mm)	LL	PL	PI	USCS Classification
US-75 #2	36	99	0.015	53	23	30	CH
US-75 #3	28	99	0.011	58	23	35	CH
US-75 #4	25	98	0.015	47	24	23	CL
US-75 #5	30	96	0.009	50	26	24	CH

Table A.14: Erosion Test Results of US-75 Samples

Sample	Erosion Test Results							Critical Shear Stress, lb/ft^2 (N/m^2)
US-75 #2	Water Velocity, ft/s (m/s)	1.64 (0.50)	3.28 (1.00)	6.56 (2.00)	8.20 (2.50)	9.84 (3.00)	13.12 (4.00)	0.17 (8.20)
	Shear Stress, lb/ft^2 (N/m^2)	0.02 (0.80)	0.06 (2.80)	0.26 (12.30)	0.51 (24.50)	0.68 (32.40)	1.32 (63.00)	
	Erosion Rate, in/hr (mm/hr)	0.00 (0.00)	0.00 (0.00)	0.11 (2.90)	0.22 (5.60)	0.44 (11.10)	0.96 (24.40)	
US-75 #3	Water Velocity, ft/s (m/s)	3.28 (1.00)	6.56 (2.00)	8.20 (2.50)	9.84 (3.00)	11.48 (3.50)	16.40 (5.00)	0.39 (18.70)
	Shear Stress, lb/ft^2 (N/m^2)	0.06 (2.80)	0.24 (11.40)	0.47 (22.30)	0.76 (36.20)	0.93 (44.40)	2.02 (96.60)	
	Erosion Rate, in/hr (mm/hr)	0.00 (0.00)	0.00 (0.00)	3.90 (0.15)	9.40 (0.37)	0.52 (13.30)	1.79 (45.50)	
US-75 #4	Water Velocity, ft/s (m/s)	1.64 (0.50)	3.28 (1.00)	6.56 (2.00)	9.84 (3.00)	13.12 (4.00)	16.40 (5.00)	0.32 (15.50)
	Shear Stress, lb/ft^2 (N/m^2)	0.02 (0.80)	0.06 (3.00)	0.33 (15.80)	0.66 (31.50)	1.32 (63.20)	2.27 (108.8)	
	Erosion Rate, in/hr (mm/hr)	0.00 (0.00)	0.00 (0.00)	0.12 (3.00)	0.23 (5.90)	1.95 (49.50)	5.15 (130.9)	
US-75 #5	Water Velocity, ft/s (m/s)	3.28 (1.00)	6.56 (2.00)	9.84 (3.00)	13.12 (4.00)	16.40 (5.00)	19.69 (6.00)	0.51 (24.30)
	Shear Stress, lb/ft^2 (N/m^2)	0.06 (2.80)	0.24 (11.60)	0.64 (30.60)	1.15 (55.20)	2.05 (98.10)	3.26 (156.2)	
	Erosion Rate, in/hr (mm/hr)	0.00 (0.00)	0.00 (0.00)	0.08 (2.00)	0.11 (2.70)	2.36 (60.00)	5.40 (137.1)	

Bridge 007-0013 on US-73 Highway
(GPS Co-ordinate: 39.9686,-95.5550)

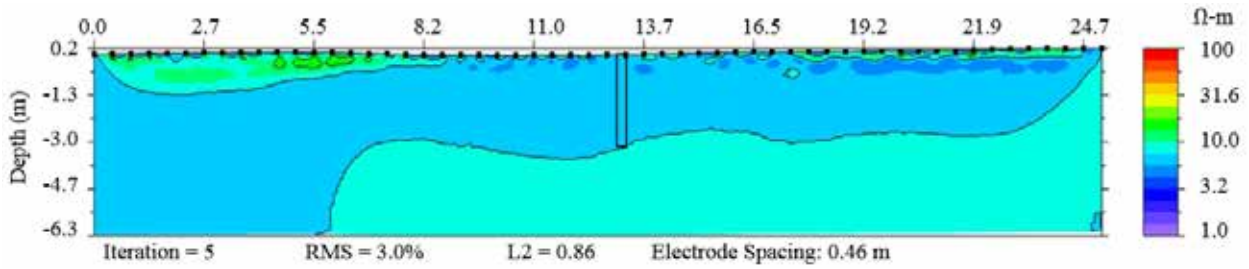

Figure A.15: Inverted Resistivity of US-73

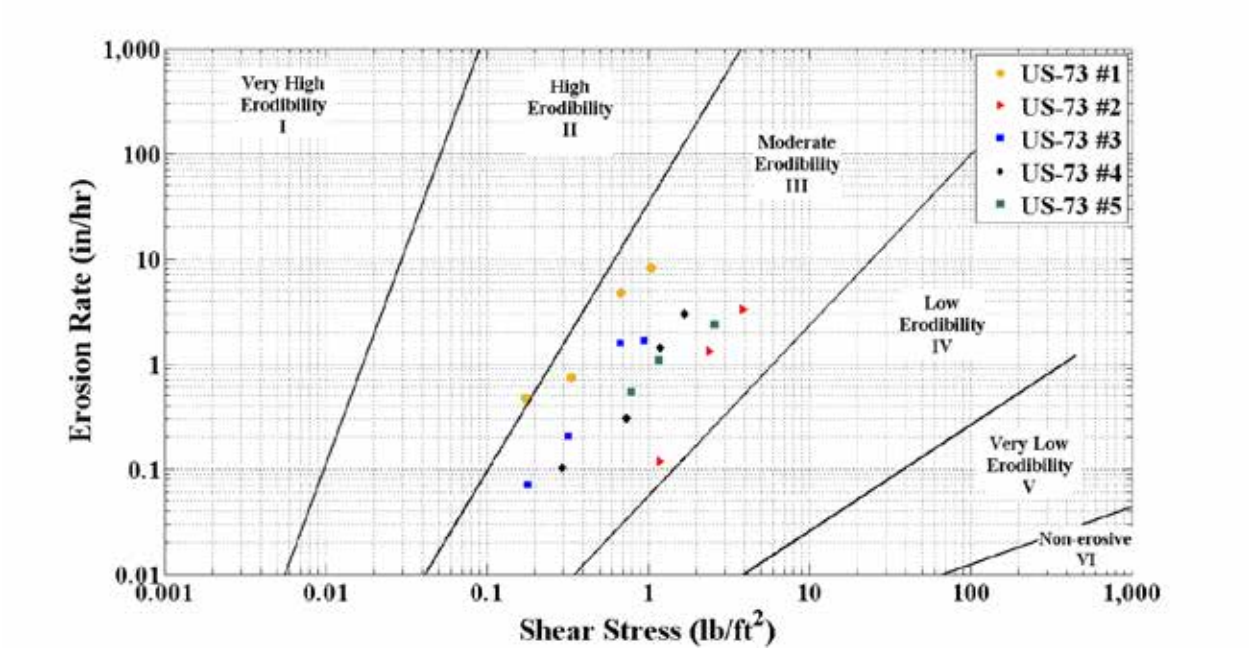

Figure A.16: Erosion Rate versus Shear Stress for US-73 Samples

Table A.15: Classification of US-73 Samples

Sample designation	Water content (%)	Percent finer than 0.075 mm (%)	Mean grain size (mm)	LL	PL	PI	USCS Classification
US-73 #1	27	95	0.010	43	16	27	CL
US-73 #2	28	97	0.006	50	17	33	CH
US-73 #3	27	98	0.007	56	17	39	CH
US-73 #4	28	98	0.004	51	17	34	CH
US-73 #5	28	96	0.010	45	16	29	CL

Table A.16: Erosion Test Results of US-73 Samples

Sample	Erosion Test Results							Critical Shear Stress, lb/ft^2 (N/m^2)
US-73 #1	Water Velocity, ft/s (m/s)	1.64 (0.50)	3.28 (1.00)	4.92 (1.50)	6.56 (2.00)	8.20 (2.50)	9.84 (3.00)	0.15 (7.40)
	Shear Stress, lb/ft^2 (N/m^2)	0.02 (0.80)	0.07 (3.10)	0.18 (8.40)	0.37 (16.10)	0.68 (32.4)	1.05 (50.10)	
	Erosion Rate, in/hr (mm/hr)	0.00 (0.00)	0.00 (0.00)	0.47 (12.00)	0.75 (19.00)	4.72 (120.0)	8.13 (206.70)	
US-73 #2	Water Velocity, ft/s (m/s)	3.28 (1.00)	6.56 (2.00)	9.84 (3.00)	13.12 (4.00)	16.40 (5.00)	19.69 (6.00)	1.05 (50.10)
	Shear Stress, lb/ft^2 (N/m^2)	0.06 (2.90)	0.28 (13.5)	0.46 (22.10)	1.18 (56.40)	2.38 (114.1)	3.88 (185.90)	
	Erosion Rate, in/hr (mm/hr)	0.00 (0.00)	0.00 (0.00)	0.00 (0.00)	0.12 (3.00)	1.32 (33.50)	3.31 (84.00)	
US-73 #3	Water Velocity, ft/s (m/s)	1.64 (0.50)	3.28 (1.00)	4.92 (1.50)	6.56 (2.00)	8.20 (2.50)	9.84 (3.00)	0.16 (7.70)
	Shear Stress, lb/ft^2 (N/m^2)	0.02 (0.80)	0.07 (3.20)	0.18 (8.70)	0.32 (15.40)	0.68 (32.60)	0.95 (45.50)	
	Erosion Rate, in/hr (mm/hr)	0.00 (0.00)	0.00 (0.00)	0.07 (1.80)	0.21 (5.20)	1.57 (40.00)	1.66 (42.20)	
US-73 #4	Water Velocity, ft/s (m/s)	1.64 (0.50)	3.28 (1.00)	6.56 (2.00)	9.84 (3.00)	11.48 (3.50)	13.12 (4.00)	0.19 (9.00)
	Shear Stress, lb/ft^2 (N/m^2)	0.02 (0.80)	0.07 (3.40)	0.29 (14.10)	0.74 (35.40)	1.19 (57.10)	1.69 (81.00)	
	Erosion Rate, in/hr (mm/hr)	0.00 (0.00)	0.00 (0.00)	0.10 (2.60)	0.31 (7.80)	1.43 (36.30)	3.01 (76.40)	
US-73 #5	Water Velocity, ft/s (m/s)	1.64 (0.50)	3.28 (1.00)	6.56 (2.00)	9.84 (3.00)	13.12 (4.00)	16.40 (5.00)	0.56 (26.80)
	Shear Stress, lb/ft^2 (N/m^2)	0.02 (0.80)	0.07 (3.30)	0.29 (13.70)	0.79 (37.60)	1.17 (55.60)	2.58 (123.40)	
	Erosion Rate, in/hr (mm/hr)	0.00 (0.00)	0.00 (0.00)	0.00 (0.00)	0.54 (13.70)	1.10 (27.90)	2.36 (60.00)	

Bridge 015-0005 on US-24 Highway
(GPS Co-ordinate: 39.3647,-97.8126)

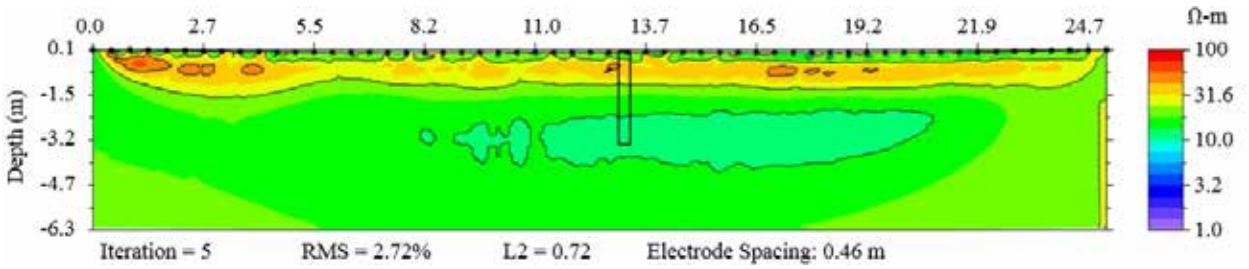

Figure A.17: Inverted Resistivity of US-24

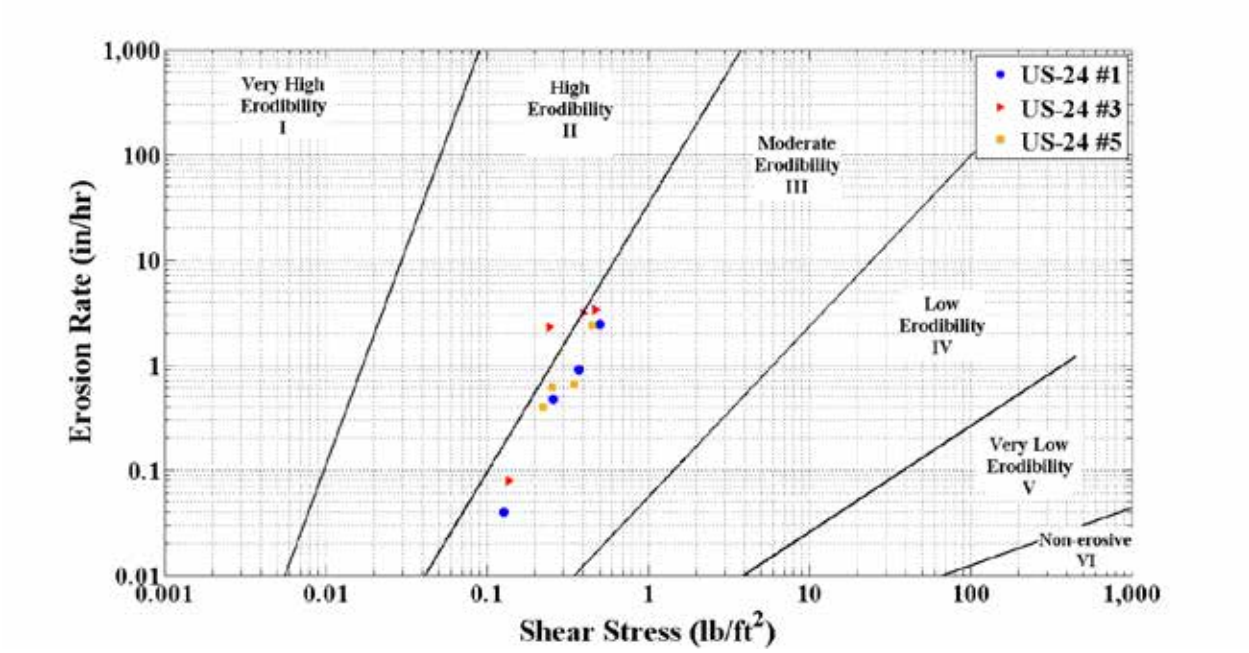

Figure A.18: Erosion Rate versus Shear Stress for US-24 Samples

Table A.17: Classification of US-24 Samples

Sample designation	Water content (%)	Percent finer than 0.075 mm (%)	Mean grain size (mm)	LL	PL	PI	USCS Classification
US-24 #1	33	96	0.023	46	21	25	CL
US-24 #3	31	96	0.023	41	24	17	CL
US-24 #5	29	97	0.023	36	19	17	CL

Table A.18: Erosion Test Results of US-24 Samples

Sample	Erosion Test Results							Critical Shear Stress, lb/ft^2 (N/m^2)
US-24 #1	Water Velocity, ft/s (m/s)	1.64 (0.50)	3.28 (1.00)	4.92 (1.50)	5.91 (1.80)	6.56 (2.00)	7.55 (2.30)	0.06 (2.70)
	Shear Stress, lb/ft^2 (N/m^2)	0.02 (0.80)	0.07 (3.30)	0.13 (6.10)	0.26 (12.30)	0.37 (17.90)	0.51 (24.20)	
	Erosion Rate, in/hr (mm/hr)	0.00 (0.00)	0.00 (0.00)	0.04 (1.00)	0.47 (12.00)	0.90 (22.90)	2.43 (61.80)	
US-24 #3	Water Velocity, ft/s (m/s)	1.64 (0.50)	3.28 (1.00)	4.92 (1.50)	5.91 (1.80)	6.56 (2.00)	7.55 (2.30)	0.08 (3.60)
	Shear Stress, lb/ft^2 (N/m^2)	0.02 (0.80)	0.07 (3.20)	0.14 (6.60)	0.25 (11.80)	0.40 (19.20)	0.48 (22.70)	
	Erosion Rate, in/hr (mm/hr)	0.00 (0.00)	0.00 (0.00)	0.08 (2.00)	2.28 (57.90)	3.11 (79.10)	3.37 (85.70)	
US-24 #5	Water Velocity, ft/s (m/s)	1.64 (0.50)	3.28 (1.00)	4.92 (1.50)	5.91 (1.80)	6.56 (2.00)	7.55 (2.30)	0.19 (9.30)
	Shear Stress, lb/ft^2 (N/m^2)	0.02 (0.80)	0.06 (3.10)	0.22 (10.70)	0.26 (12.30)	0.35 (16.70)	0.45 (21.60)	
	Erosion Rate, in/hr (mm/hr)	0.00 (0.00)	0.00 (0.00)	0.369 (10.00)	0.62 (15.70)	0.65 (16.60)	2.36 (60.00)	

Bridge 054-0030 on US-69 Highway
(GPS Co-ordinate: 38.2363,-94.6907)

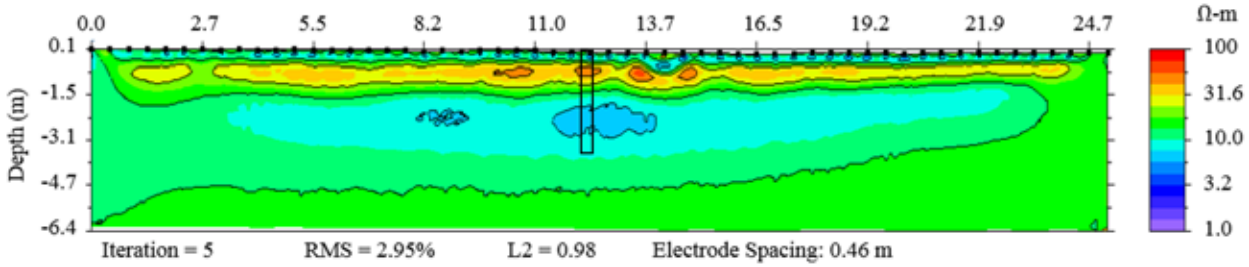

Figure A.19: Inverted Resistivity of US-69

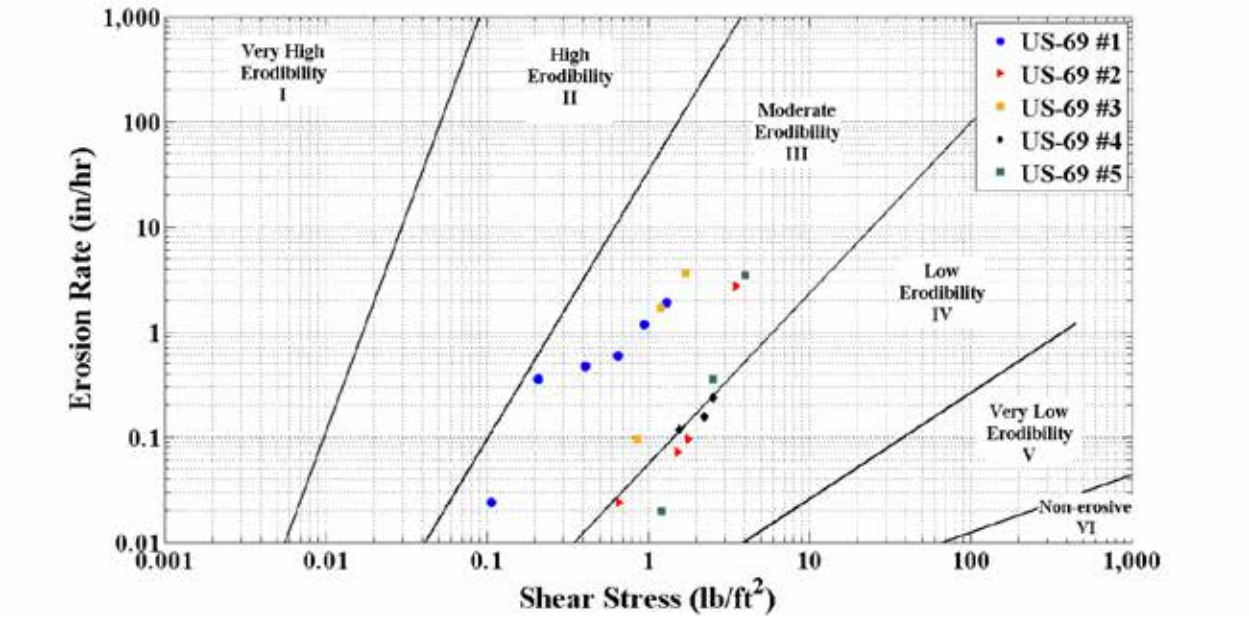

Figure A.20: Erosion Rate versus Shear Stress for US-69 Samples

Table A.19: Classification of US-69 Samples

Sample designation	Water content (%)	Percent finer than 0.075 mm (%)	Mean grain size (mm)	LL	PL	PI	USCS Classification
US-69 #1	16	61	0.031	32	29	3	ML
US-69 #2	31	98	0.008	45	10	35	CL
US-69 #3	30	99	0.005	48	20	28	CL
US-69 #4	29	99	0.006	41	24	17	CL
US-69 #5	26	99	0.010	48	17	21	CL

Table A.20: Erosion Test Results of US-69 Samples

Sample	Erosion Test Results							Critical Shear Stress, lb/ft^2 (N/m^2)
US-69 #1	Water Velocity, ft/s (m/s)	3.28 (1.00)	4.92 (1.50)	6.56 (2.00)	8.20 (2.50)	9.84 (3.00)	11.48 (3.50)	0.07 (3.50)
	Shear Stress, lb/ft^2 (N/m^2)	0.11 (5.10)	0.21 (10.00)	0.41 (19.50)	0.65 (31.30)	0.95 (45.50)	1.31 (62.80)	
	Erosion Rate, in/hr (mm/hr)	0.02 (0.60)	0.35 (9.00)	0.47 (12.0)0	0.59 (15.00)	1.18 (30.00)	1.89 (48.00)	
US-69 #2	Water Velocity, ft/s (m/s)	3.28 (1.00)	6.56 (2.00)	9.84 (3.00)	13.12 (4.00)	16.40 (5.00)	19.69 (6.00)	0.66 (31.70)
	Shear Stress, lb/ft^2 (N/m^2)	0.05 (2.60)	0.29 (13.90)	0.66 (31.70)	1.53 (73.40)	1.79 (85.60)	3.50 (167.4)	
	Erosion Rate, in/hr (mm/hr)	0.00 (0.00)	0.00 (0.00)	0.02 (0.60)	0.07 (1.80)	0.09 (2.40)	2.70 (68.60)	
US-69 #3	Water Velocity, ft/s (m/s)	3.28 (1.00)	6.56 (2.00)	9.84 (3.00)	11.48 (3.50)	3.12 (4.00)	-	0.81 (38.90)
	Shear Stress, lb/ft^2 (N/m^2)	0.06 (3.10)	0.26 (12.30)	0.85 (40.80)	1.99 (57.40)	1.71 (82.00)	-	
	Erosion Rate, in/hr (mm/hr)	0.00 (0.00)	0.00 (0.00)	0.09 (2.40)	1.70 (43.10)	3.60 (91.40)	-	
US-69 #4	Water Velocity, ft/s (m/s)	3.28 (1.00)	6.56 (2.00)	9.84 (3.00)	13.12 (4.00)	16.40 (5.00)	19.69 (6.00)	0.95 (45.70)
	Shear Stress, lb/ft^2 (N/m^2)	0.07 (3.20)	0.29 (13.90)	0.85 (40.80)	1.57 (75.00)	2.24 (107.2)	2.54 (121.5)	
	Erosion Rate, in/hr (mm/hr)	0.00 (0.00)	0.00 (0.00)	0.00 (0.00)	0.11 (3.00)	0.16 (4.00)	0.24 (6.00)	
US-69 #5	Water Velocity, ft/s (m/s)	3.28 (1.00)	6.56 (2.00)	9.84 (3.00)	13.12 (4.00)	16.40 (5.00)	19.69 (6.00)	0.91 (43.70)
	Shear Stress, lb/ft^2 (N/m^2)	0.06 (3.0)	0.28 (13.20)	0.64 (30.60)	1.21 (58.00)	2.50 (119.7)	4.04 (193.5)	
	Erosion Rate, in/hr (mm/hr)	0.00 (0.00)	0.00 (0.00)	0.00 (0.00)	0.02 (0.50)	0.35 (9.00)	3.46 (88.00)	

Bridge 011-0027 on US-166 Highway
(GPS Co-ordinate: 37.0324, -95.0511)

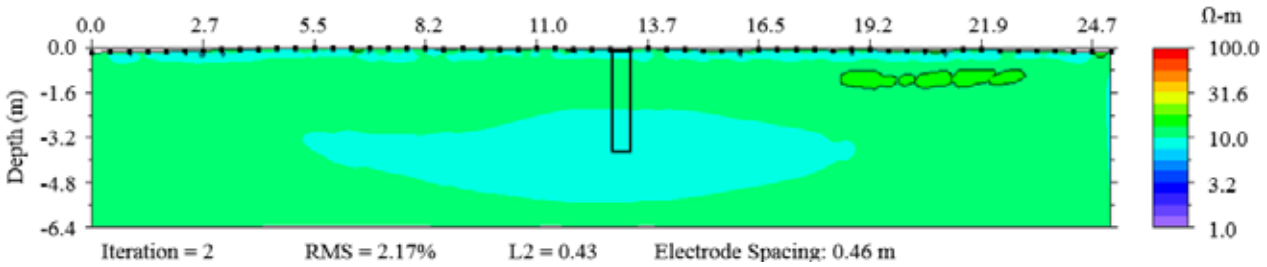

Figure A.21: Inverted Resistivity of US-166B

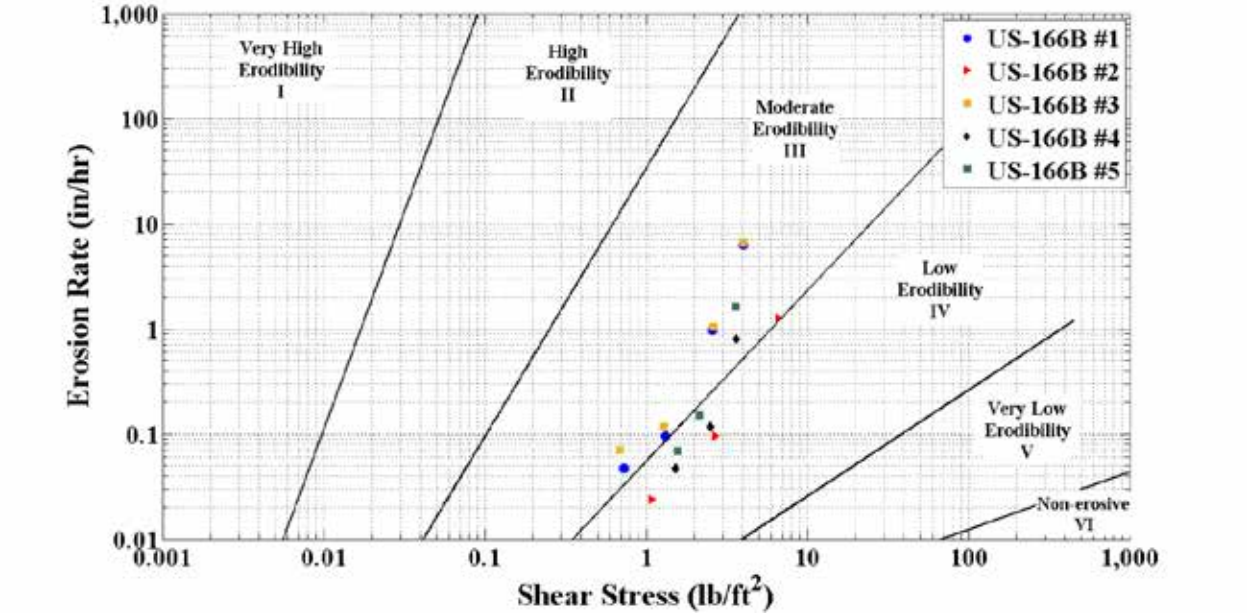

Figure A.22: Erosion Rate versus Shear Stress for US-166B Samples

Table A.21: Classification of US-166B Samples

Sample designation	Water content (%)	Percent finer than 0.075 mm (%)	Mean grain size (mm)	LL	PL	PI	USCS Classification
US-166B #1	28	99	0.006	54	19	35	CH
US-166B #2	28	94	0.011	40	23	17	CL
US-166B #3	29	94	0.014	39	16	23	CL
US-166B #4	30	98	0.007	50	20	30	CH
US-166B #5	30	98	0.009	43	21	22	CL

Table A.22: Erosion Test Results of US-166B Samples

Sample	Erosion Test Results							Critical Shear Stress, lb/ft^2 (N/m^2)
US-166B #1	Water Velocity, ft/s (m/s)	3.28 (1.00)	6.56 (2.00)	9.84 (3.00)	13.12 (4.00)	16.40 (5.00)	19.69 (6.00)	0.64 (30.50)
	Shear Stress, lb/ft^2 (N/m^2)	0.07 (3.20)	0.37 (17.50)	0.73 (34.90)	1.32 (63.40)	2.59 (124.1)	4.04 (193.5)	
	Erosion Rate, in/hr (mm/hr)	0.00 (0.00)	0.00 (0.00)	0.05 (1.20)	0.09 (2.40)	0.97 (24.60)	6.26 (159.0)	
US-166B #2	Water Velocity, ft/s (m/s)	3.28 (1.00)	6.56 (2.00)	9.84 (3.00)	13.12 (4.00)	16.40 (5.00)	19.69 (6.00)	1.05 (50.30)
	Shear Stress, lb/ft^2 (N/m^2)	0.05 (2.50)	0.31 (15.00)	0.73 (34.90)	1.09 (52.00)	2.68 (128.1)	6.58 (315.0)	
	Erosion Rate, in/hr (mm/hr)	0.00 (0.00)	0.00 (0.00)	0.00 (0.00)	0.02 (0.60)	0.09 (2.40)	1.27 (32.30)	
US-166B #3	Water Velocity, ft/s (m/s)	3.28 (1.00)	6.56 (2.00)	9.84 (3.00)	13.12 (4.00)	16.40 (5.00)	19.69 (6.00)	0.60 (28.50)
	Shear Stress, lb/ft^2 (N/m^2)	0.07 (3.30)	0.33 (16.00)	0.68 (32.60)	1.29 (62.00)	2.61 (125.0)	4.04 (193.5)	
	Erosion Rate, in/hr (mm/hr)	0.00 (0.00)	0.00 (0.00)	0.07 (1.80)	0.12 (3.00)	1.04 (26.40)	6.69 (170.0)	
US-166B #4	Water Velocity, ft/s (m/s)	3.28 (1.00)	6.56 (2.00)	9.84 (3.00)	13.12 (4.00)	16.40 (5.00)	19.69 (6.00)	1.44 (69.10)
	Shear Stress, lb/ft^2 (N/m^2)	0.07 (3.30)	0.32 (15.30)	0.71 (33.80)	1.52 (73.00)	2.52 (120.6)	3.67 (175.5)	
	Erosion Rate, in/hr (mm/hr)	0.00 (0.00)	0.00 (0.00)	0.00 (0.00)	0.05 (1.20)	0.12 (3.00)	0.80 (20.40)	
US-166B #5	Water Velocity, ft/s (m/s)	3.28 (1.00)	6.56 (2.00)	9.84 (3.00)	13.12 (4.00)	16.40 (5.00)	19.69 (6.00)	1.48 (71.10)
	Shear Stress, lb/ft^2 (N/m^2)	0.06 (3.10)	0.27 (13.00)	0.74 (35.60)	1.57 (75.00)	2.14 (102.5)	3.62 (173.3)	
	Erosion Rate, in/hr (mm/hr)	0.00 (0.00)	0.00 (0.00)	0.00 (0.00)	0.07 (1.80)	0.15 (3.80)	1.63 (41.40)	

Bridge 006-0005 on US-54 Highway
(GPS Co-ordinate: 37.8489,-94.7025)

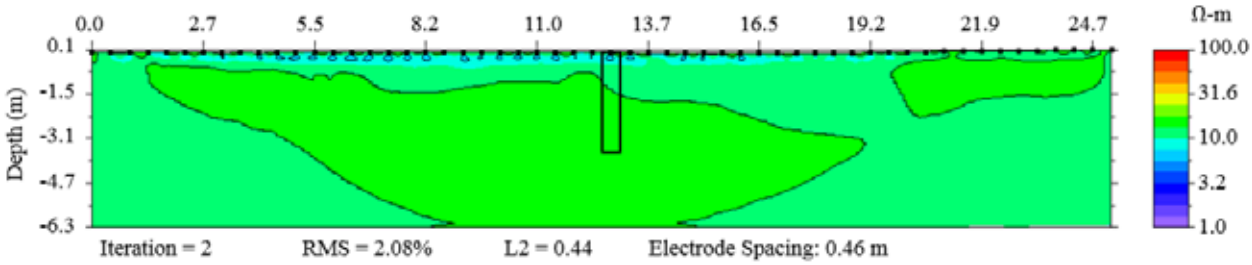

Figure A.23: Inverted Resistivity of US-54

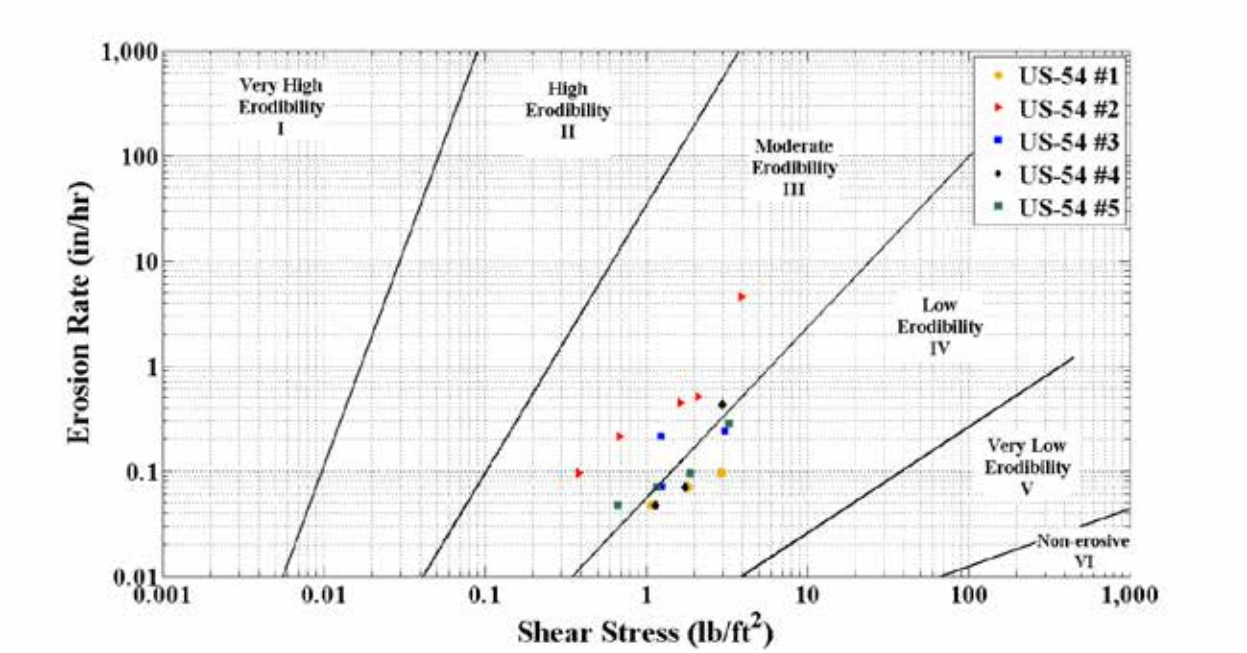

Figure A.24: Erosion Rate versus Shear Stress for US-54 Samples

Table A.23: Classification of US-54 Samples

Sample designation	Water content (%)	Percent finer than 0.075 mm (%)	Mean grain size (mm)	LL	PL	PI	USCS Classification
US-54 #1	23	99	0.007	41	20	21	CL
US-54 #2	24	99	0.008	42	22	20	CL
US-54 #3	25	98	0.007	37	19	18	CL
US-54 #4	26	96	0.011	36	20	16	CL
US-54 #5	26	92	0.012	36	16	20	CL

Table A.24: Erosion Test Results of US-54 Samples

Sample	Erosion Test Results							Critical Shear Stress, lb/ft^2 (N/m^2)
US-54 #1	Water Velocity, ft/s (m/s)	3.28 (1.00)	6.56 (2.00)	9.84 (3.00)	13.12 (4.00)	16.40 (5.00)	19.69 (6.00)	1.04 (49.80)
	Shear Stress, lb/ft^2 (N/m^2)	0.06 (3.00)	0.25 (11.80)	0.62 (29.60)	1.09 (52.00)	1.83 (87.50)	2.91 (139.5)	
	Erosion Rate, in/hr (mm/hr)	0.00 (0.00)	0.00 (0.00)	0.00 (0.00)	0.05 (1.20)	0.07 (1.80)	0.09 (2.40)	
US-54 #2	Water Velocity, ft/s (m/s)	3.28 (1.00)	6.56 (2.00)	9.84 (3.00)	13.12 (4.00)	16.40 (5.00)	19.69 (6.00)	0.25 (11.80)
	Shear Stress, lb/ft^2 (N/m^2)	0.07 (3.20)	0.38 (18.40)	0.68 (32.60)	1.63 (78.00)	2.11 (100.9)	3.95 (189.0)	
	Erosion Rate, in/hr (mm/hr)	0.00 (0.00)	0.09 (2.40)	0.22 (5.40)	0.45 (11.40)	0.51 (12.90)	4.56 (115.7)	
US-54 #3	Water Velocity, ft/s (m/s)	3.28 (1.00)	6.56 (2.00)	9.84 (3.00)	13.12 (4.00)	16.40 (5.00)	19.69 (6.00)	1.19 (57.10)
	Shear Stress, lb/ft^2 (N/m^2)	0.07 (3.40)	0.27 (13.00)	0.63 (30.40)	1.25 (60.00)	1.24 (59.40)	3.10 (148.5)	
	Erosion Rate, in/hr (mm/hr)	0.00 (0.00)	0.00 (0.00)	0.00 (0.00)	0.07 (1.80)	0.21 (5.40)	0.24 (6.00)	
US-54 #4	Water Velocity, ft/s (m/s)	3.28 (1.00)	6.56 (2.00)	9.84 (3.00)	13.12 (4.00)	16.40 (5.00)	19.69 (6.00)	1.10 (52.90)
	Shear Stress, lb/ft^2 (N/m^2)	0.06 (3.00	0.26 (12.40)	0.63 (30.40)	1.16 (55.40)	1.75 (83.80)	3.01 (144.0)	
	Erosion Rate, in/hr (mm/hr)	0.00 (0.00)	0.00 (0.00)	0.00 (0.00)	0.05 (1.20)	0.07 (1.80)	0.43 (10.80)	
US-54 #5	Water Velocity, ft/s (m/s)	3.28 (1.00)	6.56 (2.00)	9.84 (3.00)	13.12 (4.00)	16.40 (5.00)	19.69 (6.00)	0.63 (30.20)
	Shear Stress, lb/ft^2 (N/m^2)	0.06 (3.10)	0.29 (13.90)	0.67 (32.10)	1.16 (55.60)	1.86 (89.10)	3.25 (155.7)	
	Erosion Rate, in/hr (mm/hr)	0.00 (0.00)	0.00 (0.00)	0.05 (1.20)	0.07 (1.80)	0.09 (2.40)	0.28 (7.20)	

Bridge 050-0048 on US-160 Highway
(GPS Co-ordinate: 37.1649, -95.0906)

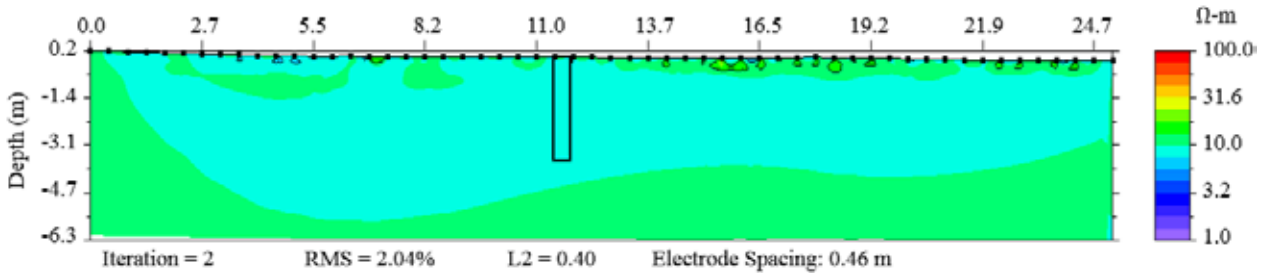

Figure A.25: Inverted Resistivity of US-160

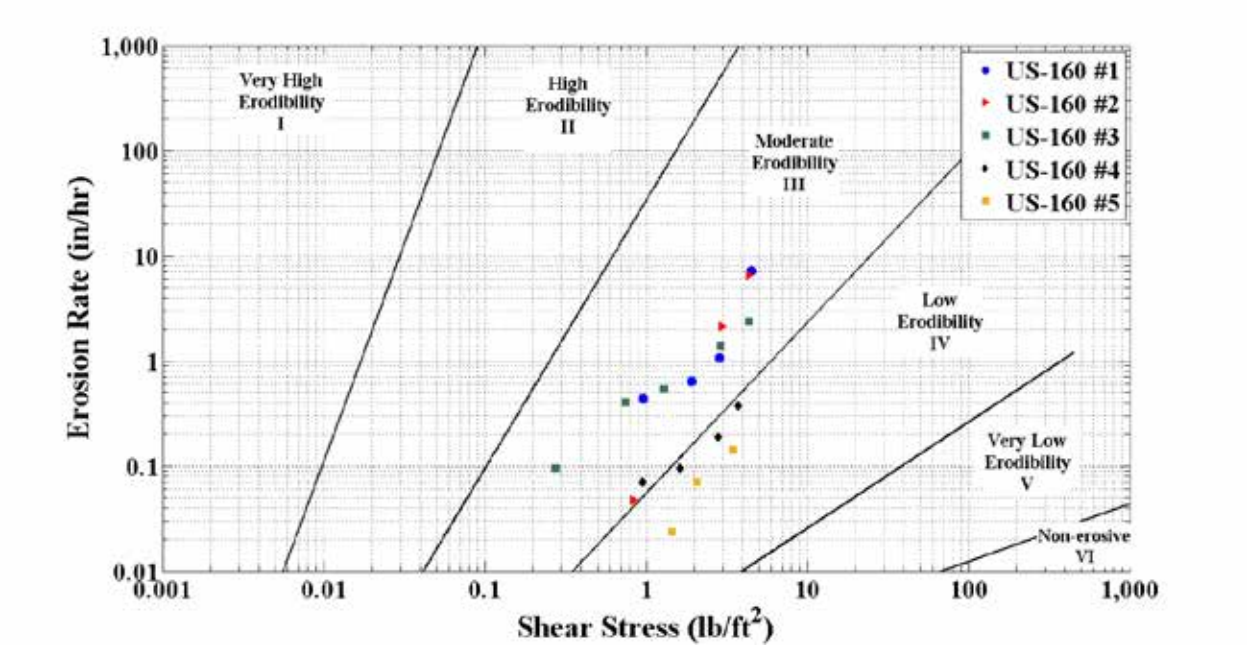

Figure A.26: Erosion Rate versus Shear Stress for US-160 Samples

Table A.25: Classification of US-160 Samples

Sample designation	Water content (%)	Percent finer than 0.075 mm (%)	Mean grain size (mm)	LL	PL	PI	USCS Classification
US-160 #1	28	98	0.003	50	26	24	CH
US-160 #2	30	98	0.005	44	22	22	CL
US-160 #3	26	98	0.006	50	24	26	CH
US-160 #4	25	97	0.006	45	20	25	CL
US-160 #5	29	98	0.005	47	22	25	CL

Table A.26: Erosion Test Results of US-160 Samples

Sample	Erosion Test Results							Critical Shear Stress, lb/ft^2 (N/m^2)
US-160 #1	Water Velocity, ft/s (m/s)	3.28 (1.00)	6.56 (2.00)	9.84 (3.00)	13.12 (4.00)	16.40 (5.00)	19.69 (6.00)	0.79 (37.90)
	Shear Stress, lb/ft^2 (N/m^2)	0.07 (3.20)	0.28 (13.30)	0.96 (46.10)	1.92 (92.00)	2.85 (136.6)	4.51 (216.0)	
	Erosion Rate, in/hr (mm/hr)	0.00 (0.00)	0.00 (0.00)	0.43 (11.00)	0.65 (16.40)	1.07 (27.30)	7.24 (183.8)	
US-160 #2	Water Velocity, ft/s (m/s)	3.28 (1.00)	6.56 (2.00)	9.84 (3.00)	13.12 (4.00)	16.40 (5.00)	19.69 (6.00)	0.79 (37.90)
	Shear Stress, lb/ft^2 (N/m^2)	0.07 (3.30)	0.29 (14.00)	0.65 (30.90)	0.84 (40.00)	2.94 (140.6)	4.32 (207.0)	
	Erosion Rate, in/hr (mm/hr)	0.00 (0.00)	0.00 (0.00)	0.00 (0.00)	0.05 (1.20)	2.11 (53.60)	6.54 (166.2)	
US-160 #3	Water Velocity, ft/s (m/s)	3.28 (1.00)	6.56 (2.00)	9.84 (3.00)	13.12 (4.00)	16.40 (5.00)	19.69 (6.00)	0.20 (9.80)
	Shear Stress, lb/ft^2 (N/m^2)	0.05 (2.60)	0.28 (13.20)	0.75 (36.00)	1.29 (62.00)	2.87 (137.5)	4.32 (207.0)	
	Erosion Rate, in/hr (mm/hr)	0.00 (0.00)	0.09 (2.40)	0.40 (10.20)	0.54 (13.80)	1.40 (35.50)	2.36 (60.00)	
US-160 #4	Water Velocity, ft/s (m/s)	3.28 (1.00)	6.56 (2.00)	9.84 (3.00)	13.12 (4.00)	16.40 (5.00)	19.69 (6.00)	0.90 (42.90)
	Shear Stress, lb/ft^2 (N/m^2)	0.06 (2.90)	0.30 (14.30)	0.96 (46.10)	1.64 (78.40)	2.81 (134.4)	3.76 (180.0)	
	Erosion Rate, in/hr (mm/hr)	0.00 (0.00)	0.00 (0.00)	0.07 (1.80)	0.09 (2.40)	0.19 (4.80)	0.38 (9.60)	
US-160 #5	Water Velocity, ft/s (m/s)	3.28 (1.00)	6.56 (2.00)	9.84 (3.00)	13.12 (4.00)	16.40 (5.00)	19.69 (6.00)	1.24 (59.60)
	Shear Stress, lb/ft^2 (N/m^2)	0.06 (2.90)	0.29 (13.80)	0.55 (26.40)	1.45 (69.20)	2.07 (99.10)	3.48 (166.5)	
	Erosion Rate, in/hr (mm/hr)	0.00 (0.00)	0.00 (0.00)	0.00 (0.00)	0.02 (0.60)	0.07 (1.80)	0.14 (3.60)	

K-TRAN

KANSAS TRANSPORTATION RESEARCH AND NEW-DEVELOPMENT PROGRAM

AD ASTRA PER ASPERA

Kansas

Department of Transportation